An Exploratory Study on Functionally Graded Materials with Applications to Multilayered Pavement Design

Ernie Pan, Wael Alkasawneh, and Ewan Chen

1. Report No. FHWA/OH-2007/12	2. Government Accession No.	3. Recipient's Catalog No.
4. Title and subtitle **An Exploratory Study on Functionally Graded Materials with Applications to Multilayered Pavement Design**		5. Report Date **August 2007**
		6. Performing Organization Code
7. Author(s) **Ernie Pan, Wael Alkasawneh, Ewan Chen**		8. Performing Organization Report No.
		10. Work Unit No. (TRAIS)
9. Performing Organization Name and Address **Department of Civil Engineering** **The University of Akron** **Akron, OH 44325-3905**		11. Contract or Grant No. **134256**
		13. Type of Report and Period Covered **Final Report**
12. Sponsoring Agency Name and Address **Ohio Department of Transportation** **1980 West Broad Street** **Columbus, OH 43223**		14. Sponsoring Agency Code
15. Supplementary Notes		

16. Abstract

The response of flexible pavement is largely influenced by the resilient modulus of the pavement profile. Different methods/approaches have been adopted in order to estimate or measure the resilient modulus of each layer assuming an average modulus within the layer. In order to account for the variation in the modulus of elasticity with depth within a layer in elastic pavement analysis, which is due to temperature or moisture variation with depth, the layer should be divided into several sublayers and the modulus should be gradually varied between the layers. A powerful and innovative computer program has been developed for elastic pavement analysis that overcomes the limitations of the existing pavement analysis programs. The new program can predict accurately and efficiently the response of the pavement consisted of any number of layers/sublayers and any number of loads. The complexity of the tire-pavement loading configuration can be modeled easily as well.

Practical pavement engineering problems have been analyzed and discussed taking into consideration the modulus variation with depth as well as the complex tire-pavement loading configuration utilizing our newly developed *MultiSmart3D* program. The analyzed problems illustrated that powerful analytical tools, such as *MultiSmart3D*, are needed to study and predict the pavement response in practical and fast manners. For example, the predicted life time of the pavement can be increased or decreased by a factor more than two if the modulus of elasticity variation with depth is taken into consideration.

17. Key Words Multilayered elastic analysis, Pavement, Temperature, Resilient modulus, Tire contact pressure, Tire footprint, Stress/strain discontinuity, Fatigue/rutting life prediction	18. Distribution Statement **No restrictions. This document is available to the public through the National Technical Information Service, Springfield, Virginia 22161**	
19. Security Classif. (of this report) **Unclassified**	20. Security Classif. (of this page) **Unclassified**	21. No. of Pages **135**
Form DOT F 1700.7 (8-72)	**Reproduction of completed pages authorized**	22. Price

An Exploratory Study on Functionally Graded Materials with Application to Multilayered Pavement Design

Prepared by

Ernian Pan, PhD
(Principal Investigator)

Wael Alkasawneh, P.E.
(Graduate Student)

Ewan Chen
(Graduate Student)

Department of Civil Engineering
The University of Akron
Akron, OH 44325-3905

Final Report
August 2007

**An Exploratory Study on Functionally Graded Materials
with Application to Multilayered Pavement Design**

TABLE OF CONTENTS

LIST OF FIGURES

LIST OF TABLES

ACKNOWLEDGMENT

ABSTRACT

The response of flexible pavement is largely influenced by the resilient modulus of the pavement profile. Different methods/approaches have been adopted in order to estimate or measure the resilient modulus of each layer assuming an average modulus within the layer. In order to account for the variation in the modulus of elasticity with depth within a layer in elastic pavement analysis, due to either temperature or moisture variation with depth, the layer should be divided into several sublayers and the modulus should be gradually varied between the layers. A powerful and innovative computer program has been developed for elastic pavement analysis that overcomes the limitations of the currently available pavement analysis programs. The new program can predict accurately and efficiently the response of the pavement consisting of any number of layers/sublayers. The complexity of the tire-pavement loading configuration can be modeled easily as well.

Practical pavement engineering problems have been analyzed and discussed taking into consideration the modulus variation with depth as well as the complex tire-pavement loading configuration utilizing the newly developed *MultiSmart3D* program. The analyzed problems showed that powerful analytical tools, such as *MultiSmart3D*, are needed to practitioners in order to study and predict the pavement response in practical and fast manners. For example, the predicted life time of the pavement can be increased or decreased by a factor more than two if the modulus of elasticity variation with depth is taken into consideration.

CHAPTER 1

INTRODUCTION

1.0 INTRODUCTION

Roads are very important in everyday transportation activities. Durability of pavement and driving convenience are very essential in pavement design and rehabilitation. The cost of pavement material and design is largely affected by the material type which can range widely based on the roadway design parameters. A maintenance-free pavement is still difficult and more research is needed to find an economical maintenance-free pavement.

Performance and durability of existing and new pavements are very important to increase the design life of pavements and to reduce the roadway hazards. In the US, a big portion of the transportation agencies budget is spent every year on pavement maintenance and improvement. In Ohio, for example, the length of public roads increased from approximately 117,000 miles to 123,000 miles between 2000 and 2003. However, the used design procedures and practice depended largely on procedures and practices that are more than 50 years old. It can be argued that the need for more practical and up-to-date procedures is inevitable these days due to the complexity of roadway design and the advancement in both technology and behavioral mechanisms of pavements.

New design approaches and procedures have been developed recently by The National Cooperative Highway Research Program (NCHRP) and the American Association of State Highway and Transportation Officials (AASHTO) Joint Task Force on Pavements. The new effort has resulted in replacing the old empirical-based pavement design procedures with mechanistic-empirical (M-E) based procedures in the new Mechanistic-Empirical Pavement Design Guide (MEPDG). The M-E approach is a very powerful approach since it combines the actual observed behavior of pavements and the analytical modeling techniques that are widely accepted. The M-E procedures are more reasonable and realistic than the empirical-based procedures since they allow for more consideration of the effects of the site actual traffic distribution, climate, material types, structure, and other design features.

Pavement behavior is a key point in the new MEPDG guide. Pavement behavior and empirical procedures have been developed based on laboratory and full scale field tests that provided valuable data base for analytical procedures. Transportation agencies under the new MEPDG are given more freedom to tailor the design procedures to suit their road and pavement conditions.

The new M-E procedures can be considered as a thickness design procedure and can be used to verify the design parameters with the actual parameters including traffic loading, material properties, and climatic conditions.

1.1 PAVEMENT LOADING RESPONSE

Understanding the pavement structural responses along the pavement section and the load capacity of the pavement requires suitable theories that represent the actual mechanical behavior. The following discusses some of the available theories that have been used to simulate pavement structural responses.

1.2 ELASTICITY THEORY

Elasticity theory was the first theory to be used for pavement analysis. Applying this theory to study the structural response of the pavement assumes that the pavement material is elastic. Elasticity theory works well as long as the stress-strain ratio is constant. This indicates that the elasticity theory is well suited for pavement sections that do not undergo stresses greater than the failure stresses. Equations derived from elasticity theory use the same basic theory but different assumptions for material properties and geometry (Bendana et. al, 1994). Pavement analysis using the elasticity theory is normally performed using Hook's law and Boussinesq theory.

1.2.1 HOOK'S LAW

Hook's law is based on the assumption that the stress-strain ratio is constant all the time in the uniaxial case of the material. Hook's law was derived assuming that the material is perfectly elastic and homogeneous.

1.2.2 BOUSSINESQ'S EQUATION

Boussinesq developed equations to compute stresses within a homogeneous, isotropic, linearly elastic half space under a point load acting perpendicular to the surface. The half-space assumption indicates an infinitely large area and an infinite depth. The value of the stress is given by (Holtz and Kovacs, 1981):

$$\sigma_z = \frac{P(3z^3)}{2\pi(r^2+z^2)^{5/2}} = \frac{P(3/2\pi)}{z^2(1+\frac{r^2}{z^2})^{5/2}} \qquad \text{Eq(1.1)}$$

where P=point load, z=depth from ground surface to the stress point, r=horizontal distance from the point load to the stress point.

Boussinesq developed other equations to compute the state of shear stresses, normal strains, and displacements under a point load in the elastic material as shown in Table 1.1 and Figure 1.1. It can be seen from the table that the normal strains, displacements, tangential stresses, and radial stresses depend on Poisson's ratio v and/or the modulus of elasticity E while the vertical stress and shear stresses are independent of Poisson's ratio and the modulus of elasticity.
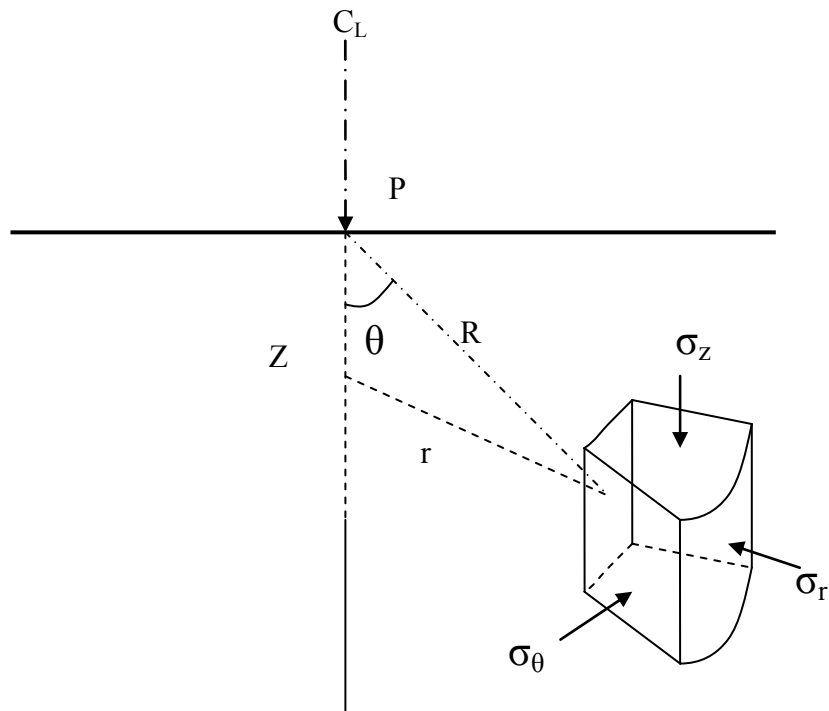
Figure 1.1, Notation for Boussinesq's Equation (Ullidtz, 1987)

Table 1.1, Boussinesq's equations for a point load

Normal Stresses

$$\sigma_z = \frac{3P}{(2\pi R^2)}\cos^3\theta$$

$$\sigma_r = \frac{P}{(2\pi R^2)}\left(3\cos\theta\sin^2\theta - \left(\frac{1-2v}{1+\cos\theta}\right)\right)$$

$$\sigma_t = \frac{P}{(2\pi R^2)}(1-2v)\left(-\cos\theta + \left(\frac{1}{1+\cos\theta}\right)\right)$$

$$\sigma_v = \frac{1}{3}(\sigma_z + \sigma_r + \sigma_t) = \frac{P}{(3\pi R^2)}(1+v)\cos\theta$$

Shear Stresses

$$\tau_{rz} = \frac{3P}{(2\pi R^2)}\cos^2\theta\sin\theta$$

$$\tau_{rt} = \tau_{tz} = 0$$

Normal Strains

$$\varepsilon_z = \frac{(1+v)P}{(2\pi ER^2)}\left(3\cos^3\theta - 2v\cos\theta\right)$$

$$\varepsilon_r = \frac{(1+v)P}{(2\pi ER^2)}\left(-3\cos^3\theta + (3-2v)\cos\theta - \left(\frac{1-2v}{1+\cos\theta}\right)\right)$$

$$\varepsilon_t = \frac{(1+v)P}{(2\pi ER^2)}\left(-\cos\theta + \left(\frac{1-2v}{1+\cos\theta}\right)\right)$$

$$\varepsilon_v = \varepsilon_z + \varepsilon_r + \varepsilon_t = \frac{(1+v)P}{(\pi ER^2)}(1-2v)\cos\theta$$

Displacements

$$d_z = \frac{(1+v)P}{(2\pi ER)}\left(2(1-v) + \cos^2\theta\right)$$

$$d_r = \frac{(1+v)P}{(2\pi ER)}\left(\cos\theta\sin\theta - \frac{(1-2v)\sin\theta}{1+\cos\theta}\right)$$

$$d_t = 0$$

Boussinesq's equation can be extended to other loading conditions such as line load over a finite area (Newmark's equation , Newmark, 1935). Westergaard (1938) derived an equation for stresses under a point load in elastic homogeneous half-space with a Poisson's ratio equal to zero. His equation is given in Eq. (1.2) where the terms are similar to the terms in Boussinesq's equation. Both Boussinesq's and Westergaard's equations provide almost the same stress value for r/z≥1.5, while for r/z<1.5 Boussinesq's equation provides larger values than Westergaard's equation (Holtz and Kovacs, 1981).

Boussinesq (1876) developed a more realistic theory for stresses in granular material assuming a variable shear modulus that changes as the hydrostatic stresses change. This assumption resembles actual stresses in materials where the shear modulus increases as the stresses increase.

Elasticity theory and Boussinesq's equations were studied by other researchers to check the validity of the theory and the accuracy of the assumptions. Frolich (1934) showed that the radial stress in Boussinesq's theory is the major principal stress which is inversely proportional to the square of the distance from the point load. Frolich (1934) generalized the theory by introducing a concentration factor (n) as shown in the following equations.

$$\sigma_z = \frac{nP}{(2\pi R^2)} \cos^n \theta \qquad\qquad \text{Eq. (1.2)}$$

$$\sigma_r = \frac{nP}{(2\pi R^2)} \cos^{n-2} \theta \sin^2 \theta \qquad\qquad \text{Eq. (1.3)}$$

$$\sigma_t = 0 \qquad\qquad \text{Eq. (1.4)}$$

$$\sigma_R = \frac{nP}{(2\pi R^2)} \cos^{n-2} \theta \qquad\qquad \text{Eq. (1.5)}$$

$$P = \frac{\sigma_R}{3} \qquad\qquad \text{Eq. (1.6)}$$

If the modulus is assumed to be constant, Frolich equations would result in deflections that are proportional to (n) and a Poisson's ratio that is equal to 0.5 as was assumed in Boussinesq's theory (Ullidtz, 1998).

On the other hand, if the modulus changes with the hydrostatic stress or the major principal stress is raised to a power factor two cases arise: The first case is resulted from the assumption that the modulus changes with the hydrostatic stress which results in a positive power factor and hence a dilation of the material since the Poisson's ratio is larger than 0.5 (based on the assumption). The second case is resulted from the assumption that the modulus changes with the major principal stress which produces a negative power factor and hence a "stress dispersion" rather than "stress concentration" as proposed by Boussinesq's theory (Ullidtz, 1998).

1.2.3 CHARTS METHOD

Boussinesq solution was extended by different researchers to account for more general loading conditions. Solutions for a circular loaded area can be obtained by integrating the Boussinesq solution for a point load. In the influence lines method, solutions for stresses and deflections can be obtained by referring to charts that had been developed by simplifying the existing conditions under a circular loaded area and by using the elastic theory as seen in Figure 1.2. These assumptions include neglecting the Poisson's ratio (Foster and Ahlin, 1954), or including the Poisson's ratio (Ahlvin and Ulery, 1962). Poisson's ratio has relatively little effect on stresses and strains in the half-space elastic theory and therefore can be neglected for simplicity (Huang, 1993).
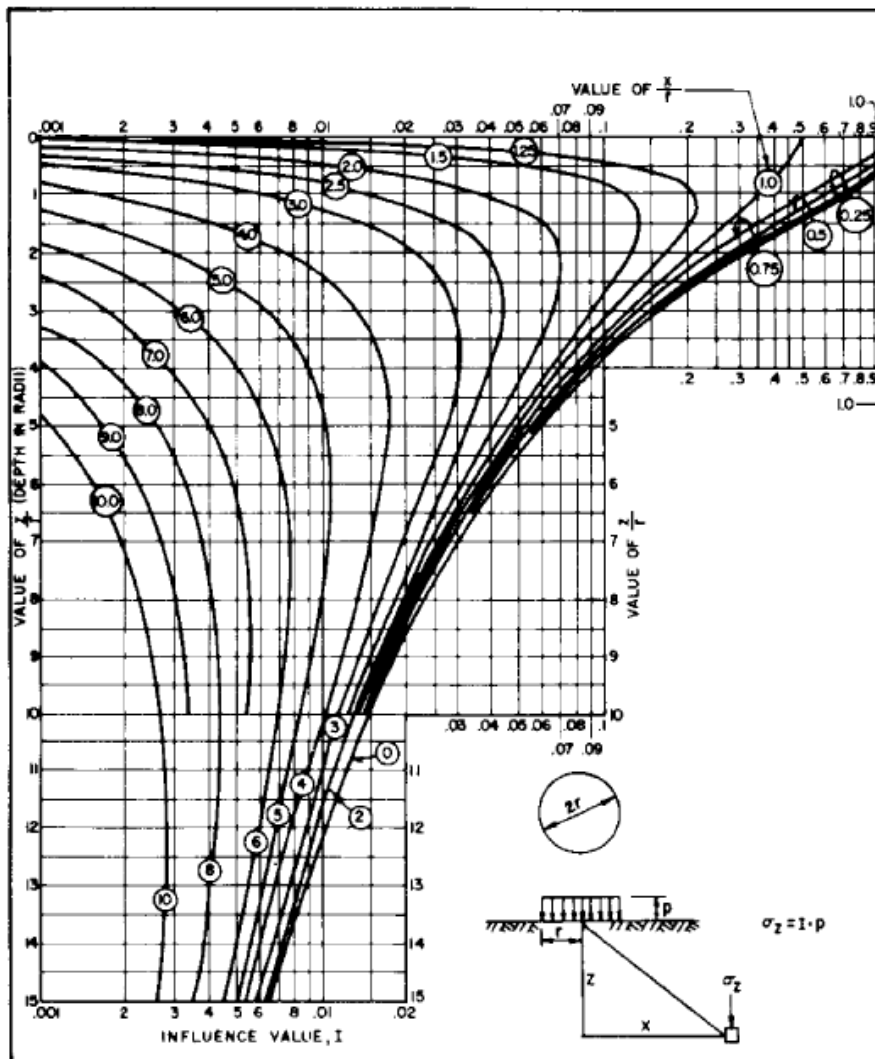
Figure 1.2, Influence lines for a circular loaded area (Holtz and Kovacs, 1981).

6

1.3 METHOD OF EQUIVALENT THICKNESS (MET)

This method was first developed by Odemark (Ullidtz, 1987). The MET method transforms a system with different moduli to a system with one modulus in order to apply the classical elasticity theories to the system. This method involves two steps in which the interface plays a key rule for the transformation. In Figure 1.3, stresses and strains above the first layer can be found by using the same modulus of elasticity and Poisson's ratio for the second layer as in the first layer and assuming a half-space case. Stresses and strains in the second layer or at the interface can be found by transforming the first layer into a layer with the same modulus of elasticity and Poisson's ratio as in the second layer but with a new thickness based on the original stiffness of the first layer.
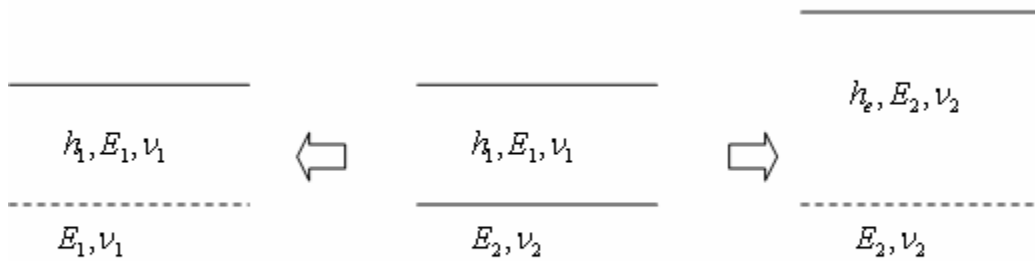
Figure 1.3, Typical transformations in the MET method (Ullidtz, 1987).

Theoretically, the MET method can be applied to any system with any number of layers as shown in Figure 1.4.
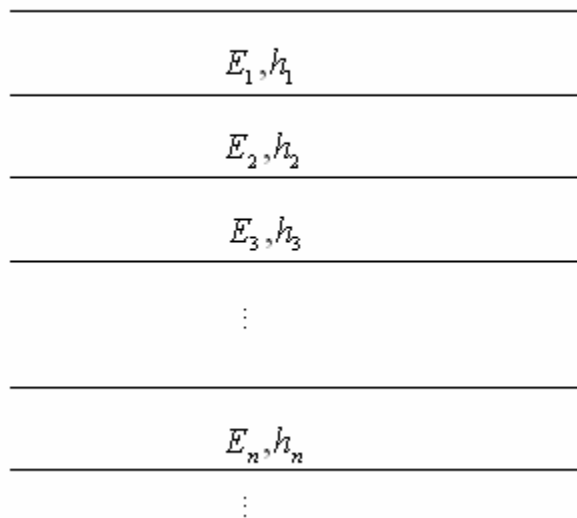
Figure 1.4, Typical multilayer system (Ullidtz, 1987).

The equivalent thickness of the transformed layer based on the original stiffness of the layer can be found using the following equation (Ullidtz, 1987):

$$h_{e,n} = f \sum_{i=1}^{n-1} \left(h_i \left[\frac{E_i}{E_n} \right]^{\frac{1}{3}} \right)$$

Eq. (1.7)

where $h_{e,n}$ is the equivalent thickness for n layers, h_i, E_i and E_n are shown in Figures 1.3 and 1.4, f is the correction factor discussed below.

The MET method is primarily based on the assumption that stress distribution below the transformed layers will be the same since an equivalent stiffness is used for each layer. Stresses and strains are assumed to be linear in each layer. However, the MET method is an approximate method and stresses and strains estimated based on this method should be corrected to improve the agreement with layered elastic theory. The correction factor should be estimated based on the number of layers in the system, Poisson's ratio, modulus of elasticity, and layer thickness. In general, the correction factor for the first interface in a two-layer system is recommended to be 0.9 while it is 1.0 in a multi-layer system. The correction factor for other interfaces in a multi-layered system is recommended to be 0.8 (Ullidtz, 1987). The MET method can overestimate or underestimate stresses and strains in the layer and at the interface and hence can produce misleading results unless a good correction factor is available.

1.4 FINITE ELEMENT METHOD

Finite Element Method (FEM) has been used to study pavement response using any material constitutive law. In the FEM method, the geometry under study is discretized into small elements connected by nodes to resemble the actual geometry or domain. Constitutive laws then applied to govern the behavior of the material, and stresses and strains can be estimated accordingly. The advantage of the FEM analysis comes from the ability to simulate any loading condition, static and dynamic, and any geometrical variation, and local discontinuities such as cracks or joints. The FEM deals with materials as continuum and therefore it simplifies the actual behavior of granular material.

Most practical FEM modeling involves only two-dimensional analysis of pavement sections due to cost, time, and modeling limitations associated with the three dimensional analysis. Three-dimensional analysis involves the discretization of the domain using sophisticated meshing techniques that adversely affect the time and cost needed to study the pavement response. Two-dimensional analysis assumes axis-symmetric equilibrium conditions that limit the simulation of the full geometry when having local discontinuities.

8

1.5 DISCRETE ELEMENT METHOD

Advanced numerical simulations assume continuum medium when dealing with pavement modeling, which indicates a compatibility assumption unless special considerations are allowed to account for discontinuities like special finite elements in finite element.

Granular materials like asphalt can be described using the granular material physical behavior. Physical behavior of granular material includes normal and shear forces between grains and translational and rotational displacements between grains. Strains in granular materials are negligible under normal stresses.

In 1978, Cundall (1978) proposed the distinct element method which uses gravity, external forces, mass of particles, center of gravity of particles, and moment of inertia of particles with Newton's laws to describe the movement and interaction between grains. Discrete element simulation is carried out using steps in which forces and displacements are calculated for the medium and used as inputs for the next step.

Ullitdz (1995,1998), using circular disks to simulate grains, showed that the Distinct Element Method produces much larger tensile strains close to the axes of the load than continuum mechanics. This shows that continuum mechanics has some limitations when predicting stresses and strains in particulate media. In addition, it was shown that plastic strains are calculated simultaneously with the resilient or elastic strains, as well as strains at failure. However, this advanced simulation technique is far from being available to engineers and is still a research tool.

1.6 VISCOELASTICITY METHOD

Materials deformation can be elastic, plastic, viscous, and viscoelastic. Based on the physical behavior, these deformations can be categorized as energy-storage processes and dissipative viscous processes (time-dependent). Viscoelastic behavior is time dependent while elastic deformations can be time-independent. Plastic materials are somewhat viscous but for simplicity they can be assumed to be time-independent.

Viscoelastic models are composed of different parts including (Ancey, 2005):

Spring: according to Hooke's law, the strain (ε) is proportional to the applied stress (σ) according to

$$\sigma = E\varepsilon \qquad \text{Eq. (1.8)}$$

with E the elastic modulus. In this law, deformations are time independent and elastic elements represent the possibility of storing energy.

Dashpot: the response of the dashpot, the plunger of which is pushed at velocity $\dot{\varepsilon}$ is described by

$$\sigma = \mu\dot{\varepsilon} \qquad \text{Eq. (1.9)}$$

where (μ) is the viscosity.

The dashpot element represents a dissipative process that occurs as a result of the relative motion between particles. This motion induces friction when there is contact between elements or viscous dampening if there is an interstitial fluid.

Viscoelaticity is described by one or more of the above two elements. If the spring and dashpot are mounted in series, the resulting model is called the Maxwell model and it is best suited for viscoelastic fluids. If the spring and dashpot are mounted in parallel, the resulting model is called the Kelvin-Voight model and it is best suited for viscoelastic solids. These models are elementary models and can be combined to get more representative models like the Burgers model. These methods can describe some aspects of the physical behavior, but they still have their own limitations.

1.6.1 MAXWELL MODEL

In this model the dashpot and spring are connected in series, therefore the total deformation is the sum of both deformations:

$$\frac{d\varepsilon}{dt} = \frac{1}{E}\frac{d\sigma}{dt} + \frac{\sigma}{\mu} \qquad\qquad \text{Eq. (1.10)}$$

which has the following solution

$$\sigma(t) = Ke^{-\frac{Et}{\mu}} + \int_{-\infty}^{t} Ee^{\frac{E(\tau-t)}{\mu}} \dot{\varepsilon}(\tau)d\tau \qquad\qquad \text{Eq. (1.11)}$$

where K is an integration constant, the lower boundary in the integral is arbitrary. K is equal to zero when the stress is finite at t= $(-\infty)$. The following two cases arise from this equation(Ancey, 2005).
1– for steady state, this equation simplifies to the Newtonian equation $\sigma = \mu\dot{\varepsilon}$.
2– for sudden changes in stress, the time derivative dominates.

Equation 1.10 can be written as $\sigma(t) = \int_{-\infty}^{t}\left[\frac{\mu}{t_r}e^{\frac{\tau-t}{t_r}}\right]\varepsilon'(\tau)d\tau = \int_{-\infty}^{t}\Gamma(t-\tau)\varepsilon(\tau)d\tau$

where $t_r = \dfrac{\mu}{E}$ is a relaxation time. The term within the brackets is called the *relaxation*

modulus and the integral takes the form of a convolution product of $\Gamma(t) = \mu\dfrac{e^{-\frac{t}{t_r}}}{t_r}$ and $\dot{\varepsilon}$.

If the above equation is used in the creep testing it will be reduced to

$$\varepsilon = \sigma\left(\frac{1}{E} + \frac{t}{\mu}\right) \qquad\qquad \text{Eq. (1.12)}$$

In the Maxwell model, stresses at time t depend on strains at time t and on the strain rate at past time t' but to within a weighting factor that decays exponentially.

1.6.2 KELVIN-VOIGT MODEL

The deformation is described using

$$\varepsilon = \frac{\sigma}{E}\left(1 - e^{-\frac{t}{t_r}}\right)$$
Eq. (1.13)

where $t_r = \frac{\mu}{E}$ is the relaxation time.

1.6.3 BURGERS MODEL

This model is a combination of the Maxwell model and the Kelvin-Voight models. Deformations are described using

$$\varepsilon = \sigma\left(\frac{1}{E_1} + \frac{1}{E_2}\left(1 - e^{-\frac{t}{t_r}} + \frac{t}{\mu_1}\right)\right)$$
Eq. (1.14)

where $t_r = \frac{\mu_2}{E_2}$ is the relaxation time.

1.6.4 CREEP TESTING

Creep testing is used to describe the response behavior of solids. In this test, a constant stress is suddenly applied to the material and the strain variation over a range of time is then monitored (Ancey, 2005). Results from the creep test can be used to describe the three distinct responses of the material during the testing. These responses are: (1) the immediate elastic response, (2) delayed elastic response (glassy behavior), where the deformation rate slows with time but becomes steady after long time, (3) the steady state viscous response (when the shear rate of the material is constant so the material is in steady flow).

Visco-elastic models are used to describe material responses during creep testing. Maxwell model is used to describe the immediate elastic response and the steady state response while Burgers model is used to describe the three responses including the glassy response.

1.7 LAYERED SYSTEMS

It is known that the modulus of elasticity of soil and pavement materials is not constant but changes as a function of different factors such as the stress level, moisture content, and temperature (Ullidtz, 1987). On the other hand, the assumption that pavement and subgrade materials are linear does not resemble the actual conditions. Depending on the stress level and strains, the physical response of soil and pavement materials can be categorized as elastic, plastic, viscous, and viscoplastic. Therefore,

modeling the pavement and subgrade using only elastic theory might result in inaccurate predictions. This problem can be tackled by assuming nonlinear elastic behavior and by using different techniques to handle the nonlinearity.

1.7.1 ELASTIC MULTI-LAYER THEORY

This method was first proposed by Burmister (1943, 1945) as an effort to tackle the limitations of Boussinesq's method. Burmister (1945) simplified the conditions between two layers assuming that all layers are isotropic, elastic, and homogeneous. The top layer, in a two layer system, was assumed to be infinite in extent in the horizontal direction but of finite thickness in the vertical direction. The bottom layer, in a two-layer system, was assumed to be of infinite extent in both horizontal and vertical directions. In addition, Burmister (1945) assumed that the shear and normal stresses outside the limits of the surface loading are equal to zero. Continuity conditions along the interface between layers were considered using two cases. In the first case, full continuity of stress and displacement across the interface was considered assuming full contact between the two layers and a fully activated shear resistance between the layers. In the second case, continuity of normal stresses and normal displacements was only considered by assuming a frictionless interface between the layers.

Vertical stresses based on the two-layer theory are shown in Figure 1.5. As it can be seen from the figure, Burmister's method gave more accurate results than Boussinesq's method since infinite half-space condition is not applicable in pavement and subbase layers because the top layer is always of a finite depth. On the other hand, Burmister's method emphasizes the importance of modeling the interface between the two layers. Boussinesq's method overestimated the vertical stresses at the interface by more than 20% compared to stresses from Burmister's method.
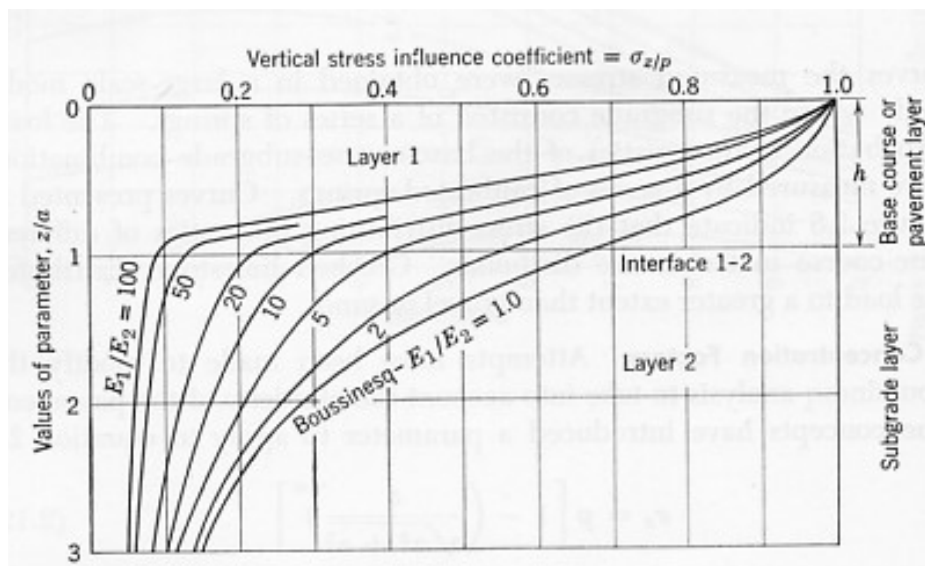
Figure 1.5, Burmister two-layer stress curves (Yoder, 1959).

Actual pavement behavior and conditions are different than those used in the multilayer theory. Pavement materials occupy a finite width and do not have a constant thickness. Spatial variations of material geometry and local discontinuities are not considered when using this method. In addition, idealizing the asphalt and soil material as homogeneous, linear elastic, and isotropic is far from real material behavior. Asphalt has a viscouselastic behavior while granular materials have a non-linear behavior. On the other hand, stresses within the pavement section are not considered in the multilayer theory. Horizontal stresses due to wheel loading and dynamic loads due to road geometry should be considered to correctly simulate the non-linear and visco-elastic responses, respectively (COST 333,1999). Anisotropy of pavement materials due to construction methods and due to the nature of the materials is inevitable and should be considered to account for stress changes in all directions within the pavement section.

Burmister extended his theory to three-layer system by deriving the settlement equation at the surface of the ground only. Based on Burmister's theory, Acum and Fox (1951) derived a closed form solution for interface stresses under the center of a circular loaded area. In 1962, Schiffman (1962) developed a solution for multiplayer elastic system which was used by many researchers to develop computer programs for pavement analysis.

1.7.2 FACTORS AFFECTING ELASTICITY

Some of the factors that affect the multi-layer elasticity are described below.

1.7.2.1 ANISOTROPY

Anisotropy has been studied by van Cauwelaet (1980) assuming a constant ratio between vertical and horizontal moduli. van Cauwelaet (1980) derived the following equations to incorporate the effect of anisotropy due to a point load and listed below are the solution below the centerline of a uniformly distributed load.

$$\sigma_z = \frac{szP}{2\pi(1-s)}\left(\frac{1}{\left(\sqrt{s^2z^2+r^2}\right)^3} - \frac{1}{\left(\sqrt{z^2+r^2}\right)^3}\right) \qquad \text{Eq. (1.15)}$$

$$\varepsilon_z = \frac{szP}{2\pi E(1-s)}\left(\frac{s^2(\rho+\nu)}{\left(\sqrt{s^2z^2+r^2}\right)^3} - \frac{1+\nu}{\left(\sqrt{z^2+r^2}\right)^3}\right) \qquad \text{Eq. (1.16)}$$

$$d_z = \frac{sP}{2\pi E(1-s)}\left(\frac{\rho+\nu}{\sqrt{s^2z^2+r^2}} - \frac{1+\nu}{\sqrt{z^2+r^2}}\right) \qquad \text{Eq. (1.17)}$$

$$s = \sqrt{\frac{\rho-\nu^2}{\rho^2-\nu^2}} \qquad \text{Eq. (1.18)}$$

For loose to medium dense granular soil with an internal friction angle equal to 30, the ratio between the vertical and horizontal stresses was found to be 2.25.

1.7.2.2 SHEAR SENSITIVITY

Shear sensitive material is a material that has a E/G ratio larger than $2(1+v)$ where E is the Young's modulus, G is the shear modulus, and (v) is the Poisson's ratio. Misra and Sen (1975) proposed the following equations for stress and displacements in shear sensitive materials with a typical value of 6 (Misra, 1979) for E/G. The solutions for a point load are

$$\sigma_z = \frac{sP}{2\pi(\alpha - \beta)}\left(\frac{1}{\left(\sqrt{\beta^2 z^2 + r^2}\right)^3} - \frac{1}{\left(\sqrt{\alpha^2 z^2 + r^2}\right)^3}\right) \qquad \text{Eq. (1.19)}$$

$$\varepsilon_z = \frac{(1+v)zP}{2\pi E(\alpha - \beta)}\left(\frac{\alpha^2 A}{\left(\sqrt{\alpha^2 z^2 + r^2}\right)^3} - \frac{\beta^2 B}{\left(\sqrt{\beta^2 z^2 + r^2}\right)^3}\right) \qquad \text{Eq. (1.20)}$$

$$d_z = \frac{(1+v)P}{2\pi E(\alpha - \beta)}\left(\frac{A}{\sqrt{\alpha^2 z^2 + r^2}} - \frac{B}{\sqrt{\beta^2 z^2 + r^2}}\right) \qquad \text{Eq. (1.21)}$$

and for a uniform distributed circular load are

$$\sigma_z = \frac{\sigma_o}{\alpha - \beta}\left(\alpha - \beta + \frac{z}{\sqrt{\alpha^2 z^2 + a^2}} - \frac{z}{\sqrt{\beta^2 z^2 + a^2}}\right) \qquad \text{Eq. (1.22)}$$

$$\varepsilon_z = \frac{(1+v)\sigma_o}{(\alpha - \beta)E}\left(\beta B\left(\frac{\beta z}{\sqrt{\beta^2 z^2 + a^2}} - 1\right) - \alpha A\left(\frac{\alpha z}{\sqrt{\alpha^2 z^2 + a^2}} - 1\right)\right) \qquad \text{Eq. (1.20)}$$

$$d_z = \frac{(1+v)\sigma_o}{(\alpha - \beta)E}\left(A\left(\sqrt{\alpha^2 z^2 + a^2} - \alpha z\right) - B\left(\sqrt{\beta^2 z^2 + a^2} - \beta z\right)\right) \qquad \text{Eq. (1.21)}$$

where α^2 and β^2 are the roots of the following equations
$x^2 + (K' - 2)x + 1 = 0$ where

$$K' = \frac{1-K}{1-v}$$

$$K = \frac{E}{(1+v)G} - 1$$

$$A = \frac{K - \alpha^2}{\alpha^2 - 1}$$

$$B = \frac{K - \beta^2}{\beta^2 - 1}$$

14

CHAPTER 2

RESILIENT MODULUS VARIATION STUDIES

2.0 INTRODUCTION

The response of flexible pavement is largely influenced by the resilient modulus of the pavement profile. Different methods and different approaches have been adopted in order to estimate or measure the resilient modulus of each layer assuming an average modulus within each layer. The resilient modulus can be estimated either by laboratory testing or by nondestructive testing such as the Falling Weight Deflectometer (FWD). The resilient modulus of pavement material is affected by many factors among which the temperature profile in the pavement, the stress or loading applied to the pavement profile, pavement drainage and moisture, frost, pavement compaction, and pavement material play a main part in the pavement behavior. Typical sections for flexible pavements are shown in Figure 2.1.
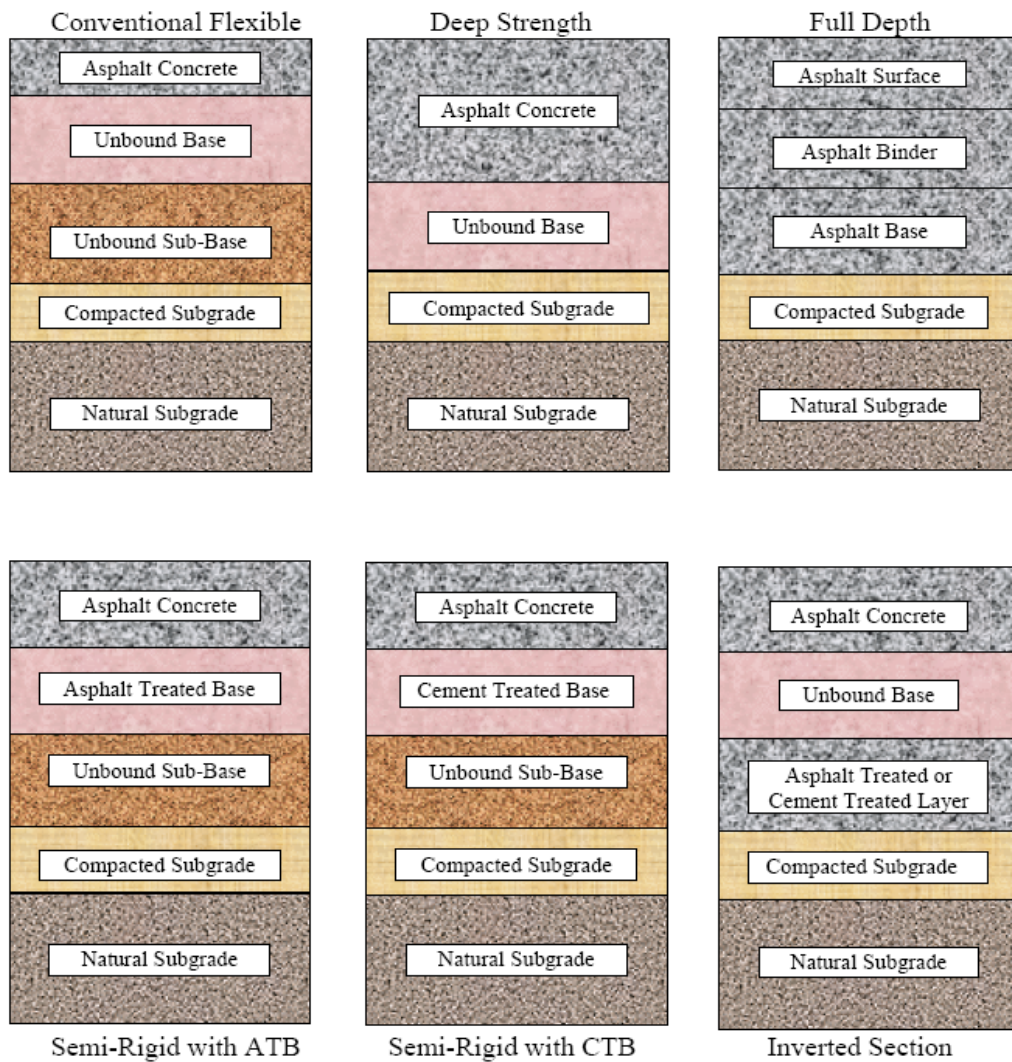
Figure 2.1, Typical flexible pavement sections (MEPDG, 2004).

Temperature variation along the pavement profile is mainly affected by the temperature variation along the surface of the pavement which varies continuously during the year. Such variation is anticipated to affect the stiffness of the pavement profile and therefore to affect the pavement responses such as rutting and load carrying capacity. In general the pavement-temperature variation can be divided into four different periods (Scrivner, et. al, 1969): (1) deep frost and high strength period, (2) rapid strength loss period, (3) rapid strength recovery period, and (4) slow strength recovery period.

Assuming a single modulus of elasticity for the pavement based on averaging the temperature during the year can result in overestimation or underestimation of the stiffness properties of the pavement depending on the prevailing climate conditions during the year. A site or more appropriately a statewide study of the temperature variation can be of significant importance to the pavement engineers due to the variation in the environmental and climatic conditions between two sites. Such studies can give information regarding the assumptions during pavement analysis and design and hence controlling the load capacity and the cost associated with each design.

Temperature variation along the pavement profile has been studied by many researchers to address its variation with depth and its relation to the surface temperature only. Other researchers studied the variation of the resilient modulus due to temperature variation to address the load carrying capacity of the pavement profile and to study the responses of the pavement during different temperature cycles. In all research the resilient modulus along the pavement profile was averaged to eliminate the complexity of the modulus variation with depth within the same layer, and due to the lack of appropriate analytical tools that can handle such variations in appropriate timely, costly and user-friendly manners.

Analytical methods that can model the temperature variation along the pavement profile without analytical limitations are limited so far to the finite element and the finite difference methods since the stress concentration, the large number of layers, computational time, input complexity, computational complexity are among the many factors that impose the limitations on such modeling. However, the boundary element method is an advanced and powerful analytical method that can be geared toward pavement analytical computation with many advantages over the existing analytical methods.

The following sections address the changes in the resilient modulus and the Poisson's ratio due to temperature and seasonal variations.

2.1 MECHANISTIC-EMPIRICAL PAVEMENT DESIGN GUIDE

The Mechanistic-Empirical Pavement Design Guide (MEPDG) addresses the importance of temperature and other environmental factors in the pavement analysis and design. The change in the temperature in the pavement profile is considered using a sophisticated climatic model called the Enhanced Integrated Climatic Model (EICM). The EICM model is a one-dimensional coupled heat and moisture flow program that uses

16

the climatic conditions of the material over several years to predict the temperature, resilient modulus adjustment factors, pore water pressure, water content, frost and thaw depths, frost heave, and drainage performance at any point within the entire pavement/subgrade profile of asphalt concrete (AC) or Portland Cement Concrete (PCC) pavements. The EICM model uses data from the Long Term Pavement Performance (LTPP) Seasonal Monitoring Program (SMP) test sections.

Based on the MEPDG guide and the EICM model, a software product was developed to incorporate the power of both (MEPDG, 2004). The MEPDG software applies an adjustment factor at the desired point within the pavement/subgrade profile to an initial user supplied resilient modulus. Initial resilient modulus of unbound material is the modulus at or near the optimum water content and maximum dry density. The adjustment is used to estimate the new resilient modulus at any time and depth.

The MEPDG method suggests the use of average temperature values for the analysis period, with a minimum of one year of hourly temperature data, to estimate the resilient modulus of the AC layer for rutting and fatigue cracking predictions. The MEPDG software allows the analysis to include only a maximum of three asphalt layers including the surface, binder, and base layers. Sub-layering of the asphalt layer is recommended to account for the temperature variation within the pavement.

Sub-layering of the pavement layers is done internally in the MEPDG program for the different layers to account for the temperature and resilient modulus variation in all layers/sublayers. Temperature variation in the layers through sub-layering is recommended to study the distress in the pavement due to seasonal variation. Pavement distress includes asphalt fatigue fracture (top down and bottom up), permanent deformation, and asphalt thermal fracture. Sub-layering is controlled by the number of layers and the depth of each layer. As the thickness of layers increases the number of sublayers increases leading to more computational time using the current available methods. However, the maximum allowed number of sublayers in the MEPDG software cannot exceed 20 or the maximum number of evaluation points cannot exceed 26 points.

Sublayering of the asphalt concrete layers is carried out to estimate the thermal stresses and the crack propagation within the asphalt concrete sublayers as a function of time and depth. A typical sublayering of the asphalt concrete layer is shown in Figure 2.2 where the top 12.7 mm (0.5 inch) is typically the first sublayer (Witczak et. *al.* 2000). A typical sublayering for a flexible pavement section is shown in Figure 2.3.
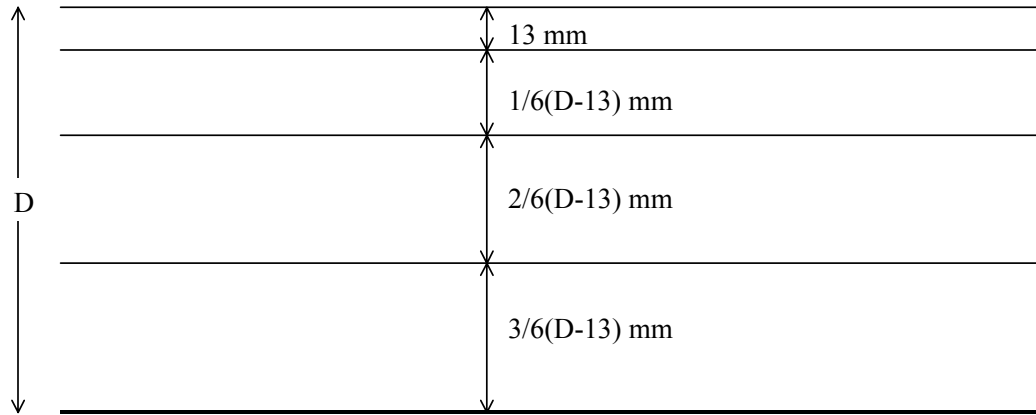
Figure 2.2, Typical AC sublayering (modified from Witczak et. *al.*, 2000).

Maximum Sublayering = 2.44 m

12.7 mm

12.7 mm

25.4 mmincrements to depth of 102 mm

Remaining thickness

$51 \text{mm} \left\{ \text{f } h_B \geq 152 \text{mm} \right\}$

$n_B = \text{int} \left(\dfrac{h_B - 51}{4} \right)$ for $h_B > 152$ mm

$n_{SB} = \text{int} \left(\dfrac{h_{SB}}{4} \right)$ for $h_{SB} \geq 203$ mm

$n_{CSG} = \text{int} \left(\dfrac{h_{CSG}}{12} \right)$ for $h_{CSG} > 305$ mm

$n_{SG} = \text{int} \left(\dfrac{h_{SG}}{12} \right)$ for $h_{SB} > 305$ mm
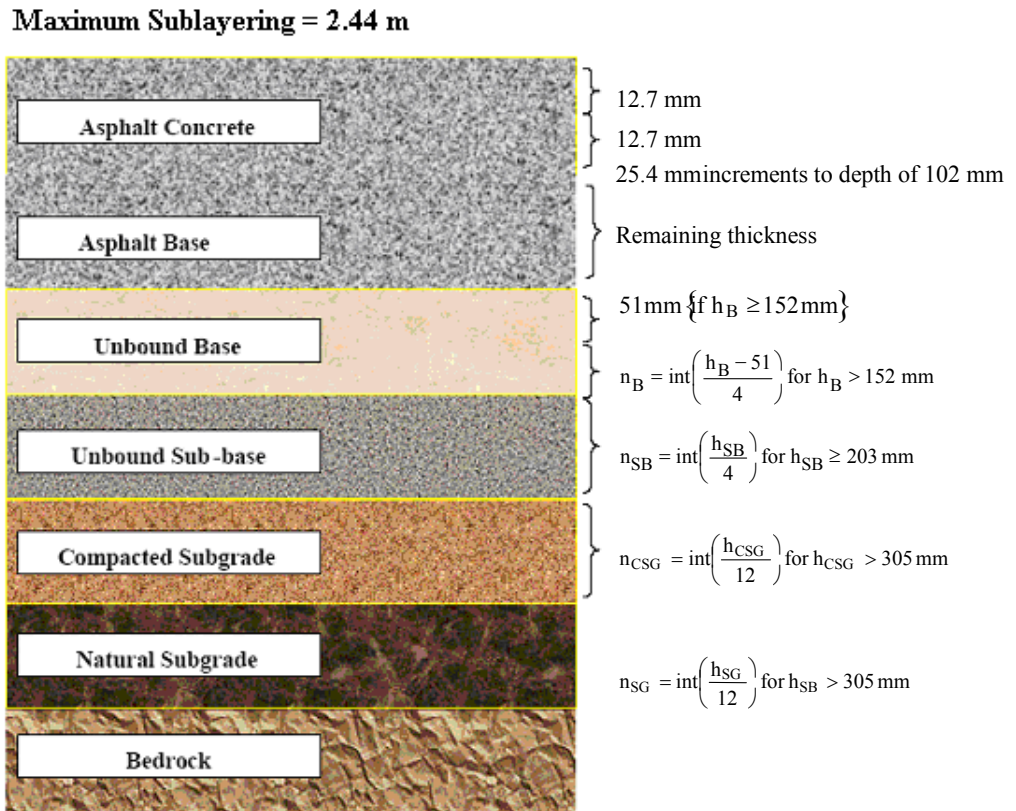
Figure 2.3, Typical sublayering of flexible pavement (modified from MEPDG, 2004)

The MEPDG software calculates the resilient modulus in the asphalt concrete layers using Witczak's equation:

$$\log(E^*) = \delta + \frac{\alpha}{1 + e^{\beta + \gamma \left[\log(t) - c \left(\log(\eta) - \log(\eta_{rt}) \right) \right]}}$$

Eq. (2.1)

where
E*: Dynamic modulus, psi

t: Time of loading, sec

η : Viscosity at temperature of interest, CPoise

η_{rt} : Viscosity at reference temperature, CPoise

$\alpha, \beta, \delta, \gamma, c$: Mixture specific fitting parameters

In addition, the software calculates the resilient modulus of the unbound and subgrade materials using Witczak-Uzban's equation

$$E = k_1 p_a \left(\frac{\theta}{p_a} \right)^{k_2} \left(\frac{\tau_{oct}}{p_a} + 1 \right)^{k_3}$$

Eq. (2.2)

where

E: Resilient modulus, psi

k_1, k_2, and k_3: parameters from physical testing or estimates

p_a: standard atmospheric pressure

θ : the bulk stress, $\theta = \sigma_1 + \sigma_2 + \sigma_3$

τ_{oct} : the octahedral stress, $\tau_{oct} = \frac{1}{3} \sqrt{\left((\sigma_1 - \sigma_2)^2 + (\sigma_1 - \sigma_3)^2 + (\sigma_2 - \sigma_3)^2 \right)}$

2.1.1 SEASONAL VARIATION OF RESILIENT MODULUS

Temperature variation output using MEPDG software for a flexible pavement section in Iowa was reported by Coree et *al.* (2005). Data extracted from the report were plotted and presented below (Figures 2.4 through 2.8). The data represent the calculated resilient modulus using weather stations input data as well as other hot mix, unbound material, and subgrade material data. The flexible pavement section and the sublayering of the layers are shown in Figure 2.4. The dashed lines represent the sublayer limit within each layer. The subgrade was divided into four sublayers with thicknesses of 0.62 m, 0.62 m, 0.62 m and 6.48 m, respectively. The sublayers of the subgrade layer are not shown in Figure 2.4. The water table at the site was reported to be at 3.66 m below the surface. The Poisson's ratio for all layers was reported to be constant during the year with a value of 0.35. Presented below in Figures 2.5 through 2.8 are some typical curves for modulus variation vs. depth in different sublayers for different months based on the profile of Figure 2.4.

Figure 2.5 shows the variation of the resilient modulus with depth in the top 381 mm of the flexible pavement system. The calculated resilient modulus was plotted at the mid-depth for each sublayer/layer to show the influence of temperature variation on the modulus as a function of depth and time.

Depth (mm)

AC
Layer

102

279

A-2-6
Base

432

A-7-5
Subbase

660

A-7-6
Subgrade
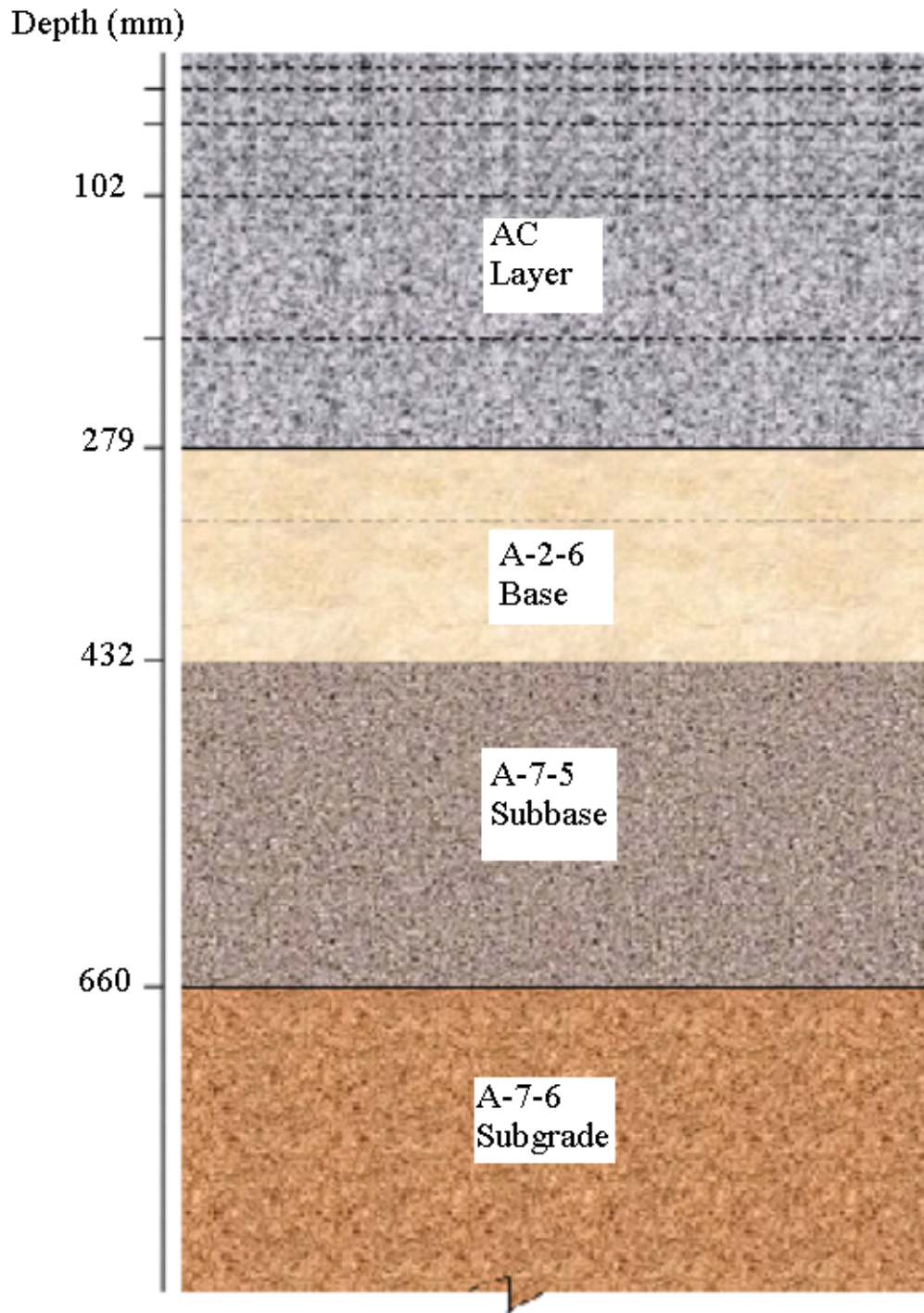
Figure 2.4, Sublayering of the flexible pavement example

Modulus of Elasticity (MPa)
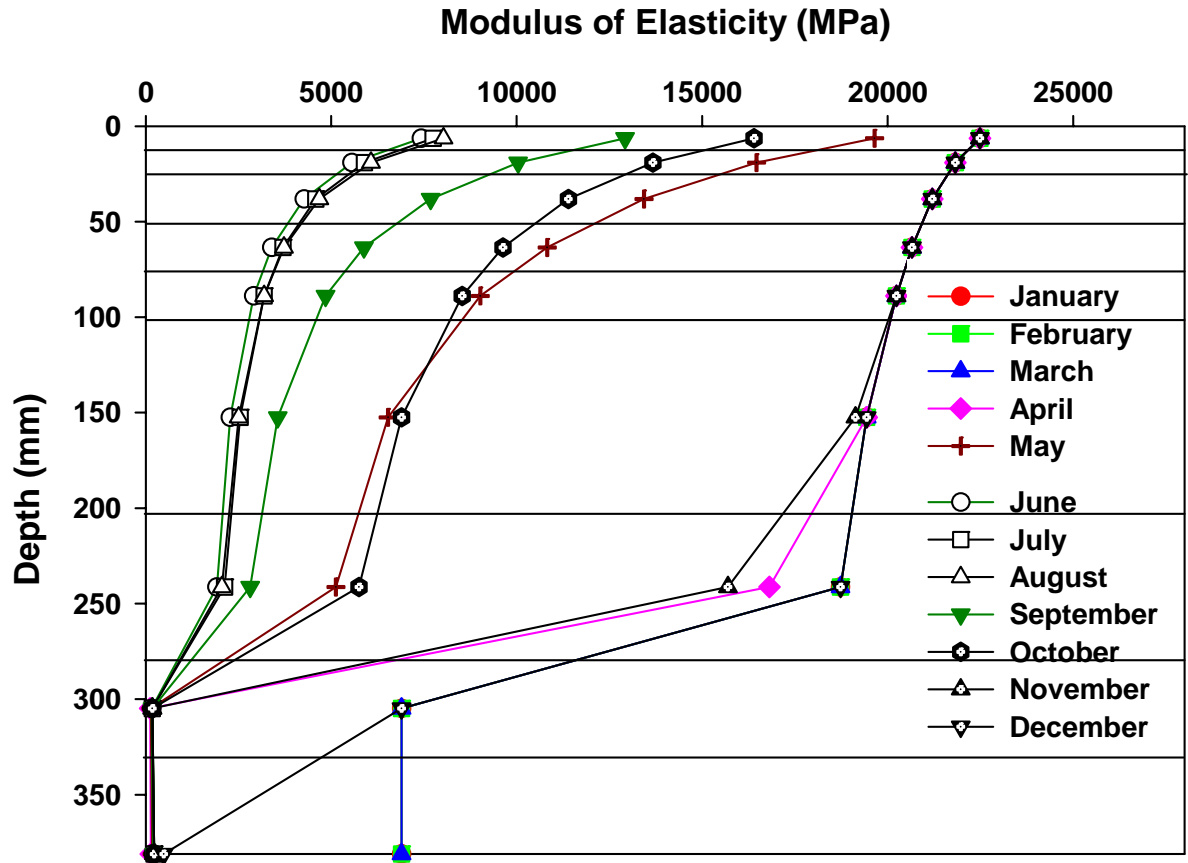
Figure 2.5, Resilient modulus vs. depth.

As can be seen from Figure 2.5, averaging the resilient modulus within the top layers based on values of one month might not be appropriate since the difference in the average monthly resilient modulus between two consecutive sublayers within the AC layer can be up to 38%. As expected, the difference in the average monthly resilient modulus between two consecutive sublayers within the base and subbase is slightly affected by the temperature variation while the difference in the subgrade layer was up to 200%. The influence of the moisture within the base, subbase and subgrade layers is larger than the influence of the temperature. However, moisture variation within the unbound layers is influenced in turn by the temperature variation.

Resilient modulus variation as a function of time within the asphalt concrete sublayers is shown in Figure 2.6. The figure shows that the temperature variation in the AC layer can reduce the maximum resilient modulus of the sublayer by a factor between 2 and 3. Therefore, averaging the modulus over a certain period of time or over the whole layer, such as the AC layer, might not be appropriate since the averaging might not capture the extreme temperatures and thus the extreme (high or low) resilient moduli.

Resilient moduli variations as a function of time within the base, subbase and subgrade sublayers are shown in Figure 2.7 and Figure 2.8. The figures show that the

temperature variation influence in the unbound layers decreases with depth. It should be noted that the temperature variation mainly influences the resilient modulus of the unbound materials within the frost depth. The figures show that the temperature variation can reduce the maximum resilient modulus, and therefore the bearing capacity, of the base and subbase layers by more than 95% during the year.
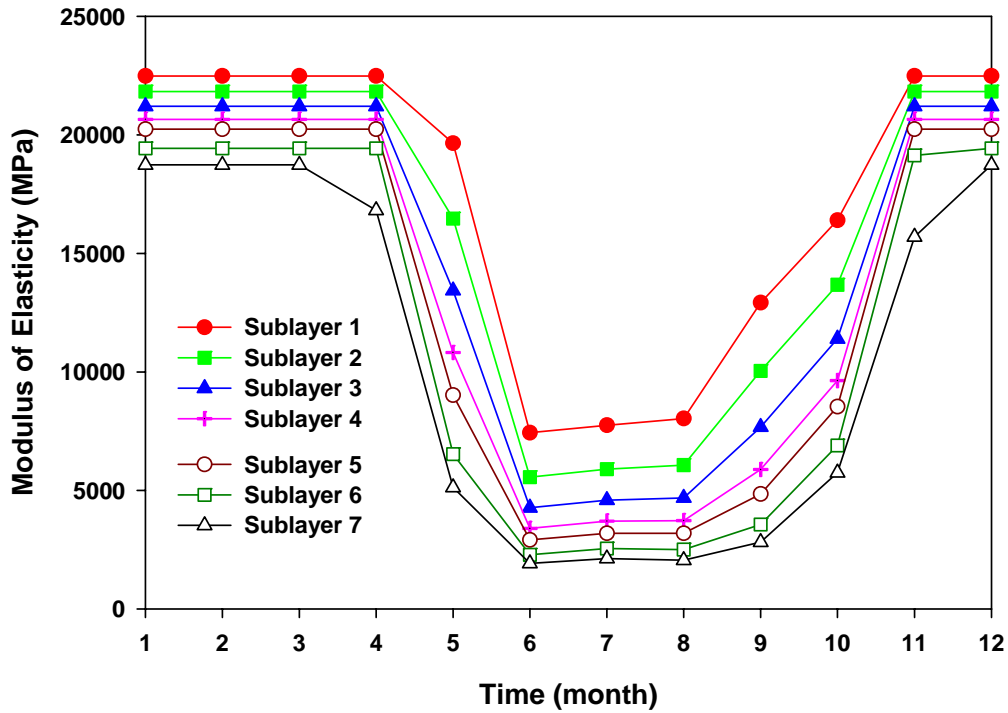
Figure 2.6, Resilient modulus vs. time in the AC sublayers
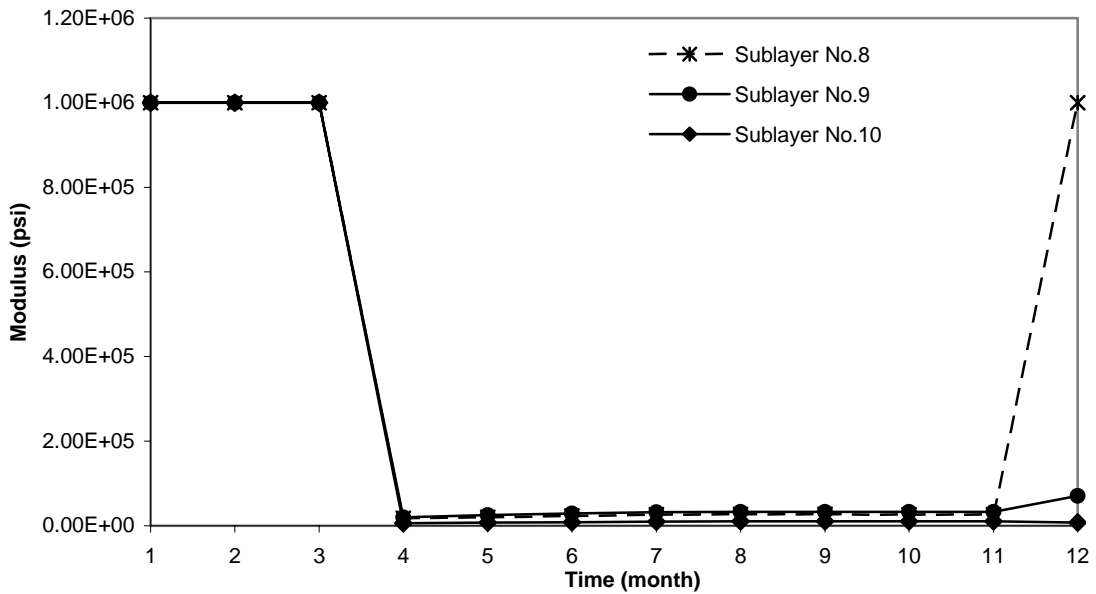
Figure 2.7, Resilient modulus vs. time in the base and subbase sublayers
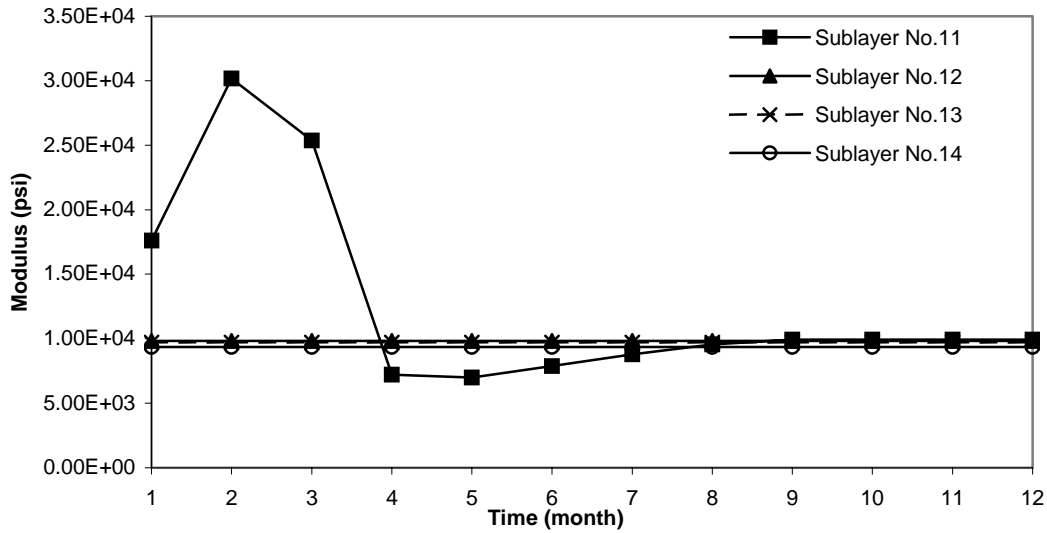
Figure 2.8, Resilient modulus vs. time in the subgrade layers

2.1.2 SEASONAL POISSON'S RATIO VARIATION

The MEPGD (2004) recommends the use of the following equation to estimate the Poisson's ratio due to the change in the resilient modulus of asphalt as a result of temperature changes.

$$\nu = 0.15 + \frac{0.35}{1 + e^{(-1.63 + 3.84x10^{-6} E)}}$$

Eq. (2.3)

where

ν : Poisson's ratio of asphalt mixture at a specific temperature.
E : Resilient modulus of asphalt mixture at a specific temperature, psi.

Figures 2.9 and 2.10 show the variation of the Poisson's ratio with depth, in the asphalt concrete sublayers, during the year. These figures were created by using results and recommendations of MEPGD (2004) and Coree et al. (2005). The Poisson's ratio can vary significantly within the same layer (in sublayers) and during the year. In this example, the variation was up to 23% between two consecutive layers in Figure 2.9, while in Figure 2.10 the maximum Poisson's ratio of one sublayer was approximately 2.4 times the minimum Poisson's ratio for the same layer during the year.
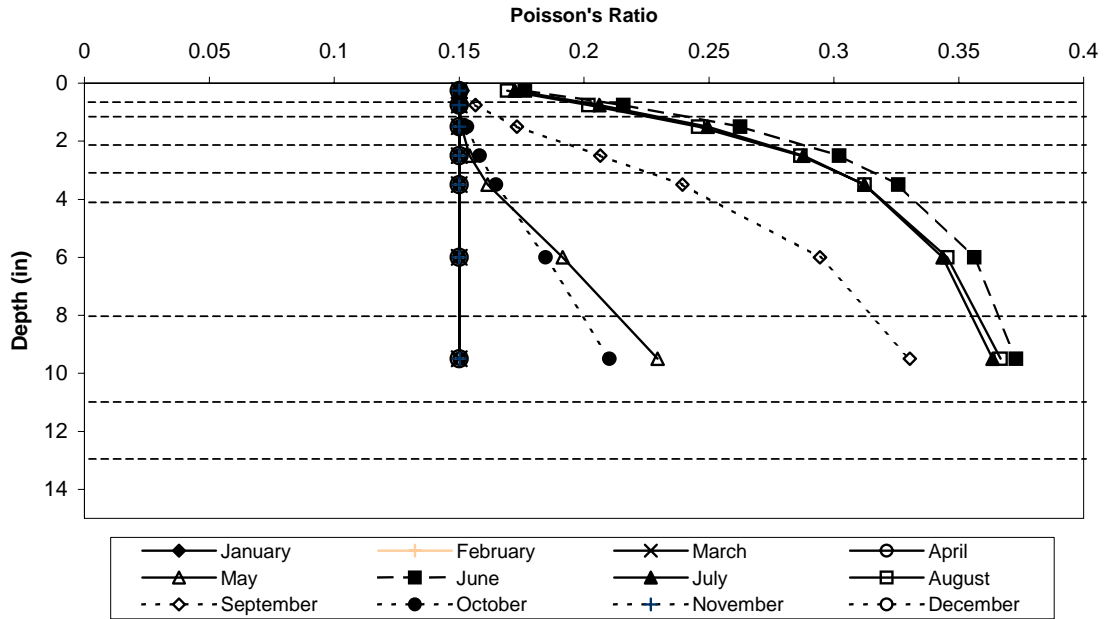
Figure 2.9, Poisson's ratio vs. depth in the AC sublayers
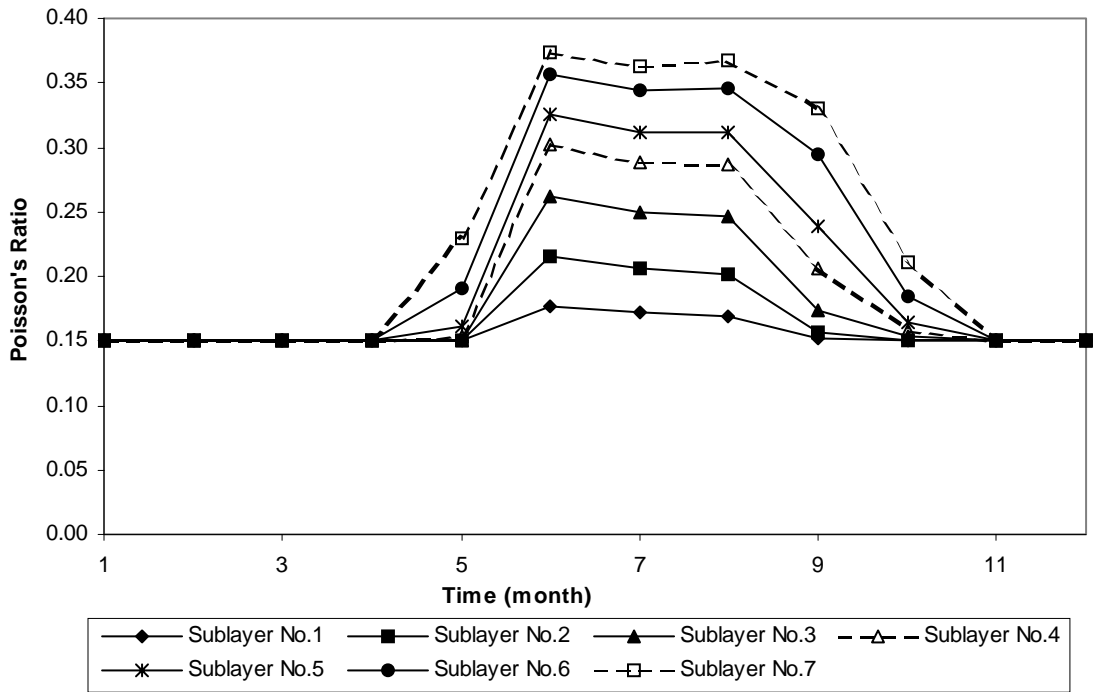
Figure 2.10, Poisson's ratio vs. time in the AC sublayers

24

2.2 TEMPERATURE VARIATION

Temperature variation within the pavement profile is monitored with field data acquisition systems as part of the Long Term Pavement Performance (LTPP) program administered and funded by the Federal Highway Administration. The collected data provided a wealth of information to the engineering community that helped in more specific state pavement-temperature studies rather than more generalized correlations or recommendations.

Seasonal and daily variation of the temperature should be addressed in any pavement analysis method since variations are largely influenced by the geographical location of the site and the environmental conditions of the pavement. The geographical location of the site can influence the freezing and thawing period and temperature gradient with time along the surface of the pavement.

Scrivner et *al.* (1969) proposed four different periods for seasonal variations in pavement based on temperature along the pavement profile and Dynaflect deflection measurements from a total of 24 sections located in Illinois and Minnesota states. The four proposed pavement-temperature periods are:

(1) Deep frost and high strength period.
(2) Rapid strength loss period.
(3) Rapid strength recovery period.
(4) Slow strength recovery period.

The proposed pavement-temperature periods show that the pavement undergoes different cycles of strength loss and recovery and therefore the selection of one representative resilient modulus is challenging. Averaging the resilient modulus based on daily, weekly or monthly records might be among the common approaches to deal with the temperature variations in the pavement during the year and a way to simplify the temperature variation.

2.2.1 PAVEMENT TEMPERATURE VARIATION

Barker et *al.* (1977) proposed the following equations to estimate the average temperature in the upper part of the asphalt layer based on air temperature:

$$T_{asphalt} = 1.2 * T_{air} + 3.2$$ Eq. (2.4)

where T is the temperature in ˚C

$$T_{asphalt} = 1.19 * T_{air}$$ Eq. (2.5)

where T is the temperature in ˚F

The above equations simplify the actual temperature variation assuming that the temperature variation in the pavement has a linear relation with the air temperature.

Another equation that estimates the mean weekly air temperature is given below (Edwards and Valkering, 1974; Ullidtz, 1987):

$$T = \frac{(T_1 + T_2)}{2} + \frac{(T_1 - T_2)}{2} \cos\left(\frac{(U - U_O)}{26} * \pi\right) \qquad \text{Eq. (2.6)}$$

where T is the mean weekly temperature (˚C or ˚F), T_1 is the maximum weekly air temperature during the year (˚C or ˚F), T_2 is the minimum weekly air temperature during the year (˚C or ˚F), U is the week number counted from new year, and U_O is the week number corresponding to the maximum temperature (T_1).

Another simplified relation was proposed by George and Husain (1986):

$$T_{asp} = T_{air}\left(1 + \frac{76.2}{h_{asp} + 304.8}\right) - \frac{84.7}{h_{asp} + 304.8} + 3.3 \qquad \text{Eq. (2.7)}$$

where

T_{asp}: Surface layer temperature (˚C)
T_{air}: Mean air temperature (˚C)
h_{asp}: Thickness of the surface layer (mm)

It can be seen from the above equations that the relation between the pavement temperature and the air temperature can be linear or nonlinear. In addition, it can be seen that temperatures within the pavement profile are higher than air temperatures above the pavement.

Baltzer and Jansen (1994) back calculated the resilient modulus of asphalt layers taking into account temperature variation of the layer. They recommended that the mean temperature of the asphalt layer be determined based on the temperature value at one-third of the asphalt thickness. Therefore, it can be concluded that most of the pavement response is based on the stiffness of the material within the top one-third of the pavement which is taken as the mean or average stiffness of the asphalt layer. However, this conclusion might be affected by the asphalt thickness and other climatic conditions that did not exist in the testing section.

More advanced temperature models for asphalt pavements were proposed by Lukanen et al (2000). The new models are non-linear and show good agreement with temperatures at one-third and one-half of the pavement depth. These models are named BELLS, BELLS2 and BELLS3, and are presented below:

BELLS equation:
$$T_d = 2.8 + 0.894 * IR + \{\log_{10}(d) - 1.5\}\{-0.54 * IR + 0.770 * (5 - day) + 3.763 * \sin(hr - 18)\} + \{\sin(hr - 14)\}\{0.474 + 0.031 * IR\}$$

BELLS2 equation:
$$T_d = 2.78 + 0.912 * IR + \{\log_{10}(d) - 1.25\}\{-0.428 * IR + 0.553 * (1 - day) + 2.63 * \sin(hr_{18} - 15.5)\}$$
$$+ 0.027 * IR * \sin(hr_{18} - 13.5)$$

BELLS3 equation:
$$T_d = 0.95 + 0.892 * IR + \{\log_{10}(d) - 1.25\}\{-0.448 * IR + 0.621 * (1 - day) + 1.83 * \sin(hr_{18} - 15.5)\}$$
$$+ 0.042 * IR * \sin(hr_{18} - 13.5)$$

where
T_d : Pavement temperature at depth (d), ˚C

IR : Infrared surface temperature, ˚C
d: depth at which material temperature to be predicted, mm
5-day: Previous mean 5-day air temperature, ˚C
1-day: Average air temperature the day before, ˚C
sin: sine function on a 24-hr clock system, with 2π radians equal to one 24-hour cycle (BELLS equation)
sin: sine function on an 18-hr clock system, with 2π radians equal to one 18-hour cycle (BELLS2 and BELLS3 equations)
hr: time of day in 24-hr system
hr_{18}: time of day, in 24-hr system, but calculated using an 18-hr asphalt concrete (AC) temperature rise- and fall-time cycle

The differences between these models are summarized below:
1-The BELLS model uses the previous mean 5-day air temperature and the 24-hr clock system (cycle).
2-The BELLS2 model uses the previous mean 1-day air temperature and the 18-hr clock system (cycle).
3-The BELLS3 model uses the previous mean 1-day air temperature and the 18-hr clock system (cycle). This model is a modification of the BELLS2 model with surface observation data adjusted to account for the sky cover or shade.

The BELLS model is not recommended since it was based on faulty infrared temperature gauges used during data collection which caused overestimation of temperatures at low asphalt temperatures and underestimation of temperatures at high asphalt temperatures. The BELLS2 model was found to overestimate high temperatures and underestimate low temperatures at mid-depth while it gave close results to field measurements for temperatures at one-third depth when compared to database temperatures predicted by Enhanced Integrated Climate Model (EICM) (Ongel and Harvey, 2004). However, the BELLS2 model is widely used to estimate temperatures in flexible pavements in the LTPP sections for back-calculation of the elastic moduli (Lukanen et. *al.*, 2000).

Based on the EICM model, the following equations were proposed for thick asphalt concrete layers (406.4-, 558.8-, and 711.2-mm thick AC)(Ongel and Harvey, 2004):

for pavement surface to quarter-depth thermal gradient:

$$TQ = -41.7 + 2.08 * T - 1.47 * t + 19.5 \left[\sin(hr - 10) * 2 * \frac{\pi}{24} \right]$$ Eq. (2.8)

for pavement quarter-depth to mid-depth thermal gradient:

$$TQ = -46.1 + 2.278 * T + 67 * t + 16.18 \left[\sin(hr - 10) * 2 * \frac{\pi}{24} \right] - 3.146 * T * t$$ Eq. (2.9)

where

TQ: Thermal gradient from top to mid-depth, (°C/m)
T: Surface temperature, °C
t: Thickness, m
hr: time of day, in 24-hour format

Ovik et. *al.* (1999) proposed the following equation using the thermal diffusivity:

$$T(x,t) = T_{mean} + A e^{-x\sqrt{\frac{2\pi}{P\alpha}}} \sin\left(\frac{2\pi}{P}(t) - x\sqrt{\frac{2\pi}{P\alpha}} \right)$$ Eq. (2.10)

where

T(x,t): Soil temperature as a function of depth and time, °C
x: depth, m
T_{mean}: Average temperature at surface, °C
A: Maximum temperature amplitude (T_{max}-T_{mean}, °C)
P: period or recurrence cycle
α : Thermal diffusivity, area/time
t: Time measured from when the surface temperature passes through T_{mean}, (days)

The above models demonstrate the variation of pavement-temperature modeling based on the depth within the pavement structure. Most of the available models consider the mid-depth as the reference point for temperature averaging for simplicity while more complex models consider the one-third depth. The temperature variation within the pavement depends on the pavement thickness, layer material, and other environmental and climatic factors. Field data presented by Ongel and Harvey (2004) showed that thin AC layers do not have large temperature differences between the top and bottom of the layer while thick AC layers have significant temperature differences only between the surface of the AC pavement and mid-depth. On the other hand, the results by Cho et *al.* (1998) showed that temperature variation within flexible pavement layers is dependent on the layer material and the sequence of the pavement layering above the unbound material.

2.2.2 PAVEMENT MODULUS VARIATION

Several researchers proposed simplified equations to estimate the resilient modulus as a function of temperature based on lab and/or field-testing.
Ullidtz (1987) proposed the following equation to estimate the resilient modulus of asphalt concrete with temperatures between 0 ˚C and 40 ˚C:

$$E = 15,000 - 7900 \log(T)$$
Eq. (2.11)

where

E: Asphalt concrete modulus (MPa)
T: Pavement temperature, (˚C)

Witczak (1989) proposed the following equation:

$$E = 10^{(6.53658-0.006447*T-0.00007404*T^2)}$$
Eq. (2.12)

where

E: Asphalt concrete modulus (psi)
T: Pavement temperature, (˚F)

Janoo and Berg (1991) proposed the following equation based on backcalculation of asphalt concrete modulus during a thaw cycle:

$$E = 5994 - 242*T$$
Eq. (2.13)

where

E: Asphalt concrete modulus (MPa)
T: Pavement temperature, (˚C)

Ali and Lopez (1999) proposed the following equation to estimate the asphalt concrete modulus when the asphalt layer temperature is known at a depth of 25 mm below the surface:

$$E = e^{(9.37196-0.03608145*T)}$$
Eq. (2.14)

where

E: Asphalt concrete modulus (MPa), T: Temperature at a depth of 25 mm in the asphalt layer(˚C).

2.3 PAVEMENT RESPONSE TO TEMPERATURE

Flexible pavements are mainly made of asphalt concrete which is a visco-elastic material. The response of viscoealstic materials is highly dependent on the temperature, time and rate of loading. The stiffness of asphalt at very cold temperatures is close to that of PCC while its stiffness at relatively high temperatures is closer to an unbound material (MEPDG, 2004).

Climatic factors that affect the pavement-temperature response include wind speed, precipitation, air temperature, solar radiation, and pavement absorptivity and emissivity. Air temperature and sun radiation are the main sources of temperature for pavement structures and surficial soils. Heat transfer from the surface of the pavement to the underlying layers is influenced by the color of the surface. During cold seasons, temperatures below the surface of black pavement surfaces are higher than those below surfaces covered by snow. The geographic location of the pavement structure affects the temperature gradient of the pavement structure.

Pavement temperature in high temperature regions is affected by the solar radiation and pavement absorptivity and emissivity more than in cold temperature regions causing pavement surface temperature to increase more noticeably in flexible pavements (Ongel and Harvey, 2004).

Due to temperature gradient variation during the year, flexible pavement structures are more susceptible to rutting, distress, and fatigue. Rutting is more noticeable in high temperature seasons due to the elevated temperature of the pavement which in turn causes lower stiffness values in the elastic layers of the pavement and higher deformations. Fatigue of the flexible pavements is influenced by the pavement temperature and repeated loading of the pavement structure. Therefore, under the same repetitive loading conditions, fatigue of thick pavement structures is critical in high temperature seasons while fatigue of thin pavement structures is more critical in cold temperature seasons. This behavior is attributed to quick stress relaxation of the tensile stresses in the pavement at high temperatures and the slow stress relaxation at low temperatures.

Surface cracking of thick flexible pavements can be attributed to age hardening of the surface bitumen. Excessive aging due to high temperatures during high temperature seasons reduces the capacity of the top section of the flexible pavement to withstand thermal stresses (Read and Whiteoak, 2003). Pavements in high temperature regions may exhibit accelerated aging resulting in a viscosity 30 times the laying viscosity after 15 years only (Rolt, 2000).

Unbound materials can lose their bearing capacity during spring thaw causing cracks in the overlying pavement layers. Temperature variation of the unbound material is highly influenced by the frost penetration depth and moisture content of the soil. Temperature gradient within the frost penetration depth is affected by the material type and physical characteristics and freeze-thaw cycles. The resilient modulus of unbound

materials during the thawing process can be 15% to 50% less than the optimum resilient modulus (MEPDG, 2004).

2.4 TEMPERATURE VARIATION IN OHIO

Temperature variation models were developed in the past based on the lab testing which mostly does not resemble the actual working and environmental conditions of the pavement. The MEPDG adopts a semi-empirical equation that can estimate the resilient modulus for a wide range of temperatures and asphalt mix conditions. However, inputs for such equations either require some assumptions or lab testing (especially when no design or historical data available), and can be appropriately applied to predict the design mix behavior.

2.4.1 PAVEMENT MATERIAL EQUATIONS

Over the last two decades, several researches in Ohio were carried out to investigate the pavement behavior under working and environmental conditions at different roadway sections. Some of the available results will be summarized in this section.

2.4.1.1 ASPHALT CONCRETE

AC Poisson's Ratio (μ)

Masada and Sargand (2002) measured the Poisson's ratio of asphalt concrete core samples obtained from the Ohio-SHRP Test Road (Rt. 23). The obtained samples were tested at different temperatures and showed the following results:

Poisson's Ratio (v) = 0.14 at 5 °C (41 °F)

Poisson's Ratio (v) = 0.35 at 25 °C (77 °F)

Poisson's Ratio (v) = 0.48 at 40 °C (104 °F)

Masada et. al (2004) recommended the use of the following equation to estimate the Poisson's ratio for asphalt concrete in Ohio as a function of temperature:

$$v = - 0.00004*T^2 + 0.012*T - 0.2837 \qquad \text{Eq. (2.15)}$$

where T: is the pavement temperature, (°F)

AC Resilient Modulus

Asphalt concrete modulus was investigated by several researchers (Sargand et *al.* (1991), Abdulshafi et *al.* (1994), Liang (1997), Liang (2001), Masada & Sargand (2002), Sargand Edwards (2002), Figueroa. (2003), and Masada et *al.* (2004)).

Figueroa (2003) proposed the following equations to estimate the resilient modulus for ODOT Item 402 & 404 asphalt concrete specimens as a function of temperature:

for Item 404 (Surface)
$$E = 0.000257*T^2 - 0.0611*T + 3.5405 \qquad \text{Eq. (2.16)}$$

for Item 402 (Intermediate)
$$E = 0.000173*T^2 - 0.0487*T + 3.1164 \qquad \text{Eq. (2.17)}$$

where

E: Resilient modulus, (million psi)

T = temperature (°F)

Masada et *al.* (2004) compiled all results obtained in Ohio for AC and proposed the following equation for the resilient modulus as a function of pavement temperature:
$$E = 0.0001*T^2 - 0.0375*T + 2.8405 \qquad \text{Eq. (2.18)}$$
Where

E: Resilient modulus, (million psi)

T = temperature (°F)

A comparison between the different equations that were mentioned previously to estimate the modulus of elasticity in the AC layer based on the pavement temperature and resilient modulus-temperature equations developed by Figueroa (2003) and Masada et *al.* (2004) is shown in Figure 2.11. As can be seen, the resilient modulus is highly dependent on the pavement temperature and therefore a more sophisticated model which can capture the detailed variation of the modulus of elasticity with depth (say due to pavement temperature variation) should be used.
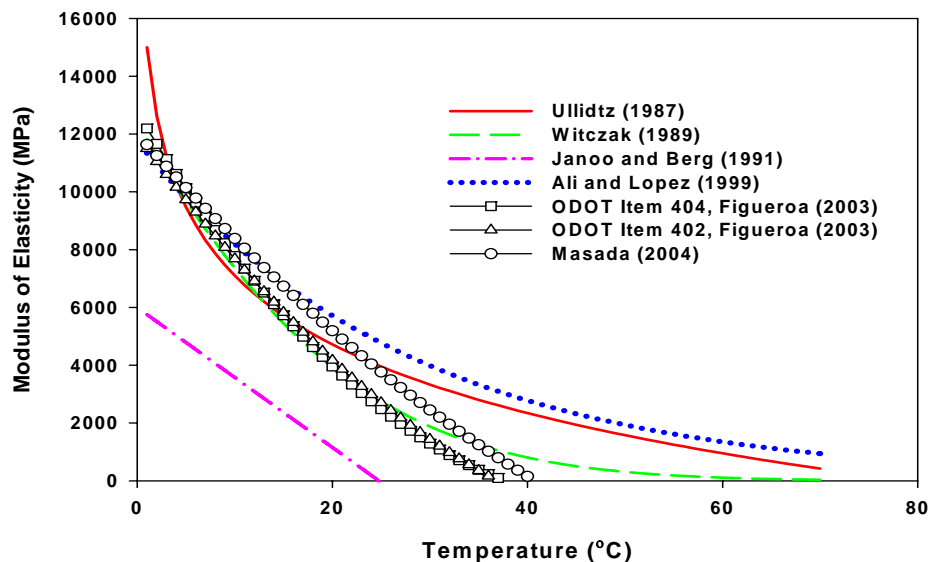
Figure 2.11, Resilient modulus vs. temperature

2.4.1.2 BASE/SUBBASE

Poisson's Ratio (v)

The recommended Poisson's ratio for untreated base and subbase layers in Ohio is reported to be 0.35 (Masada et *al.*, 2004). For cement-treated and lean concrete base/subbase Masada et *al.* (2004) recommended a Poisson's ratio of 0.15, while for asphalt-treated base/subbase layers they proposed the following:

Poisson's Ratio (v) = 0.1 at 5 °C (41 °F)

Poisson's Ratio (v) = 0.35 at 25 °C (77 °F)

Poisson's Ratio (v) = 0.5 at 40 °C (104 °F)

Masada et *al.* (2004) proposed the following equation to estimate the asphalt-treated base/subbase Poisson's ratio as a function of temperature:

$$v = 0.00004*(T^2 + T) + 0.0345 \qquad \text{Eq. (2.19)}$$

where

T = temperature (°F)

Resilient Modulus

Figueroa (2003) proposed the following equation to estimate the resilient modulus of asphalt-treated base/subbase (ODOT Item 301) as a function of the pavement temperature:

$$E = 3.0827*T^2 - 243.47*T + 5332.6 \qquad \text{Eq. (2.20)}$$

where

E: Resilient Modulus, (MPa)
T: Temperature, (°C)

Masada et *al.* (2004) proposed the following equation to estimate the asphalt-treated base/subbase as a function of pavement temperature:

$$E = 0.00005*T^2 - 0.0116*T + 1.2627 \qquad \text{Eq. (2.21)}$$

where

E: Resilient modulus, (million psi)

T = temperature (°F)

2.4.1.3 PERMEABLE ASPHALT-TREATED BASE/SUBBASE (PATB)

Figueroa (2003) proposed the following equations to estimate the resilient modulus as a function of pavement temperature for PATB (ODOT Item 302):

$$E = 0.00005 * T^2 - 0.0117 * T + 0.7481 \qquad \text{Eq. (2.22)}$$

where

E: Resilient modulus, (million psi)

T = temperature (°F)

$$E = 1.3071 * T^2 - 109.5 * T + 3118.4 \qquad \text{Eq. (2.23)}$$

E: Resilient Modulus, (MPa), T: Temperature, (°C)

2.4.2 RESILIENT MODULUS VS. TEMPERATURE

Figueroa (2003) studied the asphalt concrete temperature at different locations in Ohio. Based on the temperature and weather variations, he divided the state into three regions as shown in Figure 2.12. Temperature values in these regions are shown in Figure 2.13.
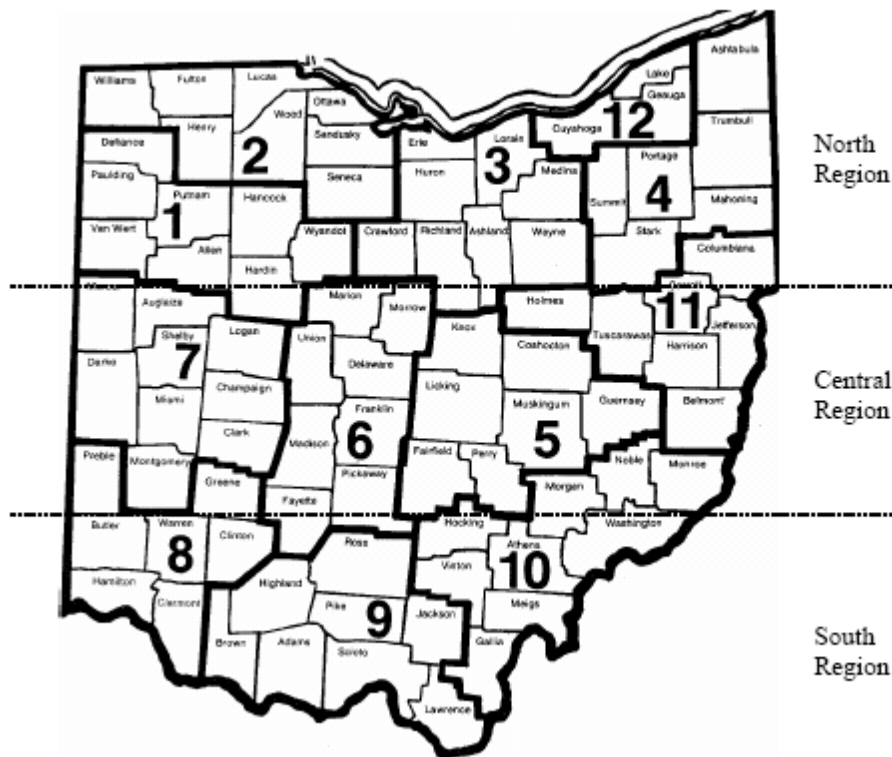
Figure 2.12, Temperature regions in Ohio (Figueroa, 2003).
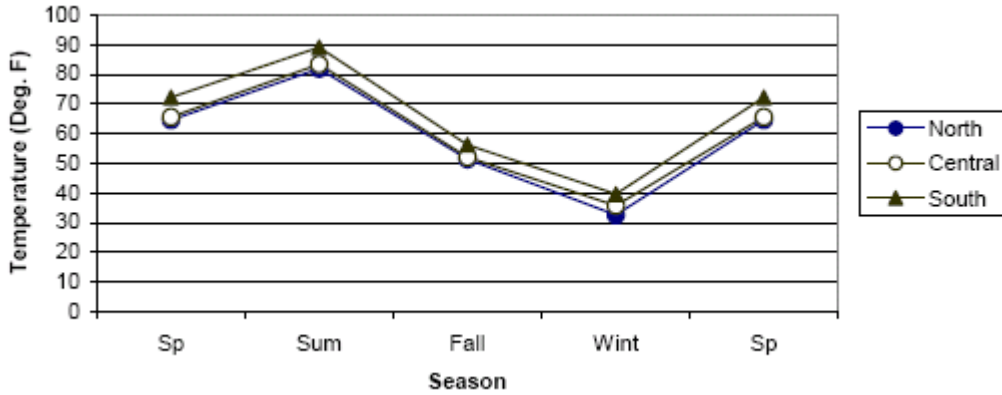
Figure 2.13, Temperature variation in AC pavements in Ohio (Figueroa, 2003).

2.4.3 POISSON'S RATIO VS. TEMPERATURE

Figure 2.14 shows the significance of the Poisson's ratio variation of the asphalt concrete layer during the year based on average asphalt pavement temperatures. This figure was created by combining the results and recommendations from Figueroa (2003) and Masada et al (2004). The figure shows that the seasonal variation can reduce the maximum Poisson's ratio by 87%, 77%, and 73% for the north, central, and south regions in Ohio, respectively. It can be seen that the lowest Poisson's ratio is observed in winter while the highest ratio is in summer, as expected.
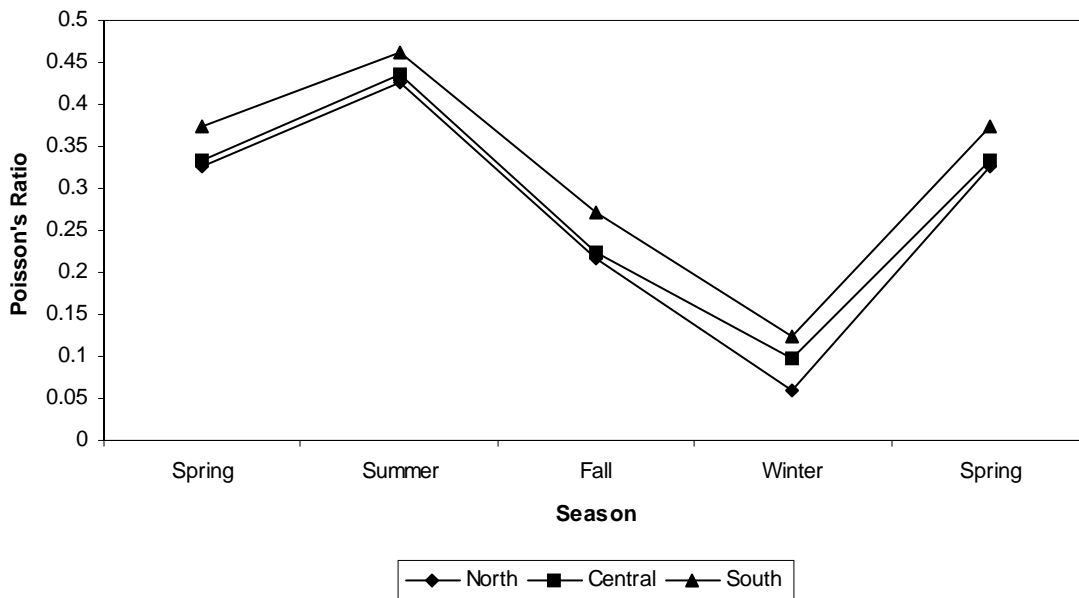
Figure 2.14, Poisson's ratio variation in Ohio.
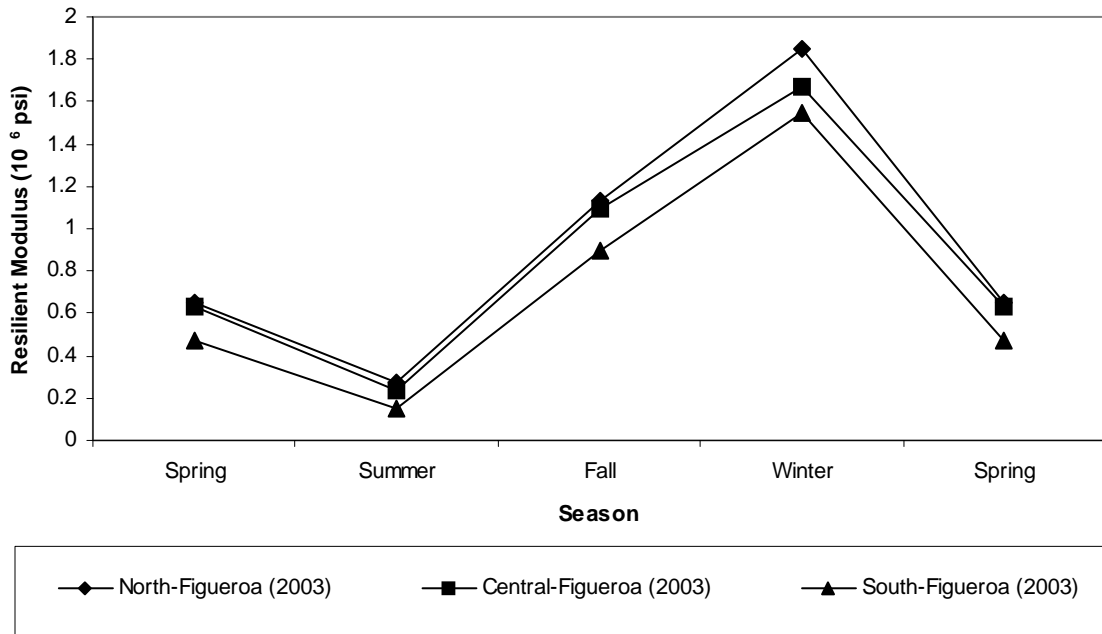
Figure 2.15, Resilient modulus variation of ODOT Item 404 (surface).
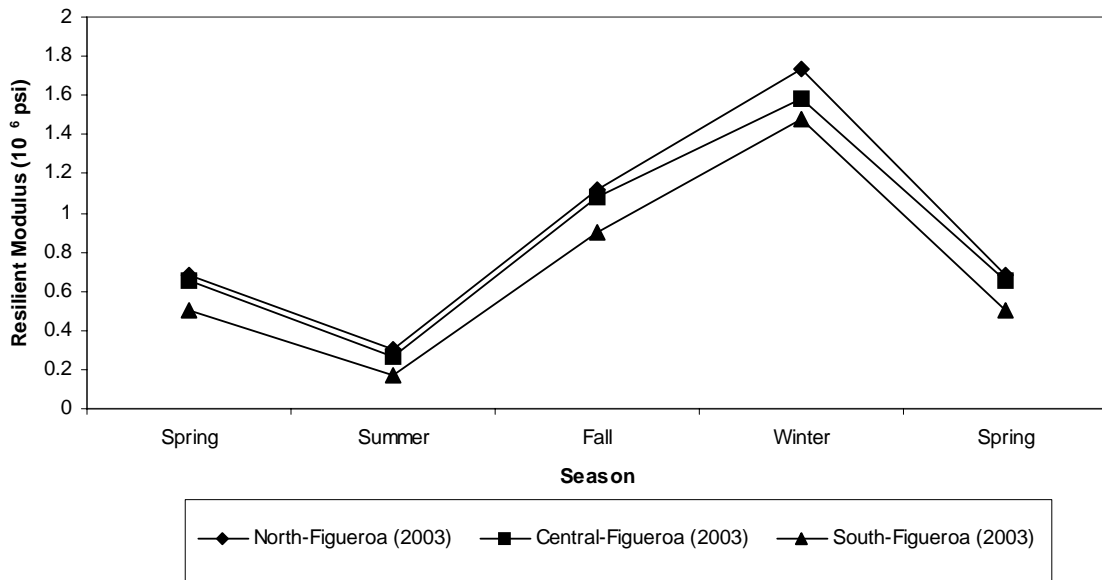
Figure 2.16, Resilient modulus variation of ODOT Item 402 (intermediate)
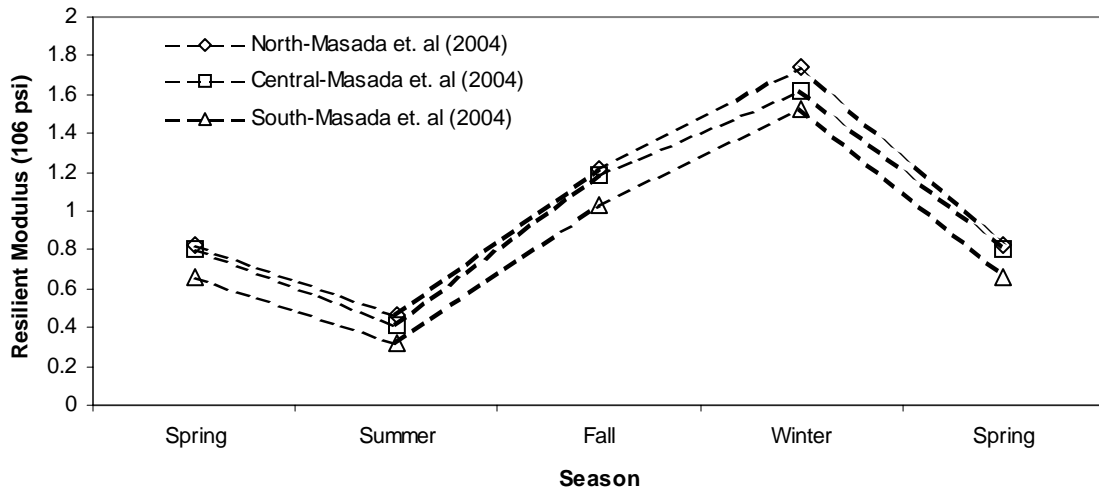
Figure 2.17, Resilient modulus variation of AC layers in Ohio

Figures 2.15 through 2.17 show the significance of the resilient modulus variation of ODOT Item 404 (Surface), ODOT Item 402, and asphalt concrete layers during the year based on average asphalt concrete pavement temperatures. These figures were created by combining the results and recommendations from Figueroa (2003) and Masada et *al.* (2004). The figures show that the reduction in the maximum resilient modulus can be between 74% and 90% in the three regions in Ohio. It can be seen that the lowest resilient modulus is observed in summer while the highest ratio is in winter, as expected.

2.5 DAILY TEMPERATURE VARIATION

Temperature gradient along the surface of the pavement varies with time during the day which in turn changes the temperature in the pavement section. For instance, temperature variation in a flexible pavement section in Los Angeles (Ongel and Harvey, 2004) is shown in Figure 2.18. It can be seen that the temperature variation in the AC layer is larger than the variation within the base, and subbase layers where the temperature gradient decreases as the depth increases. Therefore, assuming that this temperature distribution is for a pavement section in Ohio at a certain time, Equation 2.18 can be used to estimate the maximum, minimum, and average resilient moduli of the AC layer, respectively. The estimated average resilient modulus, based on this assumption, can be approximately 1.4 times the minimum resilient modulus and 0.6 times the maximum resilient modulus. Therefore, assuming an average temperature might be misleading during the design or analysis of the pavement section. On the other hand, since the temperature changes during the day, the pavement susceptibility to rutting and distresses (fatigue) changes as well.

Temperature variation in AC layers can be divided into two distinct variations. The first variation is characterized by temperature gradients that increase with depth which mainly can be observed when the surface of the pavement is colder than the

37

bottom; i.e. cold temperature seasons or during nights. The second variation is characterized by temperature gradients that decrease with depth which mainly can be observed when the surface of the pavement is warmer than the bottom of the pavement; i.e. warm temperature seasons or during the daylight. The temperature variation is influenced by the viscoelastic nature of the AC layer and the physical nature of the underlying layers. Again, variation of the temperature will result in the change of the resilient modulus, which in turn will influence the pavement response and performance.
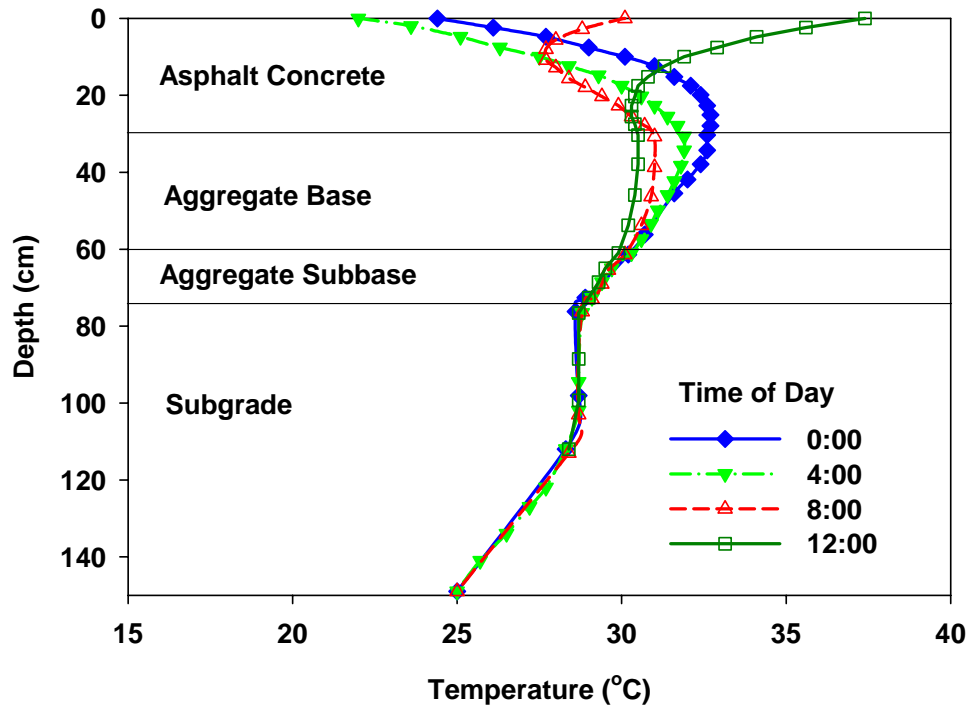
Figure 2.18, Daily temperature variation (modified from Ongel and Harvey, 2004).

2.6 RESILIENT MODULUS VARIATION EXAMPLE

Pavement responses due to the resilient modulus variation in the AC layer as a function of temperature can be better demonstrated by a numerical example. A flexible pavement section was analyzed using the *MultiSmart3D* program. The *MultiSmart3D* program is a fast and accurate software tool developed by the Computer Modeling and Simulation Group at the University of Akron, and is based on the innovative computational and mathematical techniques for multilayered elastic systems (e.g., Pan, 1989a,b, 1990, 1997). The program is capable of analyzing any pavement system regardless of the number of layers, the thickness of each layer, and the shape of the applied pressure at the surface of the pavement.

The analyzed pavement section was summarized in Table 2.1. The contact pressure at the surface of the pavement was assumed to be 690 kPa acting on a circle with a diameter of 220.3 mm. Pavement responses below the center of the contact pressure were estimated using the *MultiSmart3D* program. The used direction convention is shown in Figure 2.19.

38

Table 2.1, Parameters for the flexible pavement example

Layer	Thickness (cm)	Resilient Modulus (MPa)	Poisson's Ratio
AC Layer	15	3500	0.3
Base Layer	25	700	0.3
Subbase Layer	25	300	0.3
Subgrade Layer	Infinite Space	100	0.3
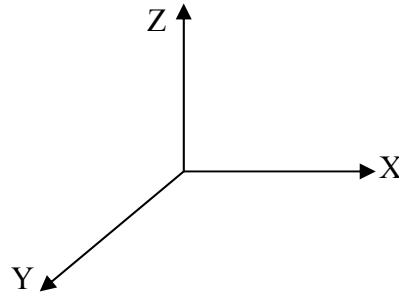
Figure 2.19, Direction convention in the *MultiSmart3D* program

Five different cases were analyzed to study the resilient modulus variation. The cases are presented in Figure 2.20 and summarized below:

Case 1: The resilient modulus was assumed to be constant in the AC layer with a value of 3500 MPa. The AC layer was modeled using the entire thickness. This case serves as the reference case since it is the common case in practice among pavement engineers.

Case 2: The resilient modulus was varied in the AC layer only using 10 sublayers. The resilient modulus increased linearly from the top to the bottom of the AC layer with an average value of 3500 MPa.

Case 3: The resilient modulus was varied in the AC layer only using 20 sublayers. The resilient modulus decreased linearly from the top to the bottom of the AC layer with an average value of 3500 MPa.

Case 4: The resilient modulus was varied in the AC layer only using 10 sublayers. The resilient modulus increased quadratically from the top to the bottom of the AC layer with an average value of 3500 MPa.

Case 5: The resilient modulus was varied in the AC layer only using 20 sublayers. The resilient modulus decreased quadratically from the top to the bottom of the AC layer with an average value of 3500 MPa.
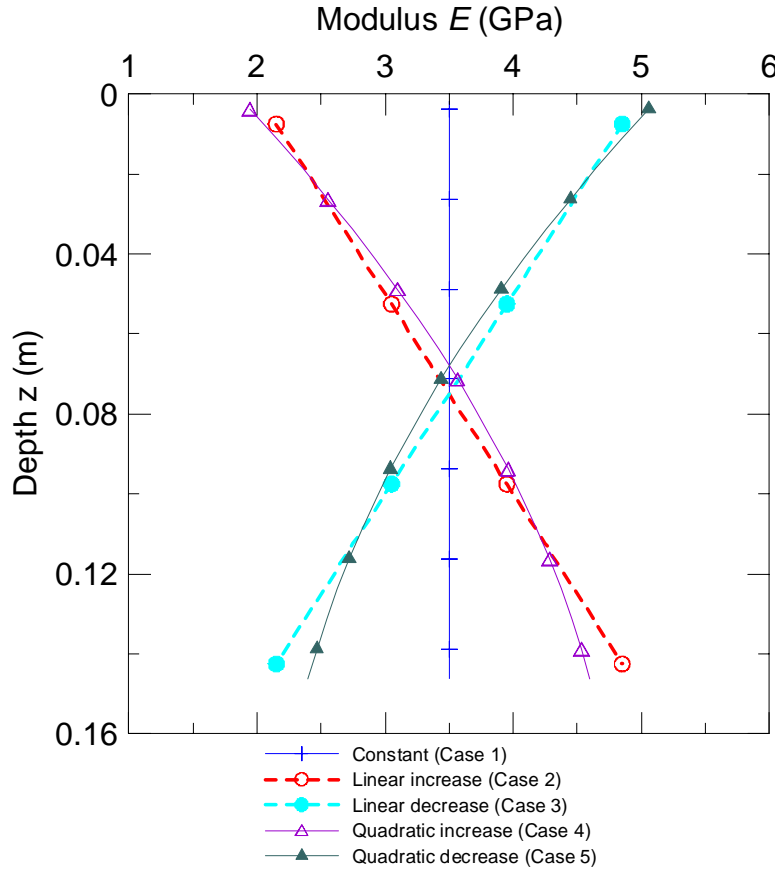
Figure 2.20, Modulus variation with depth

Vertical pavement displacements (u_z) are shown in Figure 2.21. It can be clearly seen from Figure 2.21c that Case 1 (constant modulus) underestimates the displacements in the entire AC layer as compared to Cases 2 and 4 (linear/quadratic increase), whilst it overestimates the displacements at the top and bottom as compared to Cases 3 and 5 (linear/quadratic decrease). It is further noticed that for the linear variation cases (Cases 2 and 3 in Figures 2.21a,b), using a small number of sublayers (e.g., 1, 2, 4) could result in a pavement response different to that due to the true linear variation of modulus. However, increasing the number of sublayers can improve the predicted displacements (i.e., for sublayer number=10 and 20 as in Figures 2.21a,b).
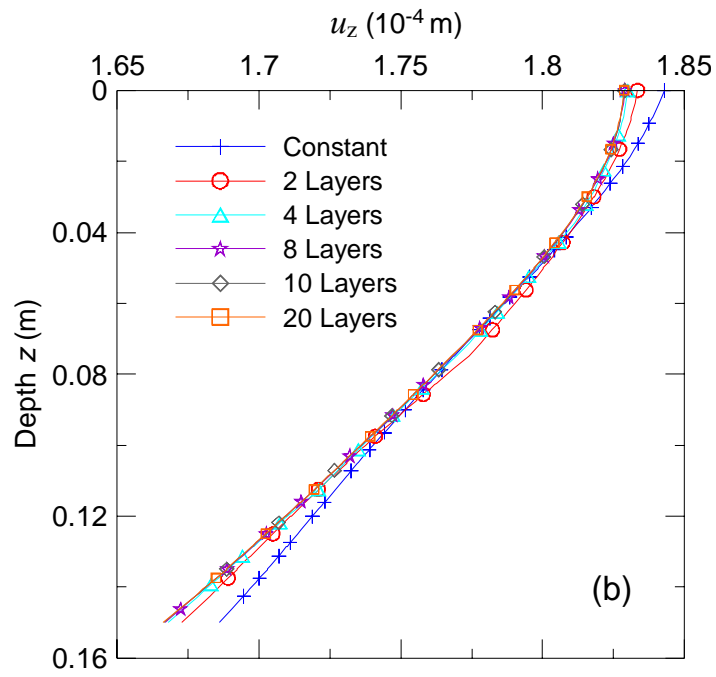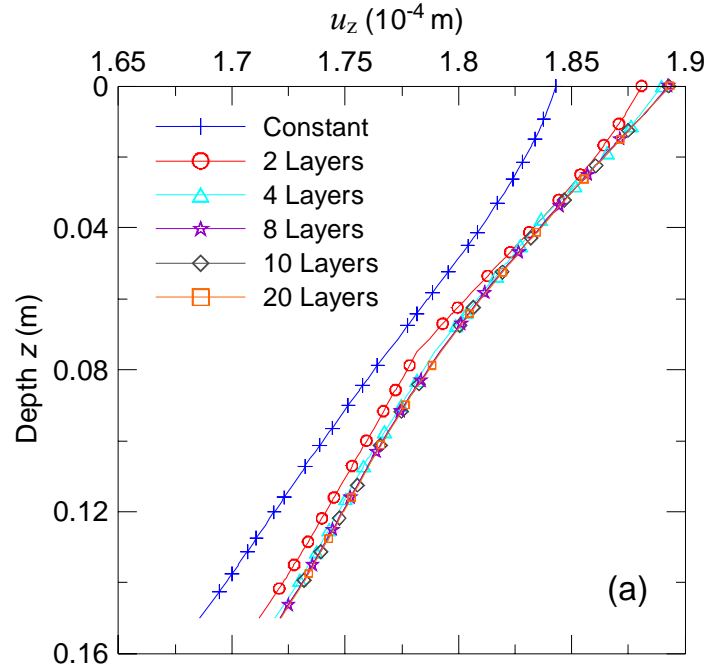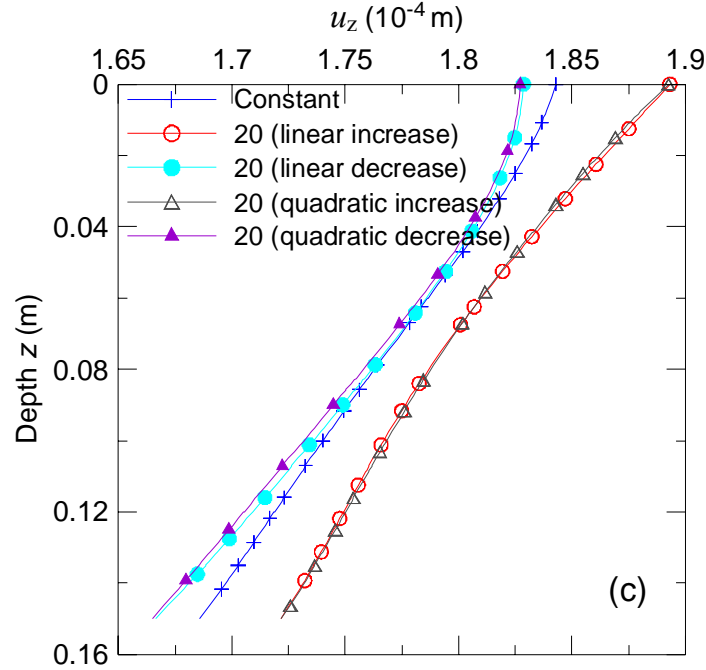
Figure 2.21, Variation of displacement u_z with depth for (a) Cases 1 and 2;
(b) Cases 1 and 3; (c) Cases 1, 2, 3, 4 and 5.

Figure 2.22 shows the variation of the horizontal normal stress in *x*-direction (σ_{xx}) for different modulus profiles in the AC sublayer. As can be seen in these figures, the effect of the number of sublayers is noticeable especially when the number is less than 8 sublayers and negligible when the number is larger than 8 sublayers (Figure 2.22a,b). The 20 sublayers case was shown to demonstrate the power of the ***MultiSmart3D*** program for more than 20 layers as compared to the current available programs which can consider only a maximum of 20 layers/sublayers (the total number of layers for the 20 sublayer case in our examples here is 23). On the other hand, it can be seen (Figure 2.22c) that the variation of the modulus with depth, in this example, largely controls the horizontal stress component. For example, using the average resilient modulus can underestimate the stress magnitude within the top and bottom 20% of the AC layer for Cases 3 and 5 (linear/quadratic decrease). The stresses were overestimated within the top and bottom 20% of the layer for Cases 2 and 4 (linear/quadratic increase). The stress magnitude between 20% and 80% of the layer thickness was underestimated for Cases 2 and 4 and overestimated for Cases 3 and 5. Stresses using Case 1 are approximately equal to the average of stresses from either Cases 2 and 3 or Cases 4 and 5. Due to symmetry, a similar behavior can be observed for the horizontal normal stress in *y*-direction. In addition, the stress jump between the adjacent sublayers can be clearly observed for the linear decrease Case 3 (Figure 2.22b).
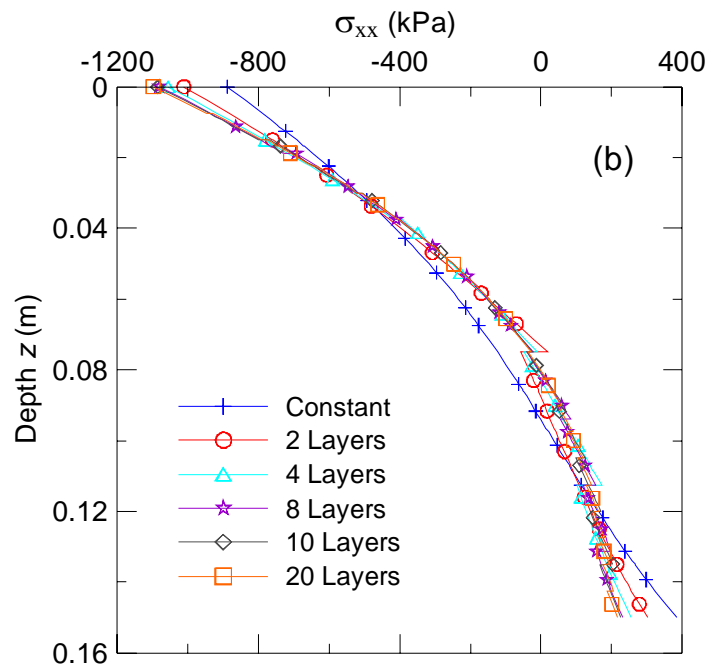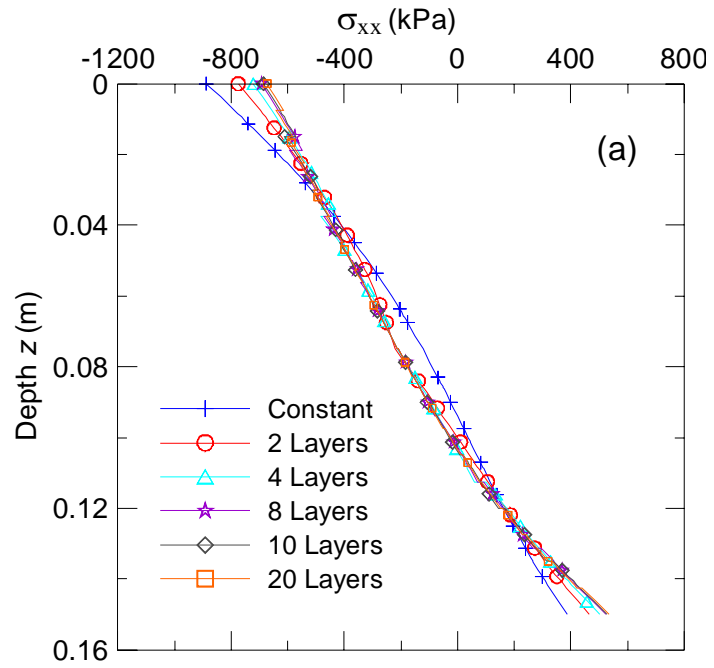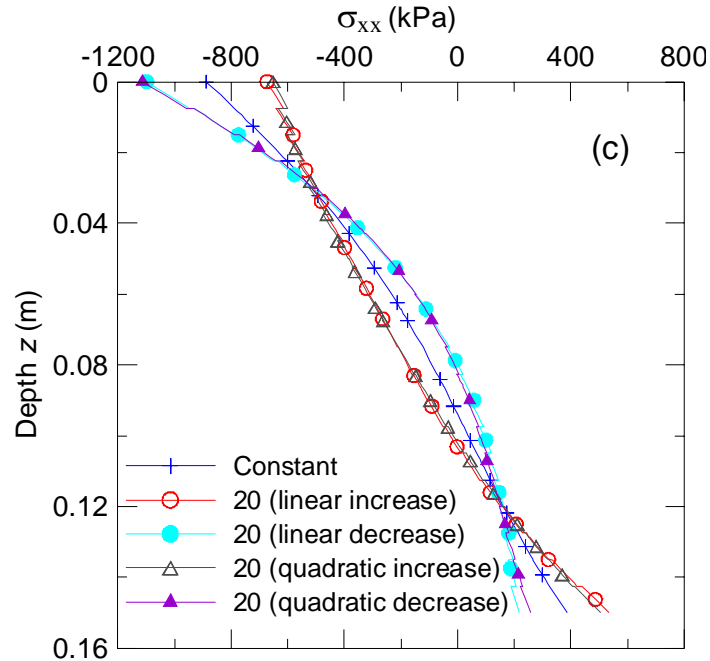
Figure 2.22, Variation of horizontal normal stress component σ_{xx} with depth for (a) Cases 1 and 2; (b) Cases 1 and 3; (c) Cases 1, 2, 3, 4 and 5.

The effect of different resilient modulus profiles on the vertical normal stress in z-direction (σ_{zz}) is shown in Figure 2.23. It is observed from Figure 2.23 that, compared to Figure 2.22 for horizontal stresses, the vertical stress is relatively insensitive to the different profiles used. It can be seen (Figure 2.23c) that using the average resilient modulus can underestimate the vertical stress magnitude for Cases 2 and 4 whilst it overestimate it for Cases 3 and 5. The difference between the stresses using Case 1 and those using other cases is more noticeable between 15% and 85% of the layer thickness (Figure 2.23c).

The effect of the resilient modulus profiles on the normal strain in x-direction (ε_{xx}) is shown in Figure 2.24. Similar to Figure 2.22 for vertical stress, it can be seen that using the average resilient modulus can either underestimate or overestimate slightly the strains (Figure 2.24c). The difference between the strains using Case 1 and those using other cases is more noticeable between 15% and 85% of the layer thickness. Due to symmetry, a similar behavior can be observed for the normal strain in y-direction.
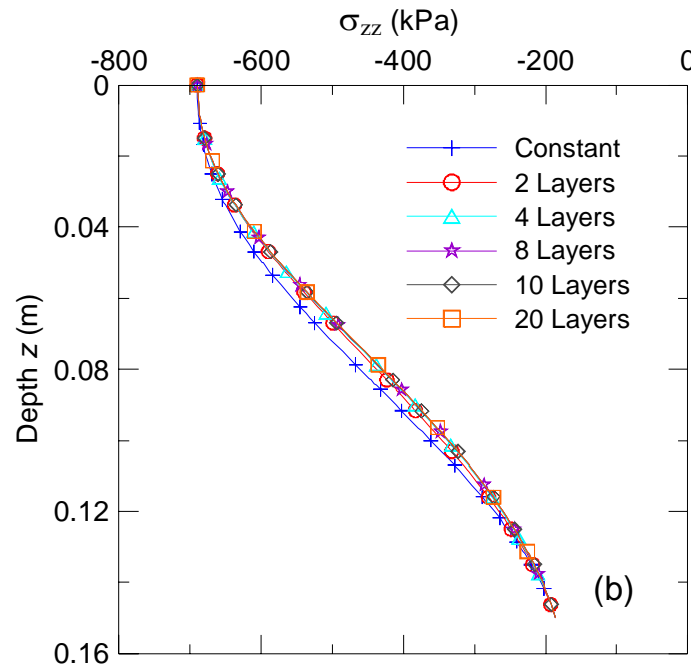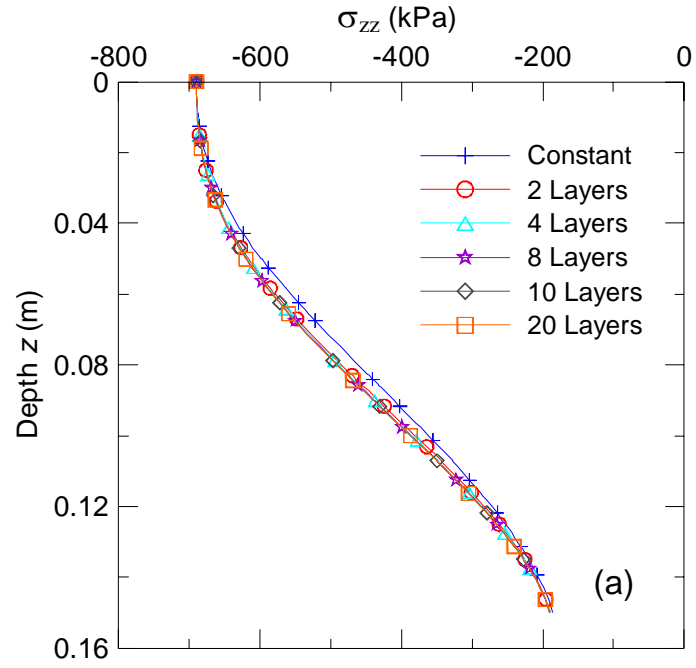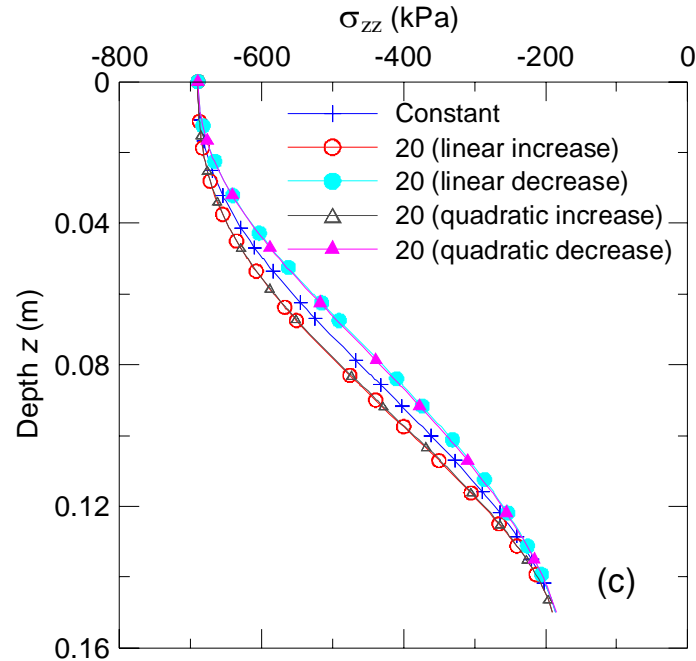
Figure 2.23, Variation of vertical normal stress component σ_{zz} with depth for (a)

Cases 1 and 2; (b) Cases 1 and 3; (c) Cases 1, 2, 3, 4 and 5.

Figure 2.25 shows the vertical strain variation (ε_{zz}) with depth below the center of the contact pressure. It can be seen that using the average resilient modulus can overestimate the strain magnitude within the top half of the AC layer whilst it can underestimate the strains within the bottom half for Cases 3 and 5 (Figure 2.25c). On the other hand, using the average resilient modulus can underestimate the strains within the top half of the AC layer whilst it can overestimate the strains within the bottom half for Cases 2 and 4 (Figure 2.25c). It is observed that the number of sublayers beyond four for Case 2 (Figure 2.25a,b for linear increase) could be enough for estimating the strain at the bottom of the AC layer whilst it showed a considerable difference near the top part of the AC layer (which requires at least 8 sublayers). An opposite trend is observed for the linear decrease case (Figure 2.25b). Therefore, the vertical strain component is very sensitive to the variation of the modulus profile and its value is highly dependent on the number of sublayers. Furthermore, just as for the horizontal stress case, one can also observe sharp jumps in the strain across the interface of the adjacent sublayers (Figure 2.25a, b).

46
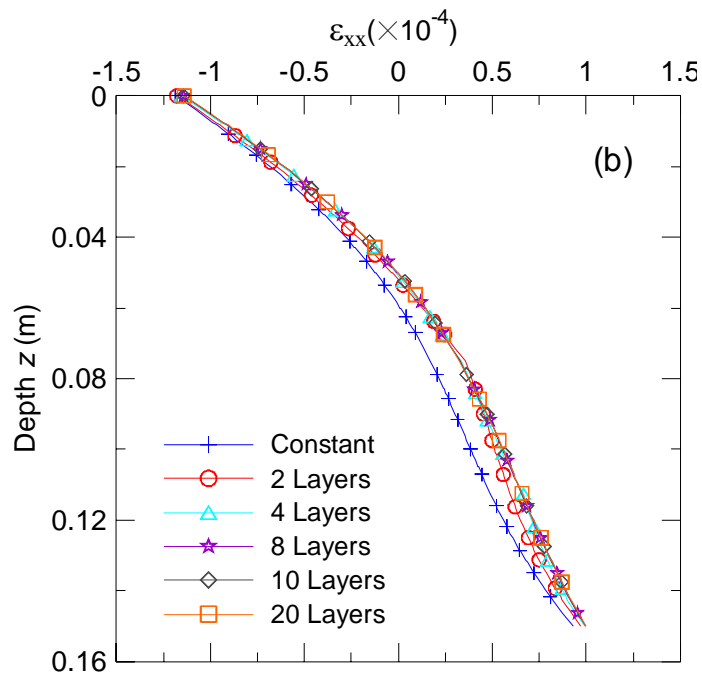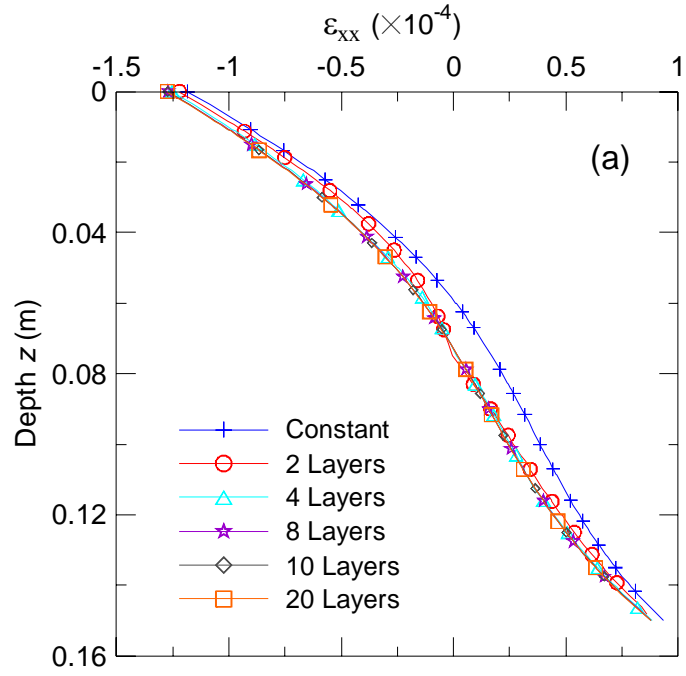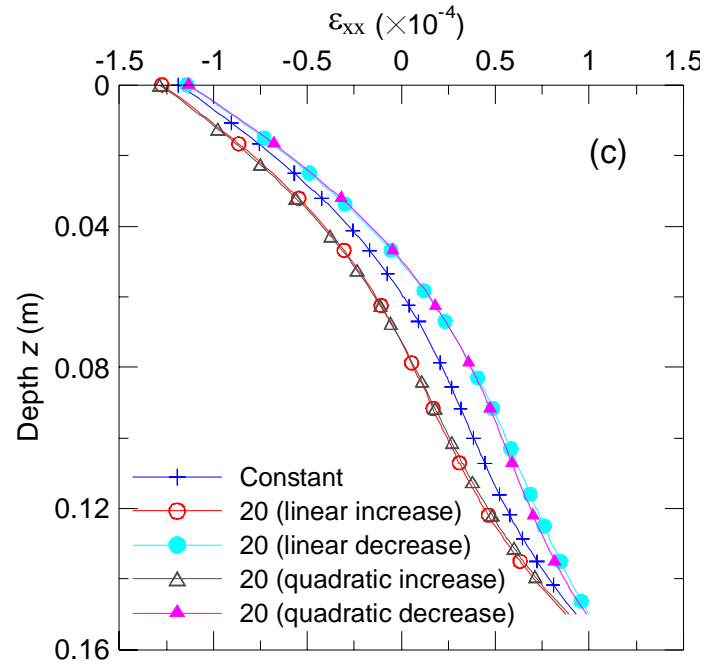
Figure 2.24, Variation of horizontal normal strain component ε_{xx} with depth for (a) Cases 1 and 2; (b) Cases 1 and 3; (c) Cases 1, 2, 3, 4 and 5.
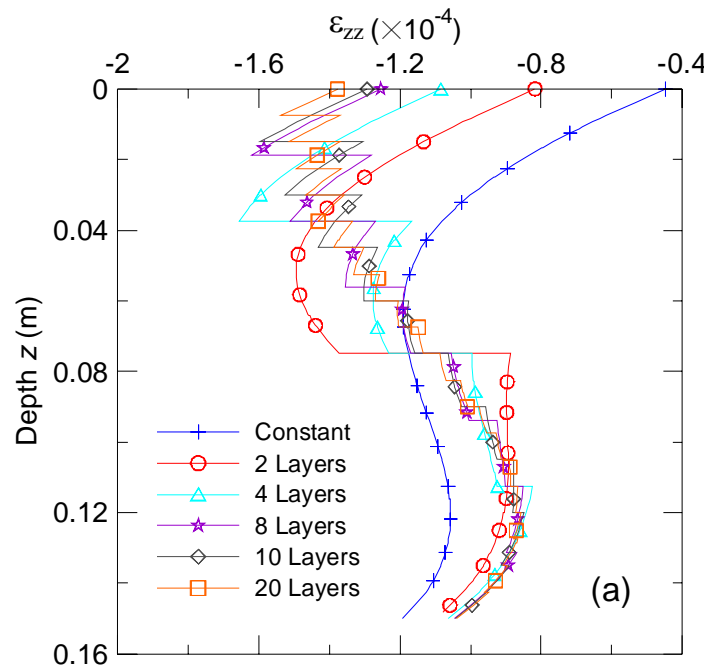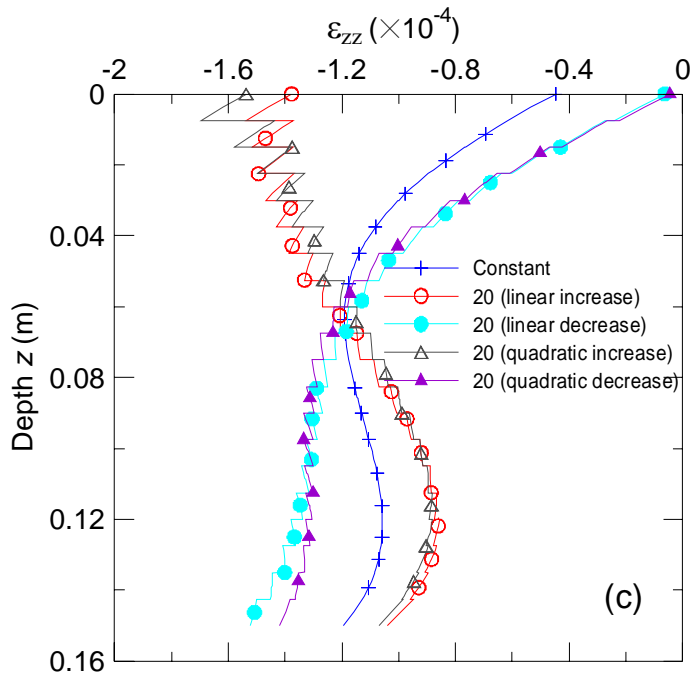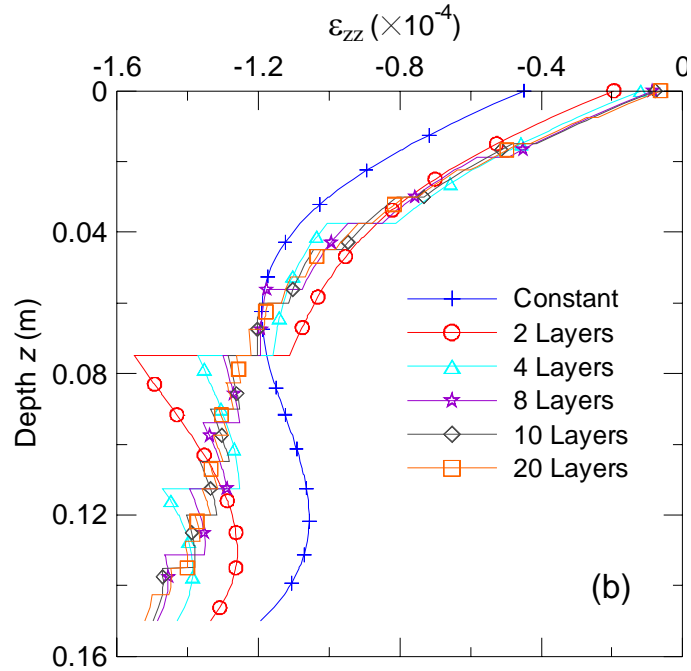
Figure 2.25, Variation of vertical normal strain component ε_{xx} with depth for (a) Cases 1 and 2; (b) Cases 1 and 3; (c) Cases 1, 2, 3, 4 and 5.

2.6.1. PAVEMENT DAMAGE PREDICTION

The predicted strain field could be applied to the damage prediction of pavement. Actually, the damage of flexible pavements can be assessed by predicting the number of

49

loads needed to initiate cracks (fatigue cracking). The Shell Model (Bonnaure et *al.*, 1980) and the Asphalt Institute Model (Shook et *al.*, 1982) are frequently used for fatigue cracking analysis in flexible pavements.

The Shell Model is based on two different loading modes, as given by:

Shell Constant Strain Model:

$$N_\varepsilon = 13909 A_f K \left(\frac{1}{\varepsilon_t}\right)^5 E_s^{-1.8}$$

Eq. (2.24)

and Shell Constant Stress Model:

$$N_\sigma = A_f K \left(\frac{1}{\varepsilon_t}\right)^5 E_s^{-1.4}$$

Eq. (2.25)

where N_ε and N_σ are the number of load repetitions to fatigue cracking using the constant strain and constant stress analysis, respectively, A_f and K are empirical parameters based on the material properties, ε_t is the tensile strain at the critical location and E_s is the stiffness of the material. The constant strain model is applicable to thin asphalt pavement layers usually less than 51 mm, whilst the constant stress model is applicable to thick asphalt pavement layers usually more than 203 mm. The Shell Model was calibrated and generalized for any thickness as given below (MEPDG, 2004):

$$N_f = A_f K F'' \left(\frac{1}{\varepsilon_t}\right)^5 E_s^{-1.4}$$

Eq. (2.26)

where N_f is the number of load repetitions to fatigue cracking, F'' is a constant that depends on the layer thickness and the stiffness of the material.

The Asphalt Institute Model is given below:

$$N_f = 0.00432 C \left(\frac{1}{\varepsilon_t}\right)^{3.291} \left(\frac{1}{E_s}\right)^{0.854}$$

Eq. (2.27)

where, similarly, N_f is the number of load repetitions to fatigue cracking, C is a constant depending on the material properties, ε_t is the tensile strain at the critical location and E_s is the stiffness of the material. The Asphalt Institute Model can be used for asphalt concrete layers of any thickness.

It can be seen from the above equations, that the critical tensile strain and the stiffness of the asphalt concrete layer are the key factors affecting the number of load repetitions needed to initiate fatigue failure. Understanding the effect of the modulus variation with depth (due to temperature variation with depth) on the fatigue cracking can be studied by finding the ratio between the estimated number of repeated loads (N_f) using the modulus variation with depth and that using the traditional assumption of a constant modulus for the entire layer. In other words, the ratio is equal to N_f (modulus variation) over N_f (constant modulus).

Figures 2.26 and 2.27 show the ratios based on the Asphalt Institute Model and the Shell Model, respectively, using the estimated tensile strains (ε_{xx}) at the bottom of the AC layer. Figure 2.24c shows that the increase of the modulus with depth will produce lower tensile strains at the bottom of the AC layer and therefore the required number of repeated loads to initiate fatigue cracks will be higher than those using the constant modulus. In this example, the increase in N_f from the modulus variation compared to that from constant modulus was approximately 22% and 16% using the Asphalt Institute Model for the linear and quadratic modulus increment case (Figure 2.26), respectively, whilst it was 35% and 26% using the Shell Model for the linear and quadratic modulus increment case (Figure 2.27), respectively.

On the other hand, the decrease of the modulus with depth produces higher tensile strains at the bottom of the AC layer (Figure 2.24c) and therefore the required number of repeated loads to initiate fatigue cracks becomes lower than that using the constant modulus. In this example, the decrease in N_f from the modulus variation compared to that from the constant modulus was approximately 21% and 17% using the Asphalt Institute Model for the linear and quadratic modulus decrease case (Figure 2.26), respectively, whilst it was 30% and 24% using the Shell Model for the linear and quadratic modulus decrease case (Figure 2.27), respectively.
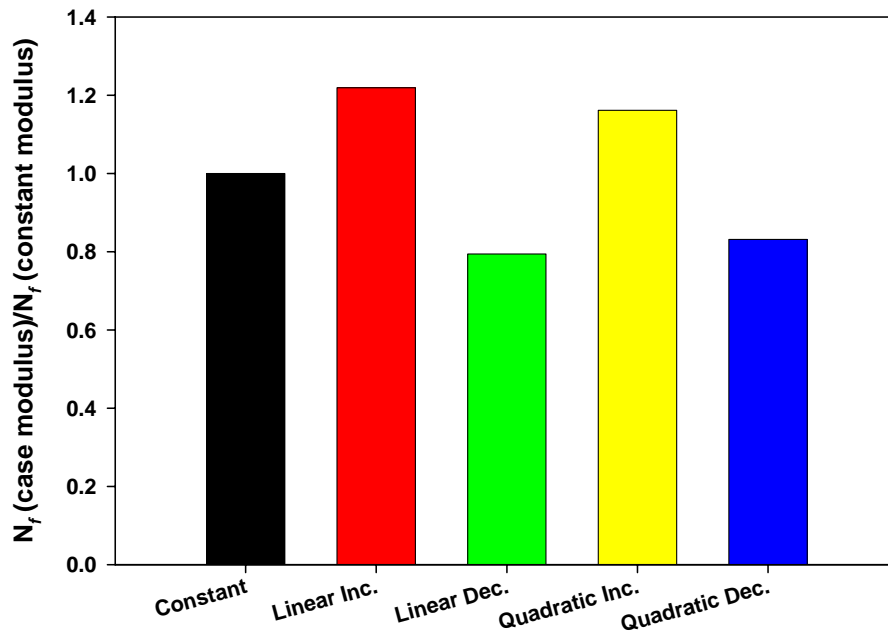
Figure 2.26, Ratio between the estimated number of repeated loads needed to initiate fatigue cracks using the modulus variation with depth and the constant modulus (Asphalt Institute Model).
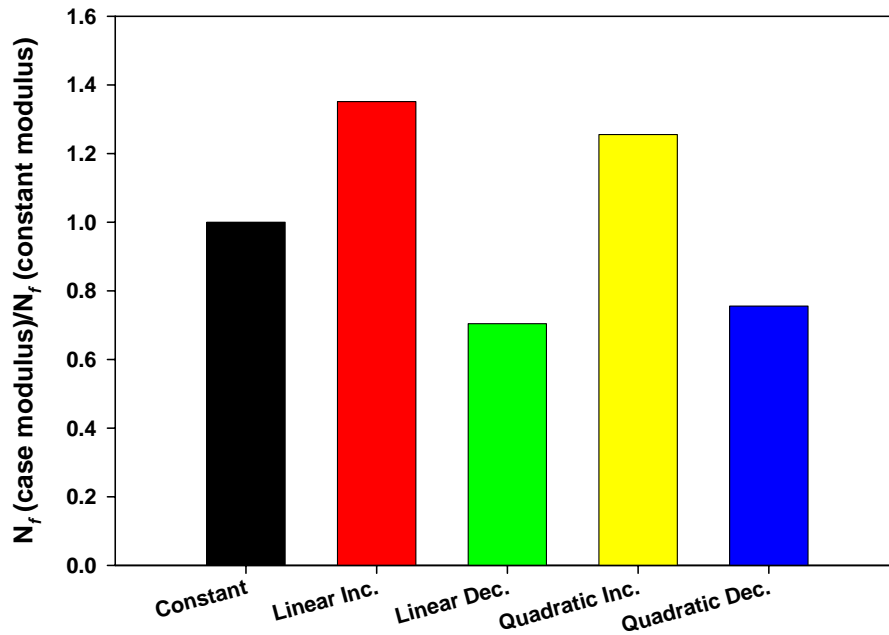
Figure 2.27, Ratio between the estimated number of repeated loads needed to initiate fatigue cracks using the modulus variation with depth and the constant modulus (Shell Model).

It is evident that the modulus variation as a result of the temperature variation with depth highly influences the predicted number of repeated loads (N_f) needed to initiate fatigue cracks in the AC layer. The predicted N_f using the constant modulus should be considered as the average value whilst those from the increase and decrease modulus variations should be considered as the upper and lower values, respectively. Therefore, modulus variation with depth can be used to create an envelope to encompass the extreme conditions that could be encountered in the AC layer.

2.7. CONCLUSIONS

The average resilient modulus is not recommended for the analysis and design of flexible pavements. Average resilient modulus can either overestimate or underestimate the pavement responses depending on the temperature variation in the AC layer. Temperature variations can be observed during the day and during the year which in turn cause different pattern of responses.

Modulus variation as a function of temperature variation can be used to create a "pavement response envelope" instead of the average pavement responses. This envelope can show the extreme pavement responses as well as the average responses, and thus can be a simple and yet a powerful approach for pavement engineers.

The modulus variation as a result of the temperature variation with depth highly influences the predicted number of repeated loads (N_f) needed to initiate fatigue cracks in the AC layer. The predicted N_f using the constant modulus should be considered as the average value whilst those from the increase and decrease modulus variations should be considered as the upper and lower values, respectively.

Increasing the number of layers is very critical especially for the vertical strain. Modeling variation of the resilient modulus using sub-layering can be difficult using most of the current commercially available programs where the maximum allowed number of layers/sublayers can not exceed 20. In addition, most multilayered elastic programs limit the number of layers, the thickness of each layer, and the total number of observation (response) points. However, the *MultiSmart3D* program can be used for any number of response points and any number of layers with any thickness so that any type of modulus variation with depth can be accurately modeled.

CHAPTER 3

EFECTIVE MODULUS VARIATION WITH DEPTH

3.0 INTRODUCTION

Material inhomogeneity within the pavement layer/sublayer can be caused by the dependency of the modulus of elasticity on the temperature, moisture, and/or other environmental factors. This fact imposes limitations on the current analytical elastic solution which does not take into consideration the variation of the modulus of elasticity with depth within the same layer. However, our newly developed multilayered program *MultiSmart3D* can be applied to any variation of modulus of elasticity in the pavement. The modulus variation within the same layer can be modeled using several sublayers where the sublayer thickness and modulus are different for different sublayers.

3.1 STRESS/STRAIN DISCONTINUITY

Displacement, strain, and stress variation with depth in multilayered systems is smooth within the same layer where the modulus of elasticity value either is the same or varies smoothly within the layer. However, the vertical strain ε_{zz} and horizontal stress σ_{xx} can be significantly different on both sides of an interface due to the large variation or jump in the modulus of elasticity in the layers above and below the interface. This discontinuity of strains/stresses can directly and significantly damage the pavement in forms of cracking. Therefore, it is important to consider the strain/stress in any flexible pavement analysis where the modulus varies with depth.

The strain/stress jumps between layers in a typical flexible pavement system (see also Table 3.1) using conventional layered elastic solution are shown in Figures 3.1 and 3.2. It can be seen clearly that the strain (ε_{zz} in Figure 3.1) and stress (σ_{xx} in Figure 3.2) discontinuity exists at the interfaces whilst the stress/strain variation within the same layer is smooth.

The problem of strain/stress discontinuity at the interface in flexible pavement analysis can be solved by reducing the discontinuity in the modulus of elasticity between the two sides of the interface. In reality, the modulus of elasticity of one layer in the pavement section can be orders higher than that in the subsequent layer. In order to ensure the continuity of the strains/stresses, the variation of the modulus of elasticity with depth should be continuous within the layer and between both sides of the interface. The modulus of elasticity variation with depth can be achieved by subdividing each layer into a number of sublayers each with a constant modulus of elasticity. The average modulus of elasticity of all sublayers should be equal to the average modulus of elasticity of the layer.
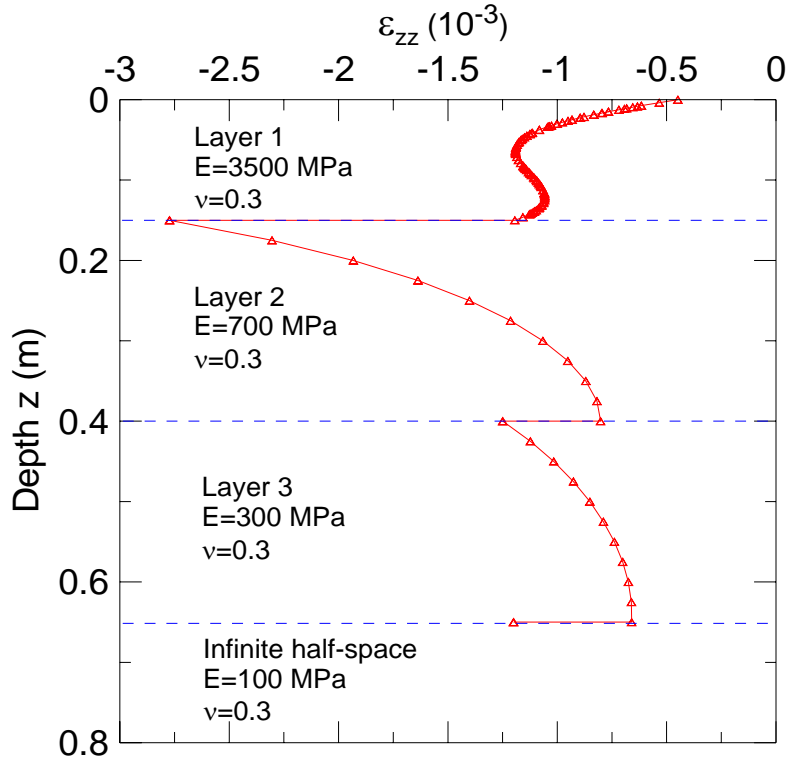
Figure 3.1, Vertical strain (ε_{zz}) jumps at interfaces in a flexible pavement system.
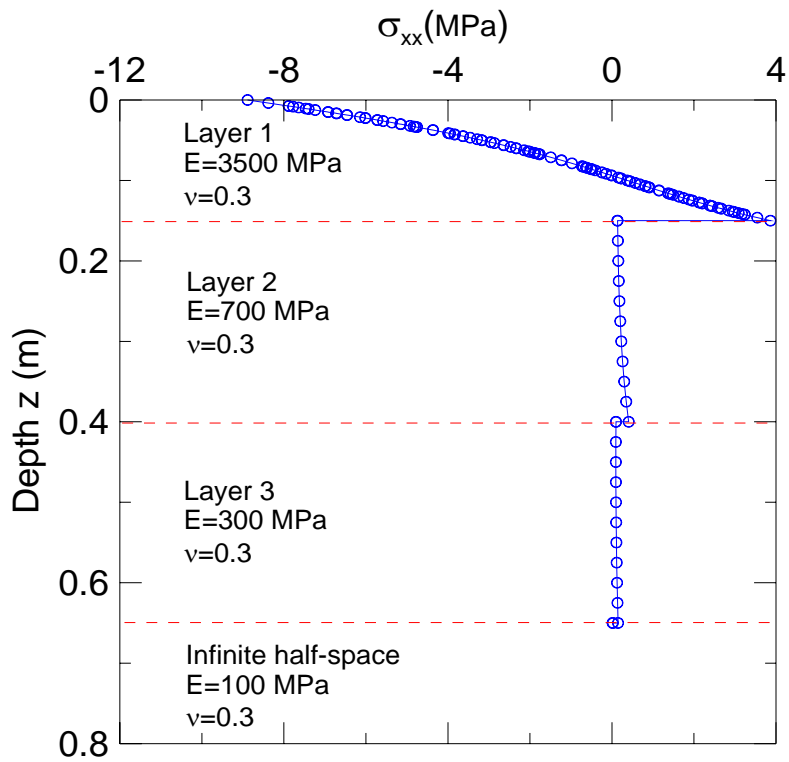
Figure 3.2, Horizontal stress (σ_{xx}) jumps at interfaces in a flexible pavement system.

Field measurement indicates that temperatures vary with depth during the day and during the year, as shown in Figure 3.3 (Ongel and Harvey, 2004). Therefore, the modulus of elasticity of a layer, in a flexible pavement system, varies with depth due to the dependency of the modulus on temperature. It was shown in the previous sections that the variation of the modulus with depth due to temperature variation is nonlinear. Other conditions that should be satisfied by the numerical variation of the modulus with depth include the continuity of the modulus of elasticity at the interfaces of the layer and the average modulus of the elastic layer. Therefore, a linear variation of the modulus with depth cannot be used and a nonlinear variation should be used instead. Using the three conditions above, the variation of the modulus with depth can be achieved using a quadratic equation.
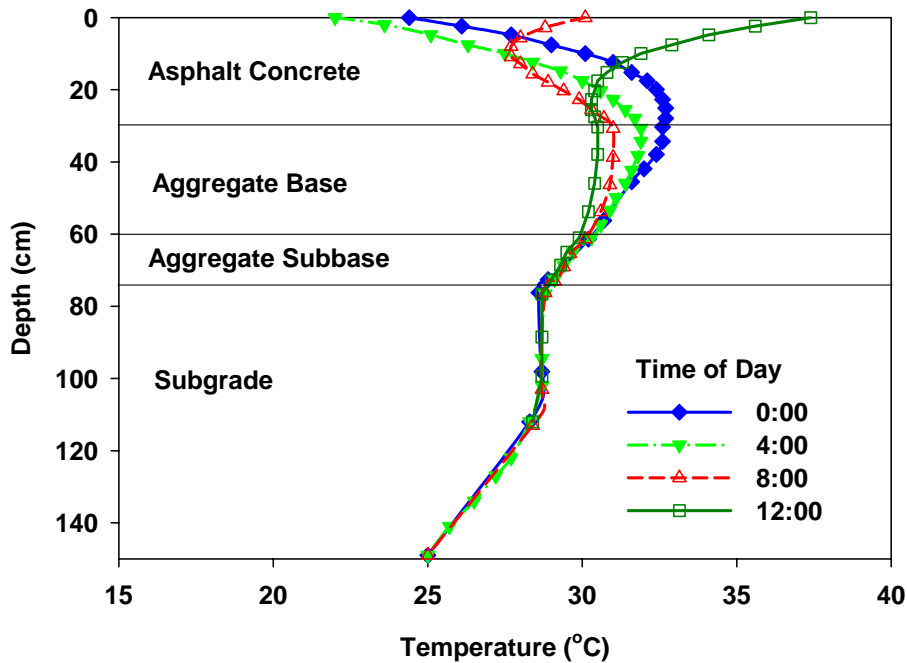
Figure 3.3, Daily temperature variation (modified from Ongel and Harvey, 2004).

A simple way to handle the strain/stress "jump" between the two sides of the interface in a multilayered elastic material is proposed. The method is based on a "controlled" variation of the modulus of elasticity within the elastic layer to ensure the lowest strain/stress "jump". Modulus variation with depth within the same layer is described below (The following steps **a)** through **d)** can be equally applied to other layers as well).

a). Select the thickness and the elasticity parameters (modulus of elasticity and Poisson's ratio) for each main layer in the multilayered elastic system, for example, layer *I* in Figure 3.4.

b). Use the modulus of elasticity in the upper layer (E_{I-1}) and the modulus of the elasticity of the subsequent layer (E_{I+1}) as boundary conditions to control the moduli variation with depth within layer *I*, see Figure 3.5.

56

c). Use the quadratic equation to describe the variation of the modulus of elasticity with depth in the layer. The resulting system of equations contains two equations and three unknowns (the three unknown constants for the quadratic equation). The needed third equation to solve the linear system of equations can be obtained using:

$$\int_0^{h_I} E(z)dz = E_I h_I \qquad \text{Eq. (3.1)}$$

where $E(z)$ is the quadratic modulus of elasticity function in layer I as a function of depth z and it is equal to $(a + bz + cz^2)$, where a, b, and c are the three unknowns. Equation (1) ensures that the resulting modulus variation within layer I will always result in the same average modulus. Therefore, the three simultaneous equations can be solved to find the three unknowns.

d). Subdivide layer I into a number of sublayers with the modulus of each sublayer being determined using the quadratic equation at the given depth. The constant modulus of elasticity within each sublayer should ensure a smooth transition of stresses/strains between two subsequent sublayers ((j-1) and (j) sublayers). This condition can be satisfied using:

$$E_{j-1}/E_j \approx 0.90 - 1.00 \qquad \text{Eq. (3.2)}$$

where E_{j-1} and E_j are the moduli of elasticity of the sublayers (j-1) and (j), respectively. This condition is very important since it will reduce the effect of the modulus variation with depth.

e). Calculate the response of the multilayered elastic system using ***MultiSmart3D*** program. Steps **a)** through **d)** can be applied to other layers as well.
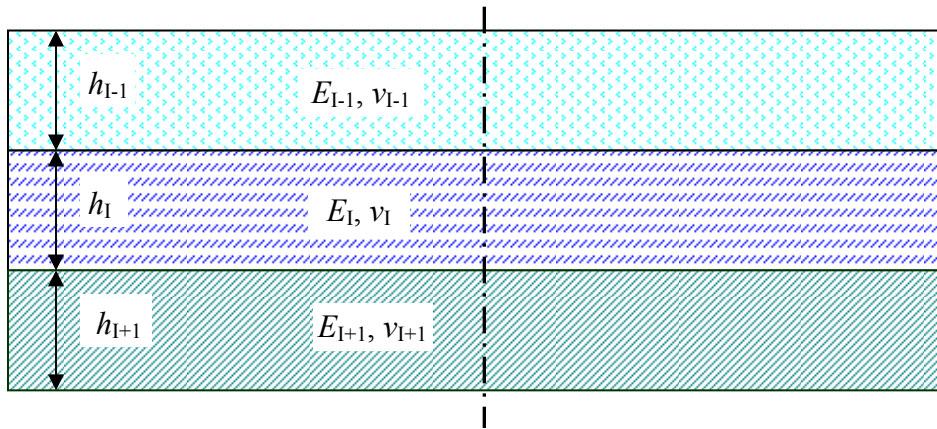
Figure 3.4, A multilayered elastic system.
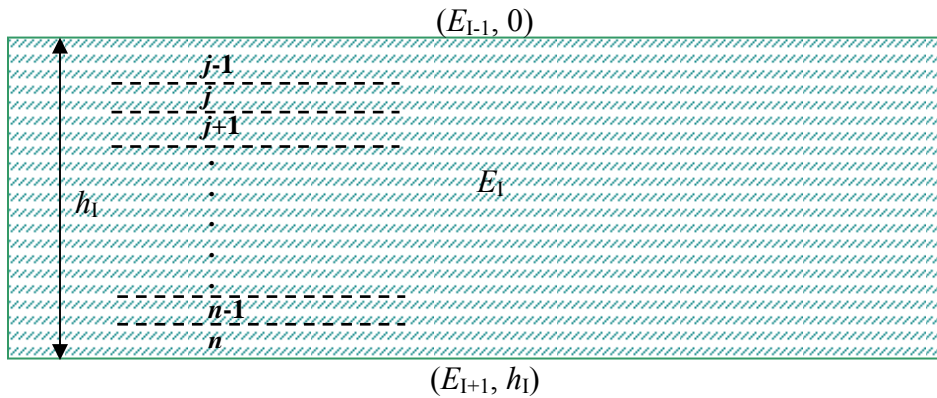
Figure 3.5, Assumed modulus boundary conditions for layer I.

3.2 FLEXIBLE PAVEMENT APPLICATION

Interface strain/stress jump in flexible pavements is very common in multilayered elastic analysis for any flexible pavement system. The above method will be applied to a flexible pavement system to demonstrate the applicability of the new method and to establish some guidelines regarding the use of the new method.

The typical flexible pavement section was summarized in Table 3.1. The contact pressure at the surface of the pavement was assumed to be 690 kPa acting on a circle with a diameter of 220.3 mm. Pavement responses below the center of the contact pressure were calculated using the *MultiSmart3D* program. The coordinate system is chosen such that the x- and y-axes are on the surface of the pavement ($z=0$) whilst the z-axis is vertical to the x-y plane and extends along the depth direction.

Table 3.1, Parameters of the flexible pavement example

Layer	Thickness (cm)	Resilient Modulus (MPa)	Poisson's Ratio
AC Layer	15	3500	0.3
Base Layer	25	700	0.3
Subbase Layer	25	300	0.3
Subgrade Layer	Infinite Half-Space	100	0.3

The interface strain/stress jump between the AC layer and the base layer was studied by the proposed method. The AC layer was subdivided into 10, 20, 50, 100, and 500 sublayers. The

modulus of elasticity within each sublayer is constant and equal to the average modulus of elasticity of the sublayer. For each sublayering model, the pavement response within the AC layer was calculated at 120 depth points using both the constant (average) and the quadratic modulus variation methods. Field response was also calculated at an additional point (a total of 121 points) which was located immediately below the interface between the AC layer and the base layer in order to study the jump of the strain/stress. The modulus variation with depth using constant and quadratic modulus variation functions is shown in Figure 3.6. The pavement responses using different models are shown in Figures 3.7 through 3.11.
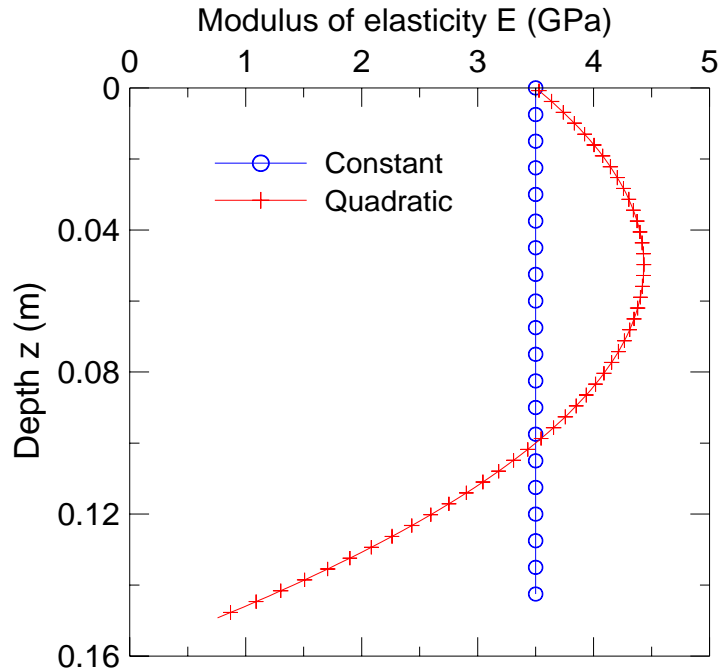
Figure 3.6, Modulus of elasticity variation with depth in the AC layer.

Figure 3.7 shows that the use of the average constant modulus can underestimate the displacement at any point within the AC layer except at the AC/base interface, as compared to the quadratic model with different sublayers. In addition, it can be seen that the number of sublayers has negligible effect on the calculated displacements in the AC layer. The maximum differences of displacements in the AC layer using the quadratic distribution compared to the displacements estimated using the average modulus was approximately 1.5%.

Figure 3.8 shows the variation of the vertical component of strain (ε_{zz}) with depth. It is clear that use of the average modulus of elasticity can underestimate the strains within approximately the top 60% of the AC layer and overestimate the strains in the lower 40% of the AC layer. In addition, the strain jump between the two sides of the AC/base interface can be up to 130% in the constant modulus case while it ranges between 42% and 1% for the quadratic variation using 10 and 500 sublayers, respectively. On the other hand, the maximum differences of strains in the upper 60% and the lower 40% of the AC layer between the quadratic and

constant models were approximately 40% and 58%, respectively. The influence of the number of sublayers is clearly seen in the figure especially near the interface.
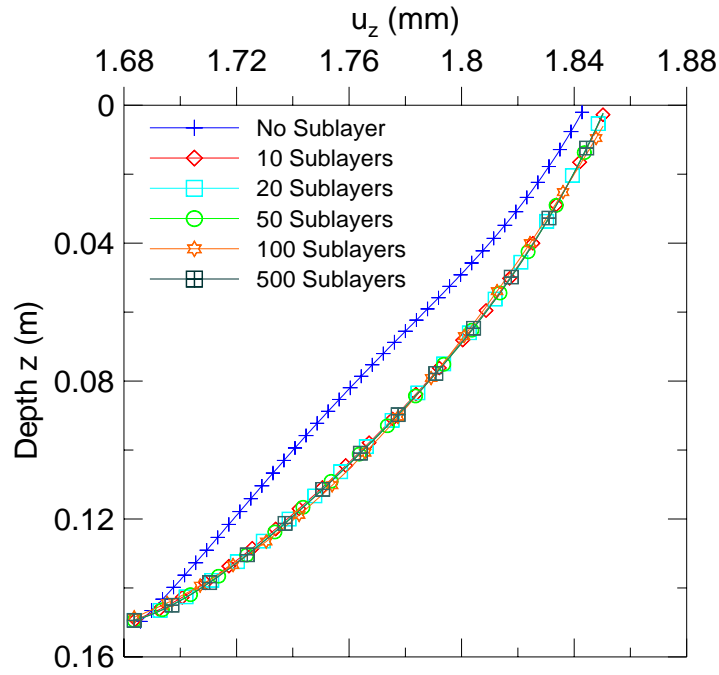
Figure 3.7, Displacement (u_z) variation with depth in the AC layer.
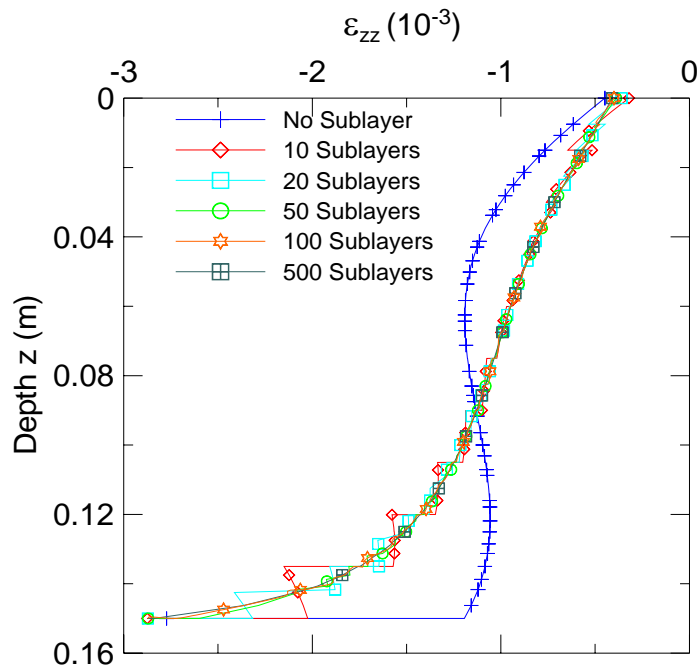
Figure 3.8, Vertical strain (ε_{zz}) variation with depth in the AC layer.

Figure 3.9 shows the variation of the horizontal component of strain (ε_{xx}) with depth. The strains in the upper 30% of the AC layer are almost identical regardless of the number of sublayers or the method of the modulus variation within the layer. However, using the constant modulus can underestimate the strains within the lower 70% of the AC layer. The maximum difference of the strains in the lower 70% of the AC layer from the quadratic and constant models is about 40%, whilst the number of sublayers has negligible effect on the strain variation with depth. Similar behavior can be observed for the other horizontal strain (ε_{yy}) due to symmetry.

Figure 3.10 shows the variation of the vertical component of stress (σ_{zz}) with depth. The difference between the stresses estimated using the quadratic and constant models is less than 10% in the top 20% and lower 80% of the AC layer, whilst it is almost the same outside the 20%-80% thickness range. The number of sublayers has negligible effect on the stress variation with depth.

Figure 3.11 shows the variation of the horizontal component of stress (σ_{xx}) with depth. The difference between the estimated stresses using the quadratic and constant models is between 3% and 480%, with the maximum difference being at the interface between the AC and base layers. It is further noticed that the number of sublayers has noticeable effect on the stress variation with depth.
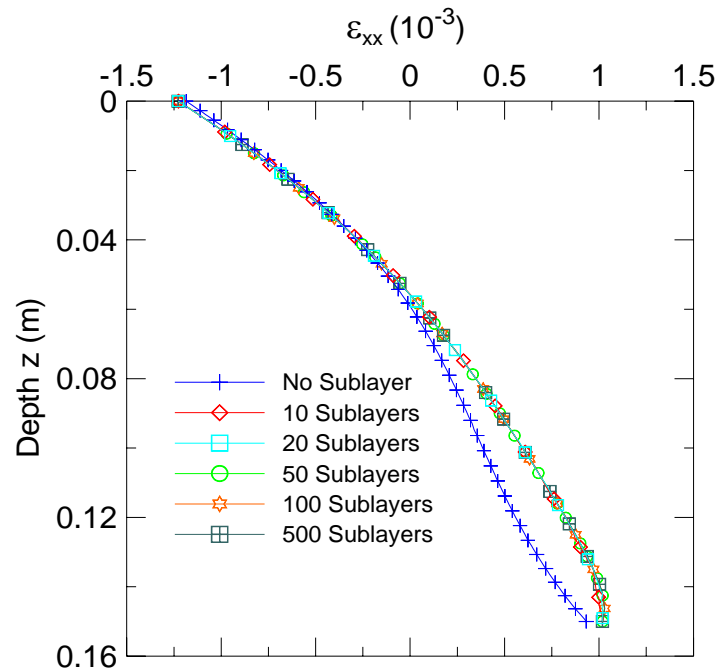
Figure 3.9, Horizontal strain (ε_{xx}) variation with depth in the AC layer.
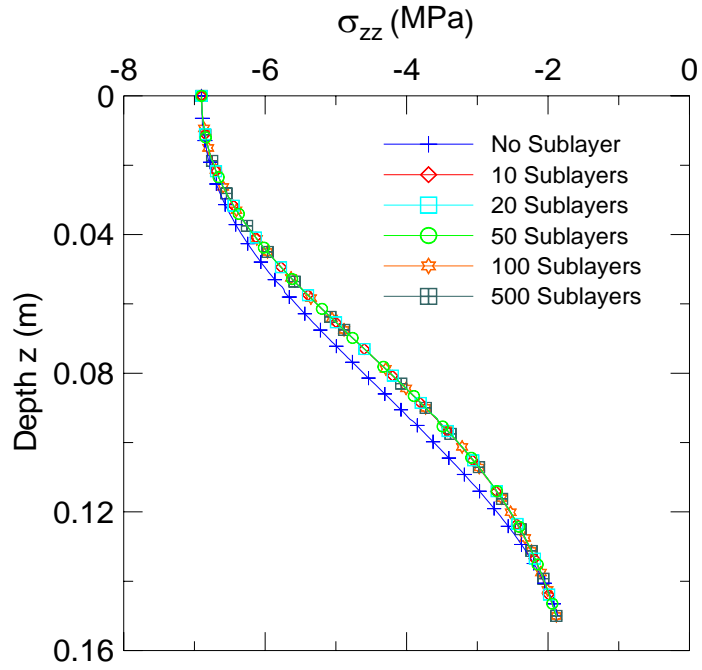
Figure 3.10, Vertical stress (σ_{zz}) variation with depth in the AC layer.
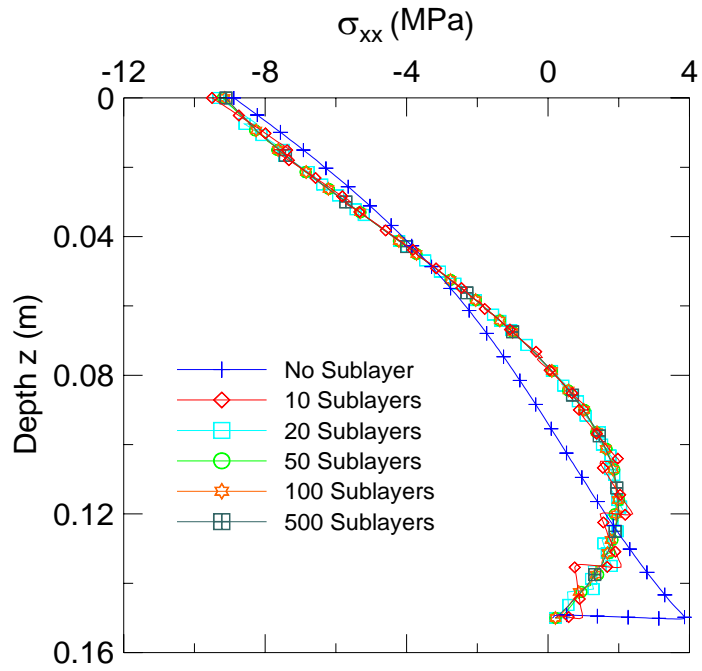
Figure 3.11, Horizontal stress (σ_{xx}) variation with depth in the AC layer.

3.2.1 EFFECT OF SUBLAYER NUMBERS

The number of sublayers, when used to vary the modulus of elasticity within the elastic layer, has a considerable effect on the strain/stress jump between the two sides of the interface. In order to investigate the effect of modulus of elasticity on the response between the two sides of the interface, the changes in the strain (ε_{zz}) and stress (σ_{xx}) are plotted against the number of sublayers in Figures 3.12 and 3.13, respectively.

It is observed that the quadratic modulus variation with depth can be used effectively to reduce the stress jump between the two sides of the interface. This jump in pavement response between the AC layer and the base layer can be reduced by increasing the number of sublayers (which is to reduce the ratio of the modulus of elasticity between two subsequent sublayers). Furthermore, from Figures 3.12 and 3.13, it can be seen that using 125 sublayers can produce smooth pavement responses between the sublayers and can effectively reduce the jump in the strain (ε_{zz}) and stress (σ_{xx}) as compared to the pavement responses using the average elastic modulus.

The effect of the ratio of the moduli between the two sides of the interface and the resulting vertical strain (ε_{zz}) and horizontal stress (σ_{xx}) can be further understood by using the "*efficiency factor*" as suggested below:

$$EF_{Strain} = \left(\frac{Strain_{j+1}}{Strain_j} \right) \bigg/ \left(\frac{E_j}{E_{j+1}} \right) \qquad \text{Eq. (3.3)}$$

and

$$EF_{Stress} = \left(\frac{Stress_{j+1}}{Stress_j} \right) \bigg/ \left(\frac{E_j}{E_{j+1}} \right) \qquad \text{Eq. (3.4)}$$

The efficiency factor can be used to easily demonstrate the relation among the number of sublayers, the change in the pavement response across the interface, and the required ratio to achieve a smooth response through the interface instead of the "jump" in the response. It can be seen from Figure 3.14 that as the number of sublayers increases, the efficiency factors for both strain and stress as defined in equations (3) and (4) approach unity, indicating a smooth transition in the pavement response between the two sides of the interface.

Figure 3.14 further indicates that the horizontal stress σ_{xx} is more sensitive to the efficiency factor than the vertical strain ε_{zz}. In practice, the horizontal stress σ_{xx} plays a major role in pavement fatigue cracking whilst the vertical strain ε_{zz} contributes substantially to pavement rutting. From Figure 3.14, we also observe that substantial reduction in the strain/stress "jump" between the two sides of the interface can be achieved using, say 125 sublayers, and that further reduction can be obtained by increasing the number of sublayers beyond the 125 sublayers threshold. It should be

noted that the sublayer thickness in this example was constant for simplicity and the variation of the sublayer thickness with depth is possible if needed.
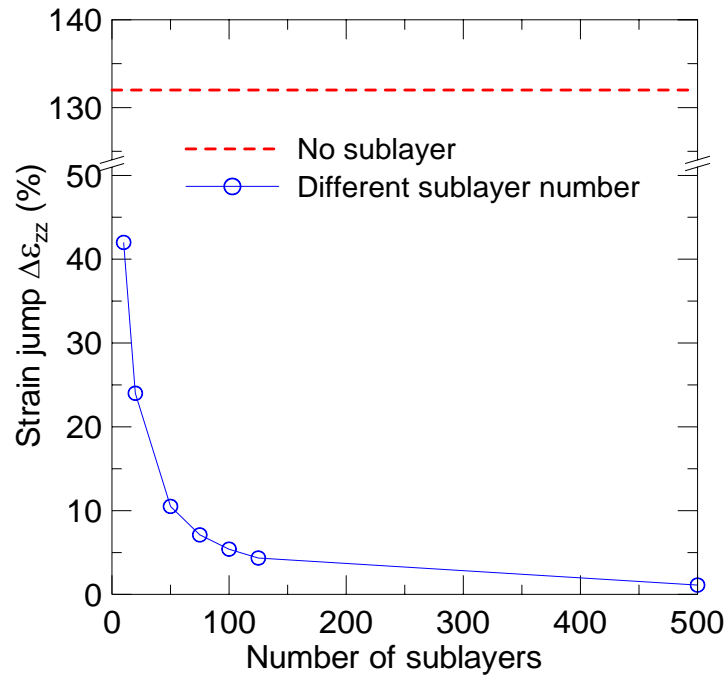
Figure 3.12, Vertical strain (ε_{zz}) jumps above and below the interface.
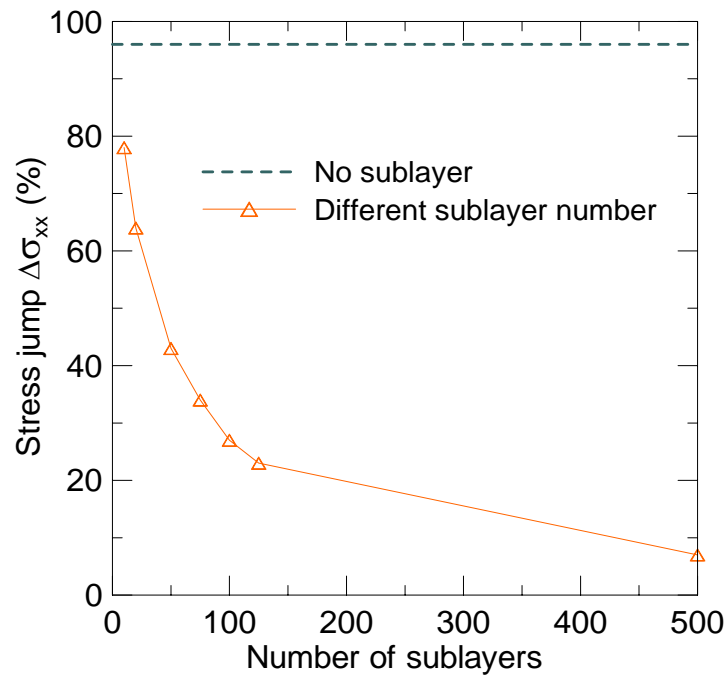
Figure 3.13, Horizontal stress (σ_{xx}) jumps above and below the interface.
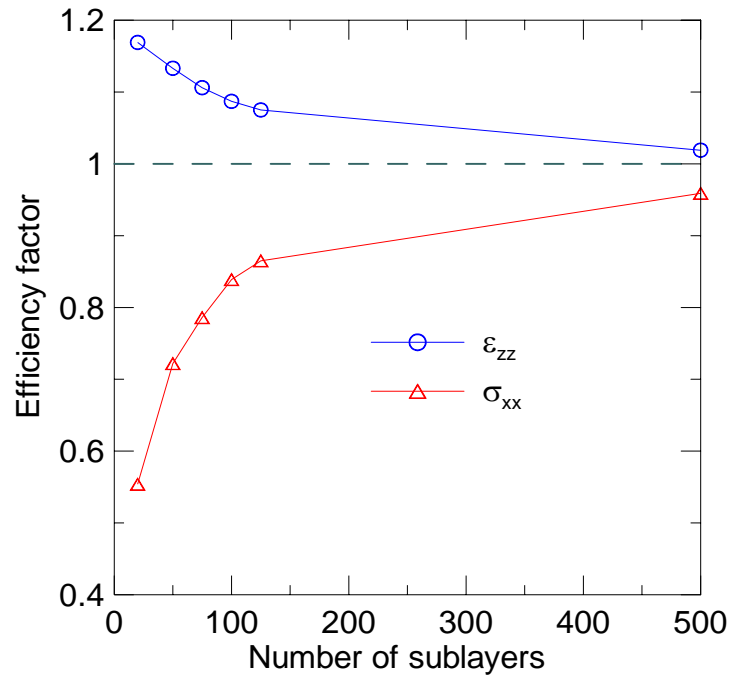
Figure 3.14, Efficiency Factor (EF) vs. number of sublayers.

3.2.2 BURMISTER SOLUTION

Burmister (1958) suggested that in flexible pavements the vertical stresses and displacements values are highly dependent on the modulus ratio between subsequent layers (E_j/E_{j+1}). On the other hand, Burmister (1945) simplified the conditions between two layers assuming that all layers are isotropic, elastic, and homogeneous. The top layer, in a two-layer system, was assumed to be infinite in the horizontal direction but finite thickness in the vertical direction. The bottom layer, in a two-layer system, was assumed to be of infinite extent in both horizontal and vertical directions. Tractions and displacements were assumed to be continuous across the interface.

As a final example, we have compared the calculated stresses using Burmister (1958) results (for 2 layers) with those using our *MultiSmart3D* program (for 125 sublayers using the quadratic variation). Figure 3.15 shows an excellent agreement between the *MultiSmart3D* analysis using the quadratic variation and that by Burmister with constant 2-layer model. This close agreement between the constant and the quadratic models suggests that instead of using the constant model which involves jumps in moduli, the quadratic model can be used where the moduli are continuous across the interface of the layers and thus the strain/stress becomes continuous without discontinuity or jump.
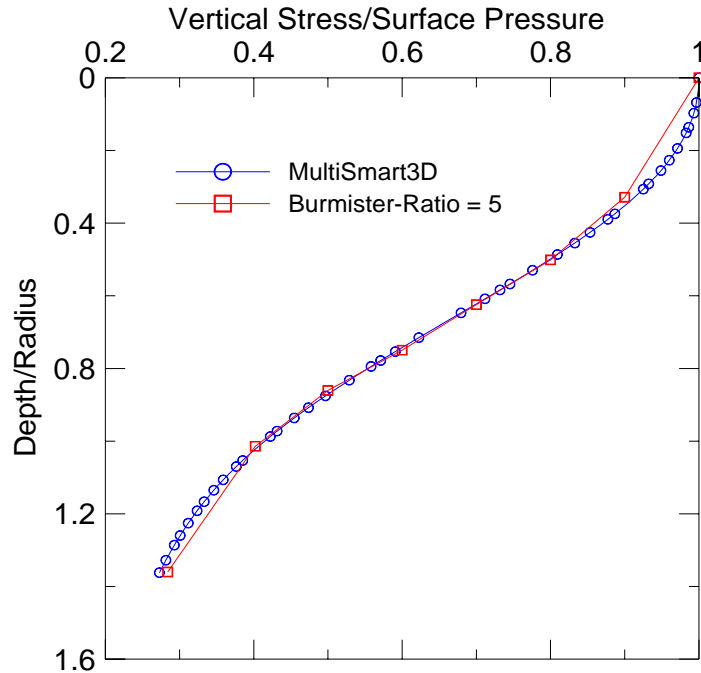
Figure 3.15, Comparison between Burmister analysis and *MultiSmart3D* analysis.

3.3 DISCUSSIONS AND CONCLUSIONS

The average modulus of elasticity is not recommended for the analysis and design of flexible pavements. The continuous variation of the modulus in the AC layer can reduce the "jump" in the stresses and strains between the two sides of the interface. The variation within any layer in the pavement system can be performed using a quadratic relation in which the average elasticity moduli are the boundary conditions. The applicability of this method is demonstrated using the *MultiSmart3D* algorithm, recently developed at University of Akron under the sponsorship of ODOT/FHWA. This new algorithm is superior to any available multilayered flexible pavement program since unlimited number of layers can be used. The efficiency factor was introduced as a new way of measuring the needed number of sublayers and the effectiveness of the modulus variation with depth in order to reduce the jump in the vertical strain and horizontal stress.

The introduced quadratic variation method showed excellent agreement with the Burmister model which was based on the constant 2-layer pavement, suggesting the practical use and importance of such assumptions. The use of the quadratic modulus variation in the pavement also shows that the inhomogeneity of the AC layer can be modeled using the effective multilayered elastic approach. By increasing the number of sublayers, which will in turn reduce the modulus variation with depth, any realistic modulus variation in pavement (due to temperature, moisture, or other environmental factors) can be accurately simulated. However, modeling variation of the resilient modulus using sublayering can be difficult using most of the commercially available programs as most existing multilayered elastic programs limit the number of input layers and the thickness of each layer.

CHAPTER 4

PAVEMENT RESPONSE VERIFICATION

4.0 INTRODUCTION

The design of flexible pavements and the prediction of pavement response are highly dependent on the multi-layer elastic theory. Since the first introduction of the method by Burmister in 1943 (Burmister, 1943), the multi-layer elastic theory has been developed further to study the response of flexible pavements under vehicle loading due to its simplicity and due to the few number of inputs needed to carry out the computation. The short computational time associated with the multilayer elastic theory makes it the most popular method among engineers. However, the method suffers from certain limitations related to the assumed linear response of the pavement system, the uniform distribution of the tire contact pressure, the circular shape of the footprint of the tire under loading, and the limited number of the layers that can be incorporated into the analysis.

In the traditional multilayer elastic pavement analysis, the pavement is modeled using several elastic layers each with its independent elastic properties characterized by the modulus of elasticity and the Poisson's ratio. Therefore, the elastic modulus of the elastic layers is considered constant regardless of the load repetition and the load level which are the main factors affecting nonlinear variation of the modulus with depth. In addition, the discrete nature of the pavement layers due to the presence of the aggregate particles that are connected by interlocking forces and cementing agents, can vary the modulus of elasticity spatially (vertically and horizontally) below the pavement/stress contact points. Considering the variation of the modulus of elasticity spatially is a very difficult task and therefore linearity or nonlinearity of the modulus have been considered below the contact stress area only within thin layers with relatively thin thicknesses and of infinite widths.

The performance of flexible pavements using analytical methods had showed limitations due to the inherited limitations associated with the analytical closed form solutions using the multilayer elastic theory which impose more limitations regarding the variation of both the modulus of elasticity and the Poisson's ratio with depth. In turn, the accuracy of the elastic multilayer solutions is largely affected by the variation of the modulus of elasticity with depth especially when the thickness of the elastic layer is relatively large and hence a constant modulus should not be used. Subdividing thick elastic layers into several thin layers was not possible due to mathematical challenges that limited the maximum number of elastic layers in the pavement system to 20 layers (MEPDG, 2004).

On the other hand, the finite element method showed less practicality when dealing with flexible pavement design due to the sensitivity associated with the element size and boundary conditions that can be case dependent. However, reducing the element thickness in the finite element analysis increases the computation time and requires high capacity storage units to perform the computations. The complexity of the input process, the sensitivity of the analysis procedure, and the associated cost of the finite element method hinder the spread of the method among engineers.

The validity of any analytical method in engineering should be verified using full scale field tests. Pavement full scale tests are of valuable importance since the performance of the pavement can be measured rather than predicted under monitored field conditions. Full scale testing is not an easy task and the accuracy of such models is highly dependent on the test setup and the test procedures.

4.1 FULL SCALE PAVEMENT TESTS

It is important to bridge the gap between the theoretical response of the pavement and the actual response of the pavement using measured data from test sections. Data obtained from full scale pavement sections helped in developing most of the pavement models and the pavement design recommendations. Full scale test sections are used to study one or more of the influencing parameters in pavement design. As in any engineering test, the total cost of the test is directly proportional to the number of studied variables and therefore, studying the effect of individual parameters on the response of pavements can be limited since the interaction between more than one parameter can lead to a different response pattern which can be complex to interpret.

Pavement analysis is normally carried out assuming the 2D plane strain condition to simplify the actual 3D condition with the former being a more time and mathematical efficient analysis procedure. This reduction can highly affect the accuracy of the analysis leading to less agreement between the predicted and the measured conditions in the full-scale tests. On the other hand, the limited accuracy of the input parameters used in the analysis method will add more to the accuracy deficiency in the simulation process.

4.2 THE EFFECT OF THE BACKCALCULATED MODULUS OF ELASTICITY

The multilayer elastic analysis methods depend mainly on two input parameters, namely: the modulus of elasticity and the Poisson's ratio. Therefore, the accuracy of the predicted response using the multilayer elastic theory is highly dependent on the accuracy of the input parameters. The needed two input parameters (modulus of elasticity and Poisson's ratio) of the theory are obtained using empirical correlations, lab testing, and backcalculation methods using results from nondestructive testing such as the Falling Weight Deflectometer (FWD) and the Spectral Analysis of Surface Waves (SASW) method (Nazarian, 1984; Mamlouk, 1985; Gucunski and Krstic, 1996).

In the FWD method a trial and error procedure is applied to the pavement section using data that include measured or assumed layer thicknesses for the pavement system, applied load (stress), measured deflections (FWD deflection basin). The trial and error uses an initial modulus value (seed) for the iteration procedure and then the deflection at the measured locations is calculated and compared to the measured results. Therefore, the modulus of elasticity and Poisson's ratio are the two important parameters in the backcalculation procedure with more emphasis on the modulus of elasticity as compared to the Poisson's ratio. The Poisson's ratio is normally assumed in the backcalculation procedure and not backcalculated, assuming its less effect on the pavement response and also due to the difficulty of including its effect in the backcalculation procedure analytically.

On the other hand, the backcalculation of the modulus of elasticity of each layer is highly dependent on the subgrade and the used response model. The subgrade can contribute to 60%-80% of the total center deflection in the FWD test and the backcalculation procedure (Ullidtz, 1987). In addition, the use of different response models in the backcalculation (such as the linear elastic model, the method of equivalent thickness (MET), and the finite element method) will result in different elastic parameters. Therefore, any forward calculation (response calculation) should be performed using the same response model that was used in the backcalculation procedure; otherwise, the predicted response can be far from the measured response.

The SASW method is a wave propagation method that is based on applying an impulse load and then measuring the surface wave velocity at different locations from the applied load using accelerometers. The modulus profile can be backcalculated using the surface or Raleigh wave. The Raleigh wave is characterized by high energy and a velocity that highly dependent on the frequency. Different methods are available to backcalculate the modulus of elasticity using the SASW results including the use of one-half of the surface wave length (Heukelom and Foster, 1960), the use of one-third of the surface wave length (Szendrei and Freeme, 1970), and the use of the wave equation solution (Yuan and Nazarian, 1993). The SASW method is not widely used due to the long time associated with the analysis procedure.

4.3 PAVEMENT RESPONSE SIMULATION

Validation of pavement response models can not be performed without the use of measured field data. The measured field data can be obtained using either real-time loading tests, or accelerated pavement tests (APT). Both performance tests are full scale tests that intend to measure the performance of the pavement under the working conditions in on site sections as in the former test and under controlled conditions in instrumented facilities as in the latter. These tests are expensive tests and the outcome results from these tests normally lead to new findings and practical design procedures. The ability to verify analytical response models using these tests is a very important task since the cost of verifying more complex cases can be a problem in such cases and the design of tests to study the interaction between different factors might not be easy.

Instrumentation of pavement sections for the full scale testing is not a trivial task and care should be taken during installation. Measured data from the test sections can be affected by the installation procedure and the type of the selected instruments. For example, strain gauges installed in asphalt concrete can measure low strain levels if the strain gauge material is stiffer than the surrounding asphalt concrete layer (Hildebrand, 2002).

4.4 PAVEMENT PERFORMANCE USING FULL SCALE TEST

Multilayer elastic theory has been used for decades to simulate the response of pavement systems under surface loading. The agreement between measured and estimated responses was always not satisfactory since limitations exist from either the testing procedure and measurements quality or the ability of the response model to predict the response accurately. The quality of the measured data can vary from test to test and even within the same test sections

affected by different factors such as the durability of the instruments during the testing and the bonding/debonding conditions that affect the measurements.

A well designed full scale test will not only aid in understanding the behavior of the system under certain conditions but also help in extending the applicability of modeling techniques in understanding the behavior of the pavement system in more complex conditions with less spending on trial testing and setup. In addition, quick and emergency jobs can be dealt with in more efficient way when the answers for critical questions can be derived from reliable and efficient response modeling tools. These tools should show time efficiency, computation efficiency, and simplicity.

The ability to back calculate the modulus of elasticity proved to add more uncertainties in the agreement between the measured and predicted values. It is common to see discrepancies between the backcalculated modulus of elasticity and the modulus of elasticity from lab-tested samples. The discrepancies can often be attributed to the difference between lab and in situ conditions such as the degree of compaction of the pavement layer or the induced fatigue after certain number of load cycles.

It is known that the elasticity of the pavement layers vary spatially as well as with depth. The ability to model the variation of the elasticity modulus with depth can reduce the uncertainties that exist between measured and predicted modulus of elasticity since more representing modeling can be employed rather than averaging the modulus within the layers. However, the number of layers that can be used in any multilayer elastic analysis is limited due to the limitation in the mathematical formulation of such solutions which require analytical treatment of the problem.

The maximum number of layers/sublayers that can be used, until recently, in the multilayer elastic analysis, is limited to 20 layers (MEPDG, 2004). Temperature variation in the layers through sub-layering is recommended to study the distress in the pavement due to seasonal variation. Pavement distress includes asphalt fatigue fracture (top down and bottom up), permanent deformation, and asphalt thermal fracture. Sublayering depends on the homogeneity of the layer, the loading of the surface, thickness of the pavement layers, and the number of the pavement layers. In most multilayer elastic pavement programs, increasing the number of sublayers will increase the computational time, which is not practical for practitioners and hence is often avoided.

4.4.1 TEST DESCRIPTION

The verification full-scale test was described in details in Hildebrand (2002). The following is aimed to summarize the pavement full-scale test and the test related information.

The test site was located in Nymølle in Denmark. The test section was constructed in a site with relatively homogeneous soil layers. The upper part of the soil section at the test site was entirely removed and replaced with compacted soil layers. The soil at the site before the pavement construction consisted of different material types as shown in Table 4.1. The constructed pavement section was approximately 6 meters wide by 10 meters long. The thickness

and the material type of the pavement layers are shown in Figure 4.1. The sand layer (Layer 1) consisted of three sublayers that were compacted using a static tandem drum roller with a total weight of 1300 kg. The degree of compaction of the constructed granular layers below the pavement section was measured using a Troxler nuclear density gauge and ranged between 93% and 97.6%.

Table 4.1, Soil profile at the test site before the pavement construction

Top of Layer* (m)	Layer Thickness (m)	Soil Designation	Classification (AASHTO)
0.616	0.25	Organic topsoil	-
0.366	0.75	Silty sand	A-2-4(0)
-0.384	2.00	Silty sand	A-4(0)
	0.50	Silty sand	A-2-4(0)
-2.884	0.50	Lean Clay	A-6(9)
-3.384	1.00	Silt	A-4(0)
-4.384	1.00	Lean Clay	A-6(9)
-5.384	4.00	Silt	A-4(8)
-9.384	N/A	Gravel	-

*Zero elevation at the top of the natural subgrade after the removal of the topsoil and part of the silty sand.
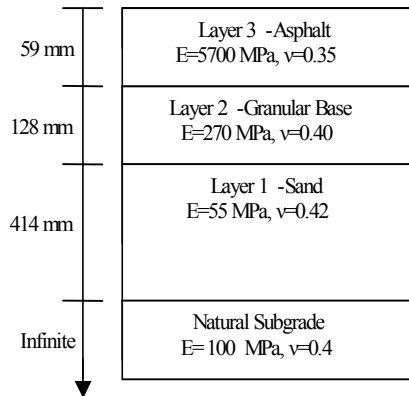
Figure 4.1, Pavement system at the test site after construction.

A total of six pressure cells and six soil deformation transducers were installed to monitor the pavement response under working conditions. Instruments were installed in the sand layer above the natural subgrade as shown in Figure 4.1. Details of the actual instruments location after installation are shown in Table 4.2.

The pavement response was measured after the construction of each pavement layer and after the construction of the asphalt concrete layer at the top. The falling weight deflectometer (FWD) was used to apply the load during the response testing. The results from the response testing after the construction of the asphalt concrete layer are included here to simulate the entire multilayer elastic system of the pavement.

Table 4.2, Instrument depth and location at the test site

Response Type	Instrument ID	X (m)	Y (m)	Depth (m)
σ_{x^*}	SRX+1.5	1.50	0.00	0.568
σ_{y^*}	SRY-1.0	0.00	-1.00	0.571
σ_y	STX-1.0	-1.00	0.00	0.569
σ_x	STY+1.5	0.00	1.50	0.566
σ_{z^*}	SVX+0.5	0.50	0.00	0.559
σ_z	SVY+0.5	0.00	0.50	0.559
ε_{x^*}	TRX+1.0	1.00	0.00	0.538
ε_{y^*}	TRY-1.5	0.00	-1.50	0.540
ε_y	TTX-1.5	-1.50	0.00	0.543
ε_x	TTY+1.0	0.00	1.00	0.539
ε_{z^*}	TVX-0.5	-0.50	0.00	0.550
ε_z	TVY-0.5	0.00	-0.50	0.552

The pavement response was measured after resetting the response instruments to zero before starting any round of measurements. Readings from the gravitational weight of soil above the instruments were subtracted from the readings observed during the testing. Climatic conditions during the test period were observed such as the rain, snow, and temperature.

Backcalculation of the modulus of elasticity was performed using the multilayer elastic program MODCOMP5 using the deviator stress model to describe the resilient modulus, as defined by

$$M_R = k_1 e^{\sigma_d . k_2}$$
Eq. (4.1)

where σ_d is dynamic deviator stress ($\sigma_d = \sigma_1 - \sigma_3$), and k_1 and k_2 are material parameters from triaxial testing.

In addition, the modulus of elasticity was further backcalculated using the SASW method. The shear wave velocity was recorded and the modulus of elasticity was calculated using the following equation:

$$E = 2(1 + v)\rho V_s$$
Eq. (4.2)

where E is the modulus of elasticity, ρ is the mass density of the soil, V_s is the measured shear wave velocity, and v is the Poisson's ratio.

The surface wave tests indicated that the modulus of elasticity below the surface varies nonlinearly. Figure 4.2 shows that the modulus of elasticity is higher at the top and changes

nonlinearly with depth based on results using either the one-half of the surface wavelength or using the one-third of the surface wavelength. This indicates that the use of the average modulus in each layer can be far from reality.
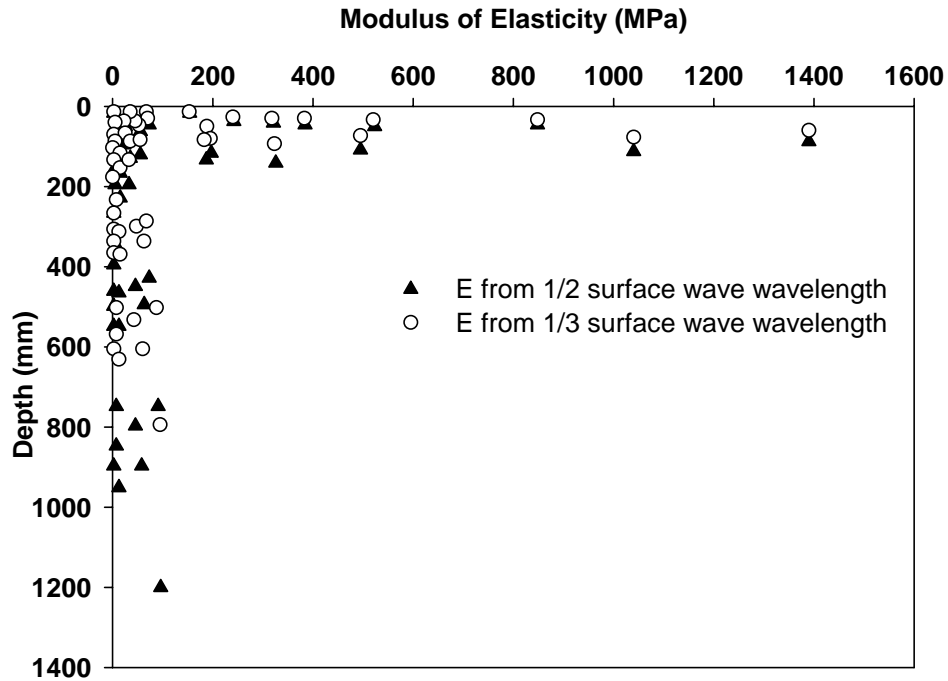
Figure 4.2, Backcalculated modulus of elasticity from SASW analysis (using results from Hildebrand, 2002).

The response at each instrument location was measured after applying the load at the surface. Then, the measured data were compared to the analysis results using the multilayer elastic program *MultsiSmart3D* and other analysis methods as reported by Hildebrand (2002). Hildebrand concluded that the agreement between the measured and calculated response is in general satisfactory. The best agreement was observed for the vertical stresses (σ_{zz}).

4.4.2 INPUT DATA SENSITIVITY ANALYSIS

The accuracy of any analysis is largely influenced by the input parameters. If the input parameters are of a good quality, one can rely on the output of the analysis method. The multilayer elastic analysis of the pavement relies mainly on two parameters: the modulus of elasticity and the Poisson's ratio. In this field-testing, the Poisson's ratios were assumed based on typical values of similar materials while the modulus of elasticity was backcalculated and averaged over the depth of each layer below the surface. The shown elasticity moduli in Figure 4.1 are based on extensive backcalculation and statistical analysis performed by Hildebrand (2002).

In order to study the sensitivity of the input parameters on the output results (stresses and strains) using the multilayer elastic analysis, the modulus of elasticity and the Poisson's ratio of the layer containing the instruments (Layer 1 in Figure 4.1) were varied linearly. Tables 4.3 and

4.4 show the results of the sensitivity analysis using Poisson's ratio for Layer 1 while Tables 4.5 and 4.6 show the sensitivity analysis using the modulus of elasticity for Layer 1.

Poisson's ratio of Layer 1 was assumed based on typical values for similar material which was 0.42. The sensitivity analysis was performed assuming fixed elastic moduli for all layers while the Poisson's ratio of Layer 1 was varied 10%, 20%, -10%, and -20% from the assumed value of 0.42. Then, pavement response was calculated using the multilayer elastic program *MultiSmart3D* at the actual depth of the instruments (Table 4.2). The corresponding Poisson's values and analysis results are shown in Tables 4.3 and 4.4.

The influence of the Poisson's ratio on the calculated stresses can be said to be significant especially for the horizontal stresses. The Poisson's ratio describes the relation between the vertical and horizontal strains which are directly related to the stresses according to the elastic theory. Increasing the Poisson's ratio by 10% and 20% increased the horizontal stresses by roughly 40% and 85%, respectively, while decreasing the Poisson's ratio by 10% and 20% decreased the horizontal stresses by roughly 30% and 55%, respectively. Therefore, increasing the Poisson's ratio has higher impact on the horizontal stresses compared to decreasing it. The Poisson's ratio showed less influence on the vertical stresses which increased or decreased slightly upon the increase or decrease of the Poisson's ratio. High Poisson's ratios are normally observed in soils with soft consistency such as loose sand. Materials around instruments can exhibit less compaction and hence higher Poisson's ratio.

Table 4.3, Stresses (kPa) sensitivity analysis using Poisson's ratio

Stress	Δ (%)[a]	v=0.336	Δ (%)[a]	v=0.378	v=0.42	v=0.462	Δ (%)[a]	v=0.499	Δ (%)[a]
σ_{x*}	-56.35	4040.24	-31.08	6379.50	9256.90	12897.80	39.33	17117.20	84.91
σ_{y*}	-55.91	4132.94	-30.84	6482.13	9372.88	13032.80	39.05	17272.70	84.28
σ_y	-56.20	4070.97	-31.00	6413.47	9295.40	12942.20	39.23	17168.30	84.70
σ_x	-56.66	3979.31	-31.25	6312.20	9181.02	12810.00	39.53	17015.90	85.34
σ_{z*}	-8.09	31662.60	-4.54	32886.90	34450.80	36502.20	5.95	38907.60	12.94
σ_z	-8.09	31662.60	-4.54	32886.90	34450.80	36502.20	5.95	38907.60	12.94

[a] Percent change between stresses calculated using v=0.42 and another Poisson's ratio.

Table 4.4, Strains (μm/m) sensitivity analysis using Poisson's ratio

Strain	Δ (%)[a]	v=0.336	Δ (%)[a]	v=0.378	v=0.42	v=0.462	Δ (%)[a]	v=0.499	Δ (%)[a]
ε_{x*}	-12.94	-1.638E-04	-7.19	-1.746E-04	-1.88E-04	-2.056E-04	9.28	-2.249E-04	19.53
ε_{y*}	-12.91	-1.623E-04	-7.18	-1.730E-04	-1.86E-04	-2.036E-04	9.26	-2.254E-04	20.99
ε_y	-12.86	-1.600E-04	-7.15	-1.705E-04	-1.84E-04	-2.006E-04	9.23	-2.221E-04	20.94
ε_x	-12.92	-1.630E-04	-7.18	-1.738E-04	-1.87E-04	-2.046E-04	9.27	-2.238E-04	19.52
ε_{z*}	7.32	5.439E-04	4.51	5.297E-04	5.07E-04	4.720E-04	-6.87	4.282E-04	-15.50
ε_z	7.48	5.407E-04	4.61	5.263E-04	5.03E-04	4.679E-04	-7.00	4.236E-04	-15.79

[a] Percent change between strains calculated using v=0.42 and another Poisson's ratio.

74

On the other hand, the influence of the Poisson's ratio on the calculated strains was almost equal in magnitude while different in behavior, as shown in Table 4.4. Increasing the Poisson's ratio increased the horizontal strains while it decreased the vertical strains by almost the same amount. In addition, decreasing the Poisson's ratio decreased the horizontal strains while it increased the vertical strains slightly.

The modulus of elasticity of Layer 1 was backcalculated based on the FWD and SASW testing results which was found by Hidebrand (2002) to be 55 MPa. The sensitivity analysis was performed assuming fixed Poisson's ratio for all layers while the modulus of elasticity of Layer 1 was varied 10%, 20%, -10%, and -20% from the assumed value of 55 MPa. Then, the pavement response was calculated using the multilayer elastic program *MultiSmart3D* at the actual depth of the instruments. The corresponding modulus of elasticity values and analysis results are shown in Tables 4.5 and 4.6.

Table 4.5, Stresses (kPa) sensitivity analysis using modulus of elasticity

Response	Δ (%)[a]	E=44 (MPa)	Δ (%)[a]	E=49.5 (MPa)	E=55 (MPa)	E=60.5 (MPa)	Δ (%)[a]	E=66 (MPa)	Δ (%)[a]
σ_{x^*}	25.71	1.16E+04	13.02	1.05E+04	9.26E+03	8.04E+03	-13.19	6.81E+03	-26.43
σ_{y^*}	25.66	1.18E+04	13.00	1.06E+04	9.37E+03	8.14E+03	-13.18	6.90E+03	-26.42
σ_y	25.69	1.17E+04	13.01	1.05E+04	9.30E+03	8.07E+03	-13.19	6.84E+03	-26.43
σ_x	25.74	1.15E+04	13.03	1.04E+04	9.18E+03	7.97E+03	-13.19	6.75E+03	-26.44
σ_{z^*}	-0.91	3.41E+04	-0.33	3.43E+04	3.45E+04	3.45E+04	0.13	3.45E+04	0.11
σ_z	-0.91	3.41E+04	-0.33	3.43E+04	3.45E+04	3.45E+04	0.13	3.45E+04	0.11

[a] Percent change between stresses calculated using E=55 MPa and another Modulus of Elasticity.

The influence of the modulus of elasticity on the calculated stresses can be said to be significant especially for the horizontal stresses. Increasing the modulus of elasticity by 10% and 20% decreased the horizontal stresses by 13% and 26%, respectively, while decreasing the modulus of elasticity by 10% and 20%, increased the horizontal stresses by 13% and 26%, respectively. Therefore, increasing and decreasing the modulus of elasticity has the same impact on the horizontal stresses. The modulus of elasticity showed negligible influence on the vertical stresses. High modulus of elasticity values are normally observed in soils with stiff or dense consistency such as dense sand.

On the other hand, the influence of the modulus of elasticity on the calculated strains is shown in Table 4.6. Increasing the modulus of elasticity decreased both the horizontal as well as the vertical strains. However, the change in the vertical strains was approximately twice the change observed in the horizontal strains indicating higher sensitivity to the modulus changes.

Table 4.6, Strains (µm/m) sensitivity analysis using modulus of elasticity

Strain	Δ (%)[a]	E=44 (MPa)	Δ (%)[a]	E=49.5 (MPa)	E=55 (MPa)	E=60.5 (MPa)	Δ (%)[a]	E=66 (MPa)	Δ (%)[a]
ε_{x^*}	7.62	-2.03E-04	3.55	-1.95E-04	-1.88E-04	-1.82E-04	-3.14	-1.77E-04	-5.96
ε_{y^*}	7.43	-2.00E-04	3.46	-1.93E-04	-1.86E-04	-1.81E-04	-3.07	-1.76E-04	-5.82
ε_y	7.13	-1.97E-04	3.32	-1.90E-04	-1.84E-04	-1.78E-04	-2.95	-1.73E-04	-5.60
ε_x	7.53	-2.01E-04	3.51	-1.94E-04	-1.87E-04	-1.81E-04	-3.09	-1.76E-04	-5.91
ε_{z^*}	14.90	5.82E-04	6.77	5.41E-04	5.07E-04	4.78E-04	-5.74	4.53E-04	-10.69
ε_z	14.83	5.78E-04	6.74	5.37E-04	5.03E-04	4.74E-04	-5.71	4.50E-04	-10.63

[a] Percent change between strains calculated using E=55 MPa and another Modulus of Elasticity.

The above results indicate that the horizontal stresses, horizontal strains, and vertical strains are highly sensitive to the variation of the Poisson's ratio and the modulus of elasticity. The vertical stresses are sensitive to the variation of the Poisson's ratio while the variation of the modulus of elasticity has negligible effect on the vertical stresses.

Poisson's ratio and the modulus of elasticity variation with depth in sand is typical due to the inhomogeneous nature of sand and the degree of compaction that differs with depth as shown in Figures 4.3 and 4.4. The figures show that the modulus of elasticity and the Poisson's ratio vary with depth as measured by the cone penetrometer tests (CPT) (Zeng and Hlasko, 2005). It can be seen that the degree of compaction and the size of the sand particles largely affect the modulus of elasticity even if the soil is uniformly compacted.
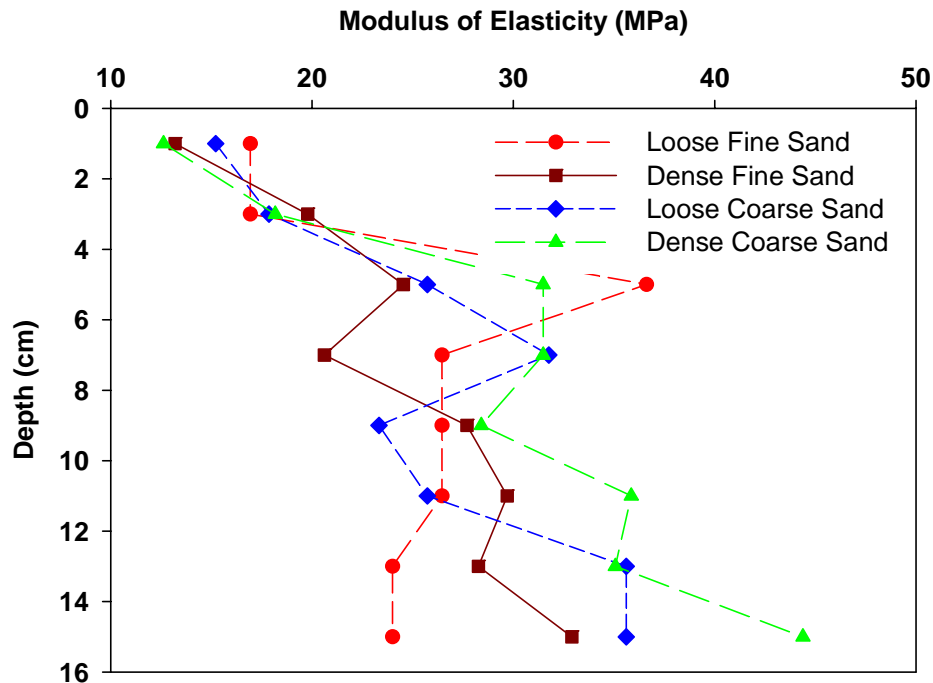
Figure 4.3, Modulus of elasticity variation with depth in sand (using results from Zeng and Hlasko, 2005).
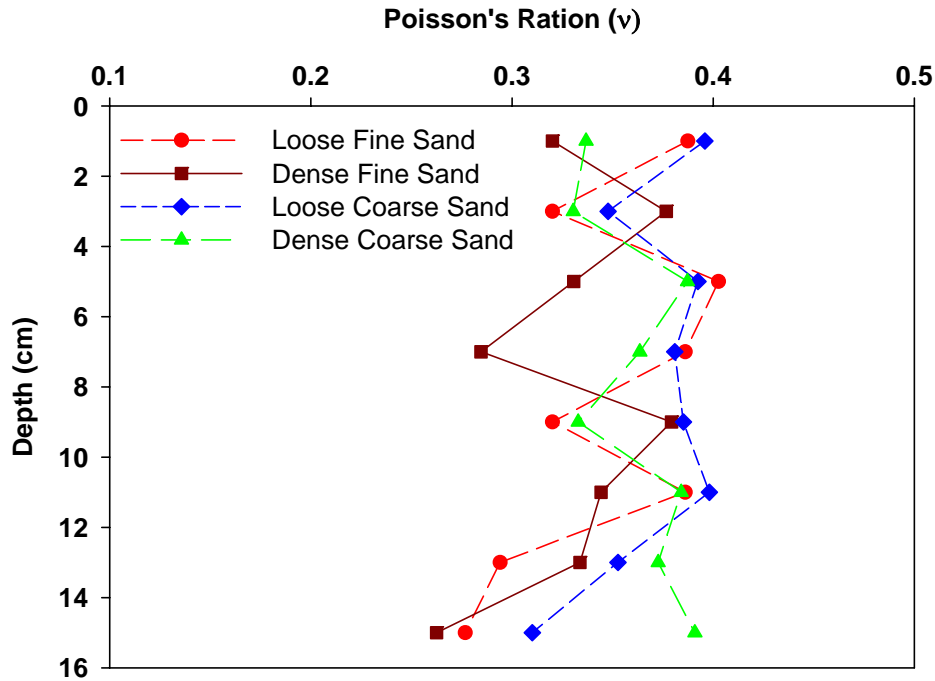
Figure 4.4, Poisson's ratio variation with depth in sand (using results from Zeng and Hlasko, 2005).

4.4.3 VARIATION OF THE MODULUS OF ELASTICITY

Soil is nonhomogenous in nature due to the irregularity in the soil particle shape, and the deposition rate. However, soil is often assumed to be homogeneous due to the simplicity in modeling. Soil homogeneity cannot be verified in sand easily due to the difficulty of obtaining undisturbed soil samples (especially for sand) from the field that represent the particle orientation and distribution at the site. As a result of the nonhomogenous nature of the soil, the modulus of elasticity varies spatially along any test section causing variation in the test results.

The variation of the modulus of elasticity largely affects the results of the elastic theory since the two main input parameters are the modulus of elasticity and the Poisson's ratio. The selection of one single modulus to represent the modulus of elasticity in the forward calculation of the pavement response is a common practice even though it is far from the in situ conditions.

Poor agreement between the lab modulus of elasticity and the backcalculated modulus of elasticity is very common. This disagreement is attributed to the fact that the backcalculated modulus is based on the seed modulus while the lab modulus is based on the physical properties of the sample. In addition, the backcalculated modulus of elasticity for each layer in the pavement system might vary based on the seed modulus but the ratio between two consecutive layers should be the same to be able to back calculate the same deflection basin.

Based on the backcalculation results of the pavement moduli, Hildebrand (2002) suggested the use of 55 MPa for the sand layer (Layer 1). This value was based on the average of the backcalculated moduli of the three compacted sublayers of the sand layer (Layer 1). The homogeneity of the compacted sand layer was assumed based on the results of the nuclear gage density, which indicated almost the same density of the three sublayers.

Using the results published by Hildebrand (2002), one can study the variation of the modulus of elasticity spatially. As can be seen in Figures 4.5 and 4.6, the vertical stresses (σ_{zz}) and vertical strains (ε_{zz}) vary spatially with the maximum values at the center of the FWD plate. The horizontal spacing between the measured responses was the same in both figures. The vertical strains were measured at a depth of 0.550 m below the surface while the vertical stresses were measured at a depth of 0.559 m below the surface. Assuming that the measurements of the vertical strains and stresses were at the same depth (difference in depth is less than 1.7%) the measurements can be used to backcalculate the spatial variation of the modulus of elasticity of the sand layer (Layer 1).

Due to the availability of two sets of vertical stresses (SVX and SVY) and two sets of vertical strains (TVX and TVY), four sets of modulus of elasticity variation as a function of the offset distance can be calculated. The modulus of elasticity variation with distance is shown in Figure 4.7. The modulus of elasticity at that depth (0.55 m below surface) varies between 37 MPa and 77 MPa with an average value of 55 MPa and a median of 54.4 MPa. The average of the modulus of elasticity below the center of the loaded area (offset=0) within the sand layer is as recommended by Hildebrand (2002) which is 55 MPa. On the other hand, the variation of the modulus of elasticity increases as the offset distance increases on both sides of the loaded area. However, the large variation in the modulus of elasticity as a function of the offset distance can affect the results and hence the interpretation of the analysis results should be done carefully. In order to study the effect of the variation of the modulus of elasticity on the calculated results, sensitivity analysis was performed on the field test section as described in the previous section.
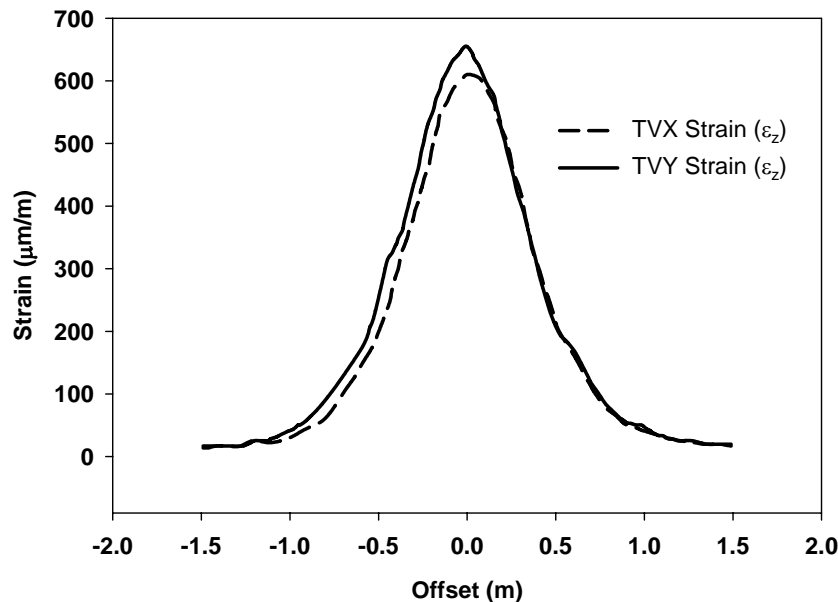
Figure 4.5, Measured strain variation in Layer 1 (using results from Hildebrand, 2002).

78
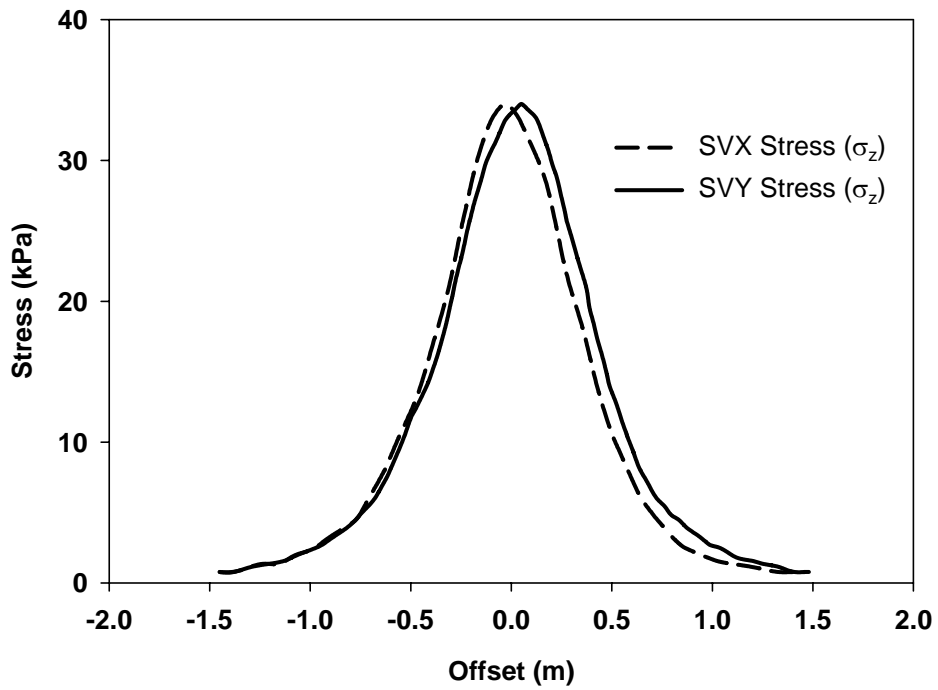
Figure 4.6, Measured stress variation in Layer 1 (using results from Hildebrand, 2002).
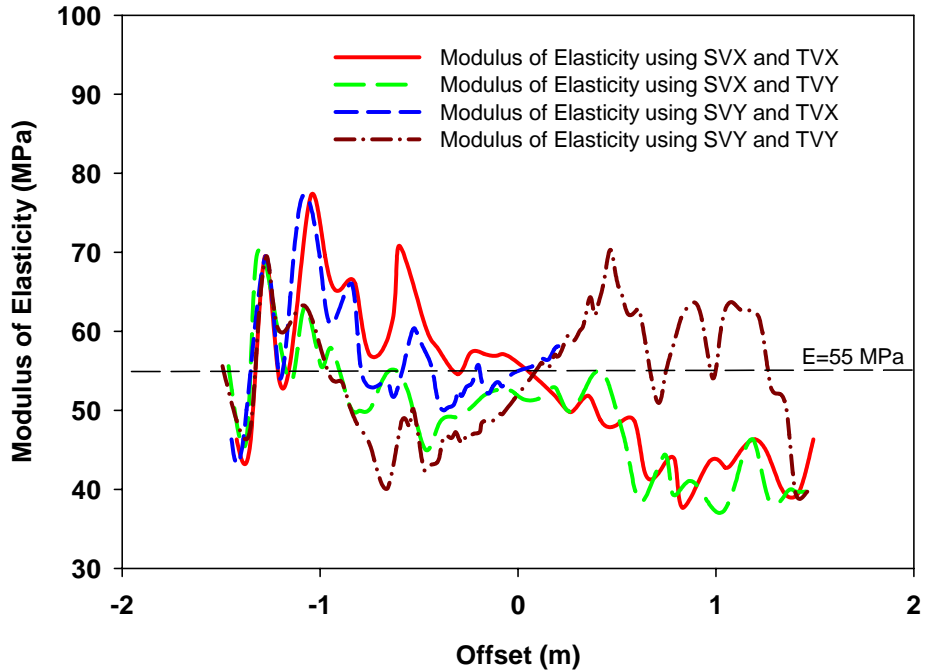
Figure 4.7, Backcalculated modulus of elasticity in Layer 1.

4.4.4 VARIATION OF THE POISSON'S RATIO

Strains were measured using LVDT type transducers. The deflections recorded by the LVDT instruments were then used to calculate the strains. Calibration of the LVDT was done only in the lab. On the other hand, no calibration was done for the in situ measurements since no method is available for in situ deflections using LVDT devices (Hildebrand, 2002). Therefore, the reliability of the measured strains can be far from the calibrated strains and hence a further reliability check should be considered before using the strains in any comparison.

However, to show the variation of the Poisson's ratio with distance, the Poisson's ratio was backcalculated at the instrument level in the sand layer (Layer 1). Assuming the 3D Hooke's law, we have the following elastic relations:

$$v = \frac{\sigma_x - E\varepsilon_x}{\sigma_y + \sigma_z}$$

Eq. (4.4)

$$v = \frac{\sigma_y - E\varepsilon_y}{\sigma_x + \sigma_z}$$

Eq. (4.5)

$$v = \frac{\sigma_z - E\varepsilon_z}{\sigma_x + \sigma_y}$$

Eq. (4.6)

Since strains are calculated from displacements measured using the LVDT transducers, the depth at each location of the instruments should be considered when comparing the strain results. Therefore, strains from TTX, TTY, and TVY, and stresses from SRX, SRY, and SVY were used to calculate the Poisson's ratio using Eq. 4.4 through Eq. 4.6. These instruments were located between 0.539 m and 0.571 m below the ground surface, therefore the effect of elevation difference should be considered negligible and the comparison should be considered valid.

The backcalculated Poisson's ratios are shown in Figures 4.8 through 4.10. The figures indicated that the backcalculated Poisson's ratio is not logical due to either the need to calibrate the measured strains or due to errors in the measurement of strains. The average backcalculated Poisson's ratio using Eqs. 4.4, 4.5, and 4.6 was 0.84, 0.68, and 0.13, respectively, whilst the assumed value is $v = 0.42$. Furthermore, the typical Poisson's ratios for loose to dense sand range between 0.2 and 0.4 (Bowles, 1996) and should always be less than 0.5 for soils.

Based on the Poisson's ratio comparison and the sensitivity analysis of the Poisson's ratio effect on the calculated strains, the measured strains in the test are not reliable without calibration and hence no further conclusions can be drawn from any analysis and comparison using the measured strains.
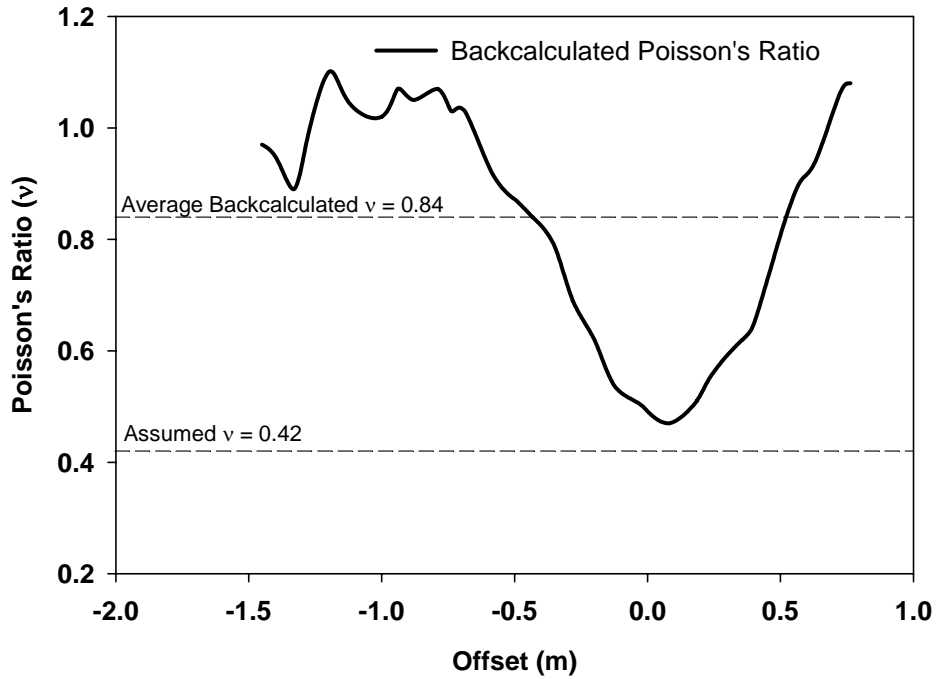
Figure 4.8, Backcalculated Poisson's ratio in Layer 1 using Equation 4.4.
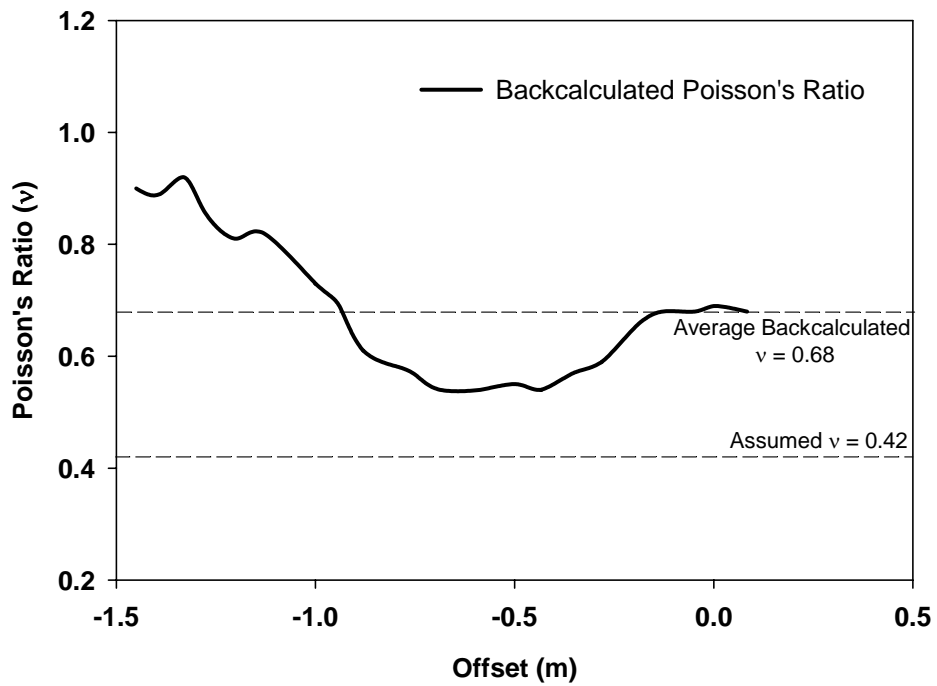
Figure 4.9, Backcalculated Poisson's ratio in Layer 1 using Equation 4.5.
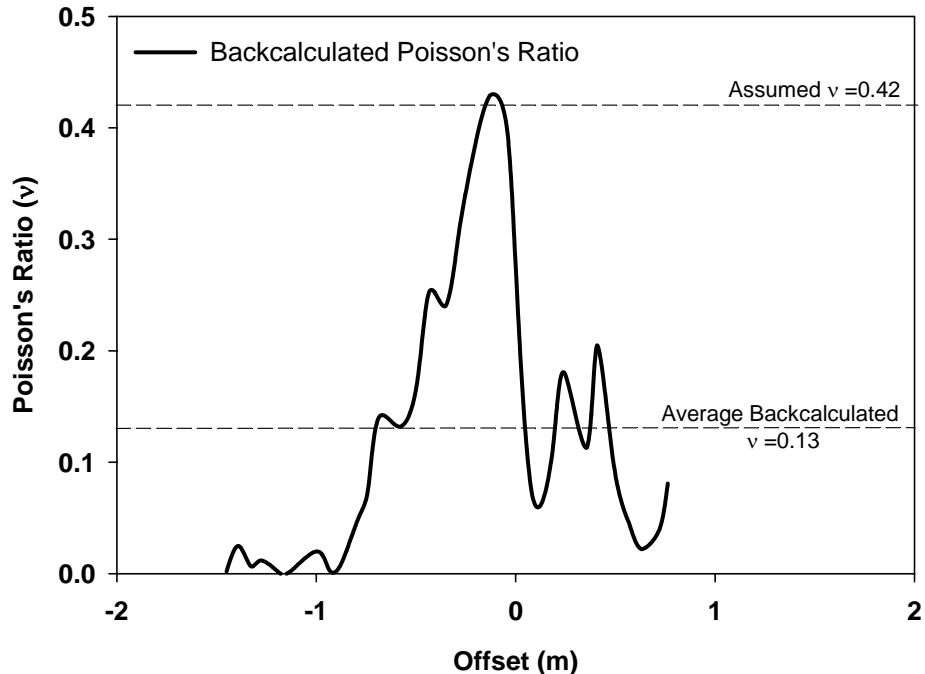
Figure 4.10, Backcalculated Poisson's ratio in Layer 1 using Equation 4.6.

4.4.5 VALIDATION OF THE QUADRATIC MODULUS OF ELASTICITY METHOD

The modulus of elasticity varies vertically and horizontally within the layers of the pavement system as indicated in Figure 4.2 and Figure 4.7 with an average of 55 MPa. In addition, Figure 4.2 indicates that the variation of the modulus can be described by a quadratic relation with depth. In the previous chapter we showed that the quadratic modulus variation with depth can be used to eliminate the stress-strain jump across the interface of the pavement layers. Furthermore, the quadratic modulus variation with depth can be used to describe the modulus variation with depth as a function of temperature.

The modulus of elasticity variation method was applied to all layers above the subgrade using the **MultiSmart3D** program developed by the Advanced Computation and Simulation Group at the University of Akron (**MultiSmart3D**, 2005). The modulus variation within all layers was achieved using 1625 sublayers (a total of 1626 layers including the sugbgrade layer) where the modulus changed smoothly with depth. The ratio of the modulus of elasticity between two consecutive sublayers was kept close to 0.97. The pavement response was calculated at the actual instrument depth at each location (as shown in Table 4.2) after applying a pressure of 500 kPa over a plate with a radius of 0.15 m to simulate the FWD pressure applied at the time of the field test.

Hildebrand (2002) reported the analysis results of the pavement response using different analytical methods and programs including the multilayer elastic theory (BISAR), the method of equivalent thicknesses (MET), nonlinear elastic layered analysis (NELPAV4), and finite element analysis (FeBack). Results from the pavement response at the actual instrument elevation are shown in Table 4.7. It should be noted that the results reported by STX-1.0 pressure gage are not accurate due to malfunctioning of the gage as reported by Hildebrand (2002).

Table 4.7, Stresses (kPa) at the actual instrument location

Instrument	Response	Measured	MultiSmart3D	BISAR	MET	NELAPAV4	FeBack
SRX+1.5	σ_{x*}	3.70	3.64	9.30	11.70	6.40	16.30
SRY-1.0	σ_{y*}	3.40	3.66	9.40	11.70	6.50	16.10
STX-1.0	σ_y	5.80	3.65	9.20	11.70	6.40	16.00
STY+1.5	σ_x	4.60	3.93	9.10	11.80	6.30	16.20
SVX+0.5	σ_{z*}	33.90	34.37	34.40	32.60	31.50	41.60
SVY+0.5	σ_z	34.30	34.37	34.20	32.60	31.30	41.60

The results show that the use of the **MultiSmart3D** program to model the modulus variation with depth can be a very powerful tool for pavement response analysis. The agreement between the calculated stresses and the actual measured stresses was satisfactory for both the horizontal and vertical stresses. As predicted by the sensitivity analysis, the effect of the modulus of elasticity on the vertical stresses is negligible to moderate, depending on the used response model.

The ratio between the calculated stresses using different models and the measured stresses is shown in Figure 4.11. It can be seen that the **MultiSmart3D** calculated vertical and horizontal stresses were approximately 0.85 to 1.08 the measured vertical and horizontal stresses from the full scale test. The use of the average modulus of Layer 1 can overestimate the vertical and horizontal stresses by a factor of 2.76, 3.44, 1.91, and 4.74 using BISAR, MET, NELPAV4, and FeBack, respectively. These significant overestimation factors and the disagreement between the measured and calculated horizontal stresses suggest the importance of considering the modulus variation with depth rather than the average modulus.

On the other hand, incorporating the modulus variation with depth in response models other than the multilayer elastic model can be complex and therefore can limit the wide spread of the use of such accurate modeling. The accuracy of such modeling is largely enhanced and verified using field test results. The accuracy of any response model should consider the accuracy of calculating both the vertical as well as the horizontal stresses since most models can model the vertical stresses with accuracy between –5% and +23% while the accuracy of modeling horizontal stresses can be significantly overestimated by a factor up to 4.74, as shown in Figure 4.11. The simplicity but yet the power of the **MultiSmart3D** program coupled by the quadratic modulus variation with depth can be used by engineers using the same current parameters and therefore highly recommended in any future analysis.
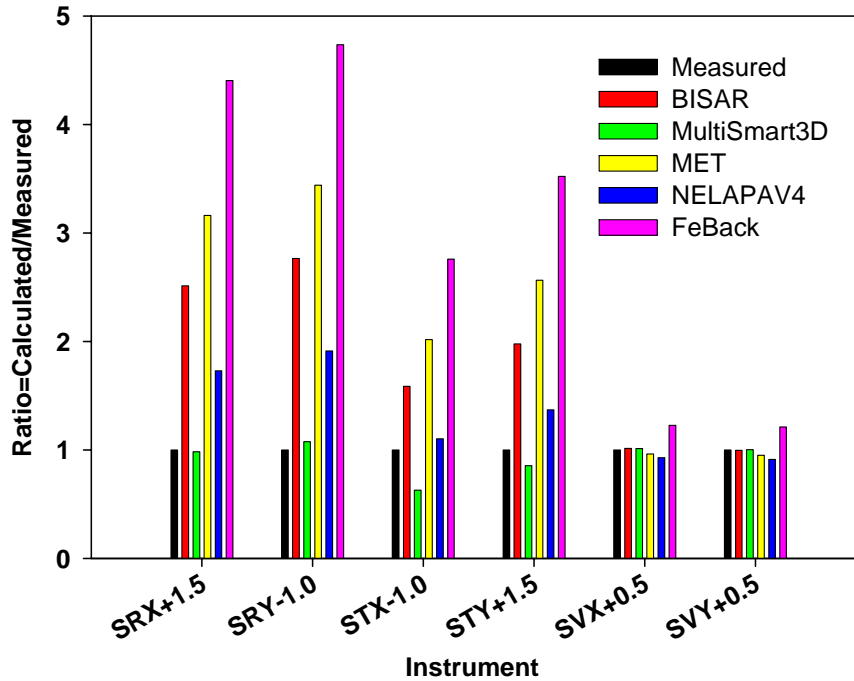
Figure 4.11, Measured and calculated stress comparison

4.5 CONCLUSIONS

Multilayer elastic analysis of flexible pavement systems is a convenient tool since less input parameters are needed in the analysis. However, the accuracy of the calculated response depends largely on the accuracy of the input parameters. The sensitivity analysis indicated that the horizontal stresses and strains are largely affected by the variation of the modulus of elasticity and the Poisson's ratio and hence, the modulus variation should be modeled in order to increase the accuracy of the calculated response. The modulus of elasticity can be backcalculated from the FWD test while, in practice, the Poisson's ratio is assumed rather than backcalculated.

The elastic modulus variation with depth can be easily incorporated into the analysis using the *MultiSmart3D* program since unlimited number of sublayers/layers can be modeled. The modulus variation with depth can be performed by varying the modulus based on the backcalculated or measured moduli with depth or by using the quadratic modulus variation method. The quadratic modulus variation with depth is based on varying the modulus of the elastic layer using a quadratic relation using the layer average modulus and the moduli of the layer above and the layer below as boundary conditions.

Full-scale field test results were used to verify the accuracy of the *MultiSmart3D* program and the power of the quadratic modulus variation method. The measured and calculated horizontal and vertical stress response using the *MultiSmart3D* program showed good agreement while other methods and models showed relatively poor agreement. The variation of the modulus with depth should be considered since the calculated response can largely be affected by averaging the modulus in the layer rather than considering the actual modulus variation with depth.

84

The **MultiSmart3D** program is a superior multilayer elastic program for pavement response. The program is able to model the modulus variation with depth and therefore it can eliminate the limitation of the current multilayer elastic programs that can handle a maximum of 20 elastic layers only. On the other hand, the variation of the modulus with depth by subdividing the elastic layer into several elastic sublayers can be used to consider the nonlinear variation of modulus of elasticity with depth in the elastic layer.

CHAPTER 5

EFFECT OF LOADING CONFIGURATION AND FOOTPRINT GEOMETRY

5.0 INTRODUCTION

Pavement design requires good approximation of the anticipated stresses and strains within the pavement structure. The distribution of the tire contact pressure along the footprint area is very important since the distribution and the magnitude of the contact tire/pavement stresses influence the response of the pavement.

The contact pressures had been measured in the past using pressure transducers at different speeds to understand the factors that affect the tire/pavement contact pressure distribution (de Beer and Fisher, 1997). The results showed that the tire type, tire geometry, applied load, inflation pressure, and vehicle speed, affect the contact pressure distribution and the shape and size of the tire footprint area. For example, increasing the applied load on the tire can increase the pressure along the sides of the footprint area compared to the pressure within the footprint area. In addition, test results (de Beer and Fisher, 1997; Blab, 1999) indicated that, depending on the tire type and structure, reducing the inflation pressure by 50% can increase the footprint area by 42%, while increasing the inflation pressure in the tire by 50% can reduce the footprint area by 33%.

Tire footprint area has been modeled for years using a circular contact area and assuming that the tire/pavement contact stresses are equal to the inflation pressure of the tire. The footprint area is obtained normally by dividing the applied load on the tire by the tire inflation pressure as follows:

$$A_f = F/P$$
Eq. (5.1)

where A_f is the footprint (contact) area, F is the applied load on tire, and P is the tire inflation pressure.

Equation 5.1 indicates that, when assuming a circular footprint area, reducing the inflation pressure by 50% can increase the footprint area by 100% while increasing the inflation pressure by 50% can reduce the footprint area by 33%. This example shows the strong effect of the inflation pressure on the footprint area as conventionally assumed. On the other hand, this example shows that the footprint area using this method can be different than the measured actual footprint area. In addition, test data from Luo and Prozzi (2005) indicated that the difference between the inflation pressure and the average contact stress over the footprint area was 18%, which contradicts the conventional assumption of equal pressures. This difference can be attributed to the distribution of the stresses within the tire itself and the tire carcass. Therefore, the assumption of having full pressure transfer of the tire pressure to the pavement should be further investigated for the benefit of pavement design.

Other typical tire footprint shapes that have been used to simulate the actual contact area are the rectangular and oval contact shapes. The circular shape has been used for decades due to its simplicity when incorporated in any elastic analysis for layered flexible pavement system and

86

the availability of closed form solutions. The rectangular and oval shapes are difficult to incorporate in elastic analysis due to the unmanageable complex expressions in the solution. Accurate selection of the tire contact area is always a challenge due to the difficulty of measuring the contact area for vehicles in motion and due to the wide range of tire types, inflation pressures, and tire boundary conditions such as the applied load, the pavement surface roughness, and the pavement temperature. In addition, simulation tools based on multilayered elastic theory that can be used in flexible pavement analysis are limited to the circular contact shape only while other advanced tools such as the finite element method are available for more complex contact geometries. However, Al-Qadi et *al.* (2004) showed that the size and thickness of the elements in the finite element model largely influenced the analysis results and the associated computation time. No guidelines are available to choose the element size and thickness for pavement analysis and therefore several analysis trials should be carried out to achieve accurate and reasonable results, which can be both time consuming and error susceptible.

Finite element models have been developed using both finite and infinite elements to reduce the computation time of the flexible pavement analysis. Hjelmstad et *al.* (1997) showed that the location of the interface between the finite elements and the infinite elements should be determined based on trial and error and can affect both the computation time and accuracy. On the other hand, the contact pressure collection rate (the interval over which the contact pressure is measured) can increase the time needed to carry out the analysis using finite element models since finer mesh sizes at the surface of the pavement should be used to account for the irregular pressure distribution. Park et *al.* (2005) calibrated the size of the elements in the finite element model both vertically and horizontally using multilayered elastic analysis.

The effect of simplifying the tire contact area and pressure distribution within the contact area using either conventional geometrical shape or uniform pressure distribution should be investigated to provide better understanding of the effect and to provide guidelines for future analysis using the multilayer elastic theory.

5.1 EFFECT OF TIRE CONTACT AREA

The effect of the tire contact area was studied by comparing the pavement response of several contact areas with the response using measured contact area and stresses. The flexible pavement response was calculated using the *MultiSmart3D* program. The *MultiSmart3D* program is a fast and accurate software tool developed by the Computer Modeling and Simulation Group at the University of Akron, and it is based on the innovative computational and mathematical techniques for multilayered elastic systems (Pan, 1989a, 1989b, 1990, 1997). The program is capable of analyzing any pavement system regardless of the number of layers, the thickness of each layer, and the shape of the applied pressure at the surface of the pavement.

The typical flexible pavement section was summarized in Table 5.1 while a summary of the studied cases is shown in Table 5.2. The contact pressure at the surface of the pavement, as shown in Figure 5.1, was measured by Texas Department of Transportation (Luo and Prozzi, 2005). The tire inflation pressure was 690 kPa acting on a circle with a diameter of 220.3 mm while the applied load was 26.3 kN (Luo and Prozzi, 2005). Pavement responses below the center of the contact pressure area were calculated using the *MultiSmart3D* program. The

coordinate system is chosen such that the *x*- and *y*-axes are on the surface of the pavement ($z=0$) whilst the *z*-axis is vertical to the x-y plane and extends along the depth direction.

Table 5.1, Parameters of a typical flexible pavement example

Layer	Thickness (mm)	Resilient Modulus (MPa)	Poisson's Ratio
AC Layer	25.4, 50.8, 76.2, 101.6, 127, 152.4, 177.8, 203.2, 228.6, 254, 279.4, 304.8	3500	0.3
Base Layer	250	700	0.3
Subbase Layer	250	300	0.3
Subgrade Layer	Infinite Half-Space	100	0.3

Table 5.2, Load configurations and footprint geometries

Case No.	Load Configuration	Footprint Geometry
Case 1	Nonuniform-Measured	Irregular
Case 2	Uniform-Tire Pressure	Rectangular
Case 3	Uniform-Tire Pressure	Square
Case 4	Uniform-Tire Pressure	Oval
Case 5	Uniform-Tire Pressure	Circular
Case 6	Uniform-Average Measured	Rectangular
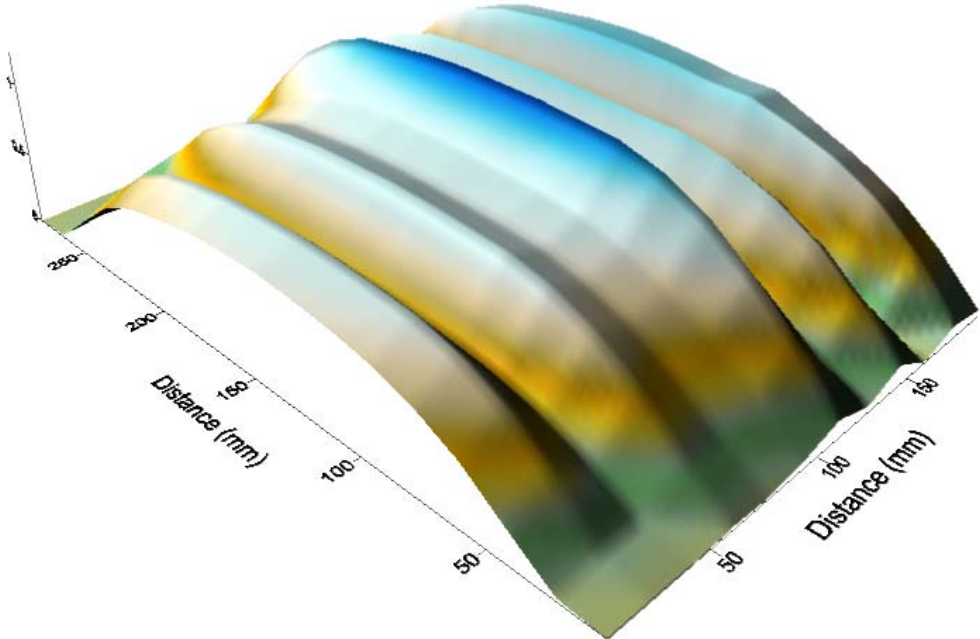
Figure 5.1, Measured nonuniform tire pressure distribution (based on data from Luo and Prozzi, 2005).

The pavement response using the measured contact area with the measured contact pressure (Case 1) was compared to the response using several regular contact areas including circular, rectangular, square, and oval contact areas (Cases 2 through 5). The pressure acting on the regular contact areas was assumed to be equal to the inflation pressure (uniform pressure) of the tire as typically used by engineers while the size of the contact area was controlled by Equation 5.1. In addition, another case (Case 6) was analyzed using the measured contact area but with a uniform pressure distribution equal to the average of the measured nonuniform pressure.

Figure 5.2 shows the dimensions of the studied contact areas. The dimensions of the rectangle were assumed based on the approximation of the dimensions of the measured contact area. The square area was added as a special case of the rectangular contact area when the ratio between the length and width is equal to one. The oval contact area dimensions were suggested by Yoder and Witczak (1974).
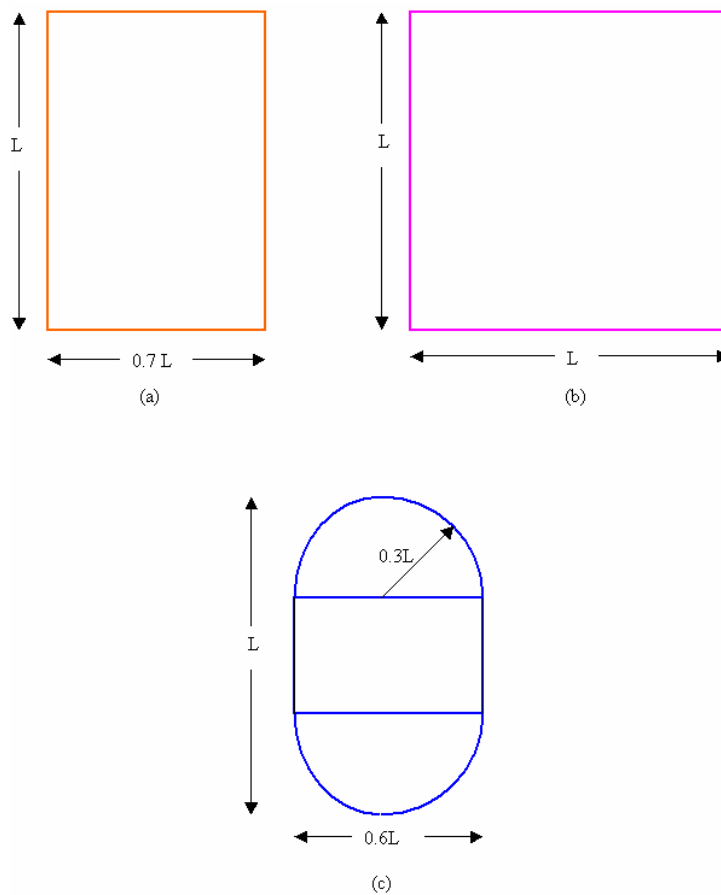
Figure 5.2, Studied contact areas; (a) rectangular (Cases 2 and 6), (b), square (Case 3), and (c) oval (Case 4).

The relation between the dimensions and the contact area for each of the studied shapes is given below:

Square	$L = \sqrt{A_f}$	Eq. (5.2)
Rectangle	$L = \sqrt{1.4286 A_f}$	Eq. (5.3)
Oval	$L = \sqrt{1.9131 A_f}$	Eq. (5.4)

where A_f is the footprint (contact) area as calculated using Equation 5.1,and L is the dimension as shown in Figure 5.2.

In order to study the effect of the contact area shape and pressure distribution on the pavement response, the thickness of the asphalt concrete (AC) layer was varied between 25.4 mm (1 inch) and 304.8 mm (12 inches), as shown in Table 5.1. The studied AC thickness range includes both thin (less than 101.6 mm) and thick pavement layers.

5.2 PAVEMENT FATIGUE PREDICTION

The damage of flexible pavements can be assessed by predicting the number of loads needed to initiate cracks (fatigue cracking). The Shell Model (Bonnaure et *al.,* 1980) and the Asphalt Institute Model (Shook et *al.*, 1982) are frequently used for fatigue cracking in flexible pavements.

The Shell Model is based on two different loading modes, as given by
Shell Constant Strain Model:

$$N_\varepsilon = 13909 A_f K \left(\frac{1}{\varepsilon_t}\right)^5 E_s^{-1.8}$$

Eq. (5.5)

and Shell Constant Stress Model:

$$N_\sigma = A_f K \left(\frac{1}{\varepsilon_t}\right)^5 E_s^{-1.4}$$

Eq. (5.6)

where N_ε and N_σ are the number of load repetitions to fatigue cracking using the constant strain and constant stress analysis, respectively, A_f and K are constants based on the material properties, ε_t is the tensile strain at the critical location and E_s is the stiffness of the material (i.e. resilient modulus). The constant strain model is applicable to thin asphalt pavement layers usually less than 51 mm, whilst the constant stress model is applicable to thick asphalt pavement layers usually more than 203 mm. The Shell Model was calibrated and generalized for any thickness as given below (MEPDG, 2004):

$$N_f = A_f K F'' \left(\frac{1}{\varepsilon_t}\right)^5 E_s^{-1.4}$$

Eq. (5.7)

where N_f is the number of load repetitions to fatigue cracking, F'' is a constant that depends on the layer thickness and the stiffness of the material.

The Asphalt Institute Model is given below:

$$N_f = 0.00432C \left(\frac{1}{\varepsilon_t} \right)^{3.291} \left(\frac{1}{E_s} \right)^{0.854} \qquad \text{Eq. (5.8)}$$

where, similarly, N_f is the number of load repetitions to fatigue cracking, C is a constant depending on the material properties, ε_t is the tensile strain at the critical location and again E_s is the stiffness of the material. The Asphalt Institute Model can be used for any thickness.

It can be seen from the above equations, that the critical tensile strain and the stiffness of the asphalt concrete layer are the main factors affecting the number of load repetitions needed to initiate fatigue failure. The effect of the contact area and pressure distribution on the fatigue in flexible pavements can be studied by finding the ratio between the estimated number of repeated loads (N_f) from the calculated pavement response using the assumed contact area and pressure and that using the measured contact area and pressure. In other words, the ratio is equal to N_f (assumed area and pressure) over N_f (measured area and pressure).

5.3 RUTTING DAMAGE

Rutting in flexible pavement is considered as a functional deterioration. Rutting is mainly predicted by calculating the vertical strains at the top of the subgrade and then estimating the allowable load repetitions until a certain rut threshold is met. For example, Shook et al. (1982) assumed a rut depth of 10 mm in their method, while Potter and Donald (1985) assumed 20-30 mm rut depth.

Recently, the results from the test sections at MnROAD were used to develop a method to predict the number of allowable load repetitions until rutting failure using a rut depth of 13 mm as shown in the following relation (Skok et al., 2003):

$$N_r = (5.5).10^{15} \left(\frac{1}{\varepsilon_v} \right)^{3.929} \qquad \text{Eq. (5.9)}$$

where N_r is the number of allowable load repetitions until rutting failure, and ε_v is the maximum compressive strain at the top of the subgrade layer.

It can be seen, from the above equation, that the vertical strain at the top of the subgrade layer is very important to predict the lifetime of the pavement due to rutting. Similar to the fatigue case, the effect of the contact area and pressure distribution on the rutting can be studied by finding the ratio between the estimated number of repeated loads (N_r) from the calculated pavement response using the assumed contact area and pressure and that using the measured contact area and pressure. In other words, the ratio is equal to N_r (assumed area and pressure) over N_r (measured area and pressure).

5.4 PAVEMENT RESPONSE

The pavement response was studied for different cases as summarized in Table 5.1 using different loading and footprint configurations. In order to study the variation of the pavement response under different conditions the analysis results for the 50.8 mm AC layer (2 inches AC layer) and the 203.2 mm (8 inches AC layer) are shown in Figures 5.3 and 5.4.

It can be seen from Figure 5.3 that the variation of the horizontal and vertical strains is linear with depth in the thin AC layer (Figures 5.3(a,b)) while it is nonlinear in the thick AC layer (Figures 5.3(c,d)) regardless of the loading configuration and footprint geometry. However, the selection of the loading configuration and footprint geometry tends to affect the calculated strains within the AC layer. The use of any footprint geometry or load configuration other than the measured ones underestimated the vertical and horizontal strains at the top and bottom of the thin AC layer (Figure 5.3(a)) while it overestimated the horizontal strain at the top of the thick AC layer (Figure 5.3(c)) and underestimated the horizontal strains at the bottom of the thick AC layer. The vertical strains in the thick AC layer (Figure 5.3(d)) were always underestimated using the assumed geometries and loading configurations. In addition, increasing the AC layer thickness decreased the horizontal strains in the AC layer while it increased the vertical strains at the top of the AC layer and decreased the vertical strains at the bottom of the layer. These findings indicate that by increasing the AC layer thickness more strains are distributed within the AC layer while less strain is transferred to the underlying layers. On the other hand, the observations indicate that fatigue cracking in thin AC layers starts faster in thin AC layers compared to thick layers.

It also can be seen that the measured load configuration and footprint area resulted in compressive strains at the top and bottom of the thin AC layer while all other cases produced tensile vertical strains at the top of the thin AC layer and compressive vertical strains at the bottom of the thin AC layer (Figure 5.3(b)). However, this contradiction is not observed in the thick AC layer when the measured load configuration and footprint area are not used in the analysis (Figure 3(d)).

92
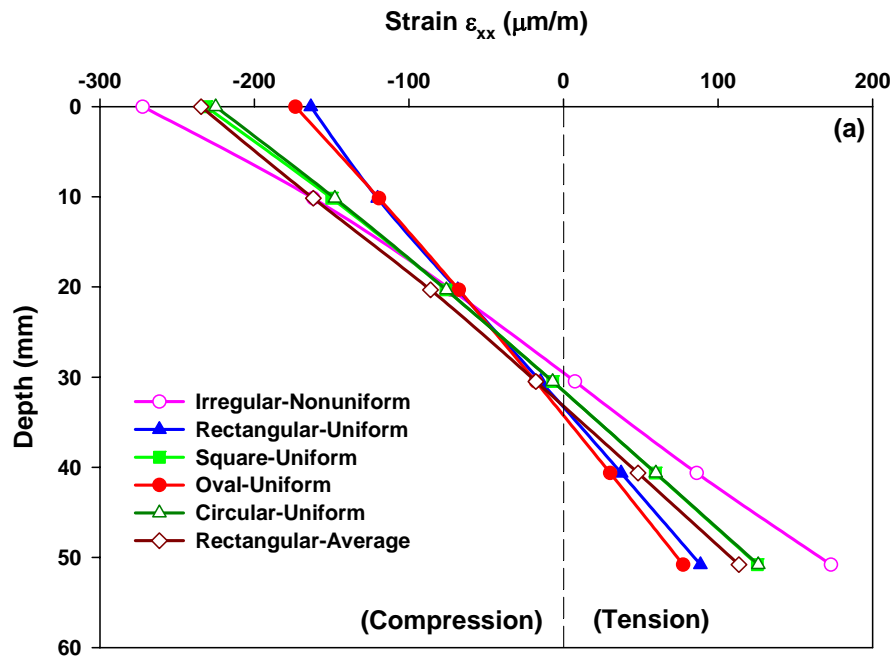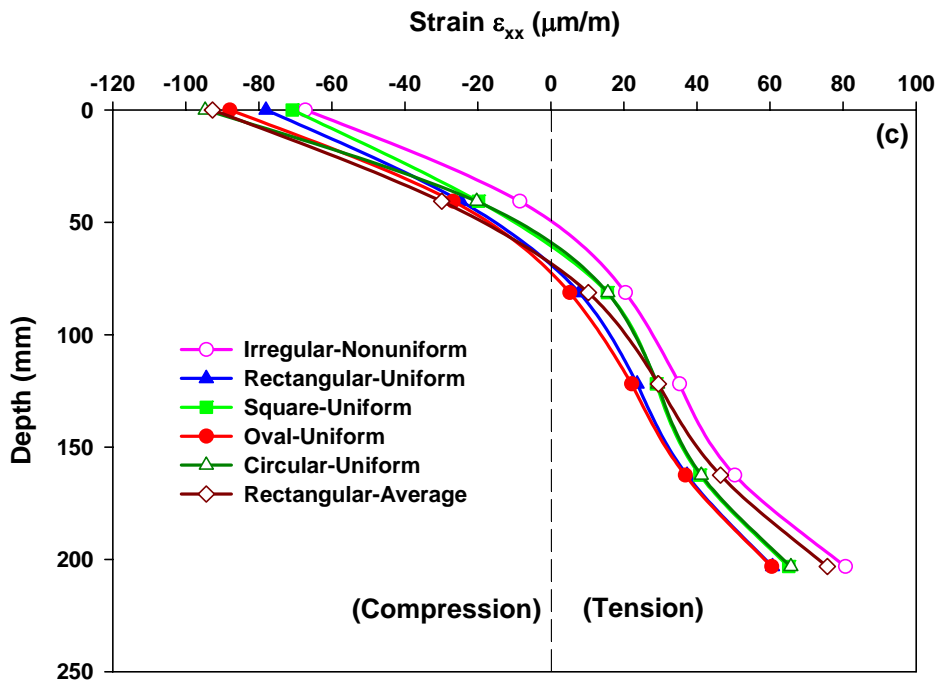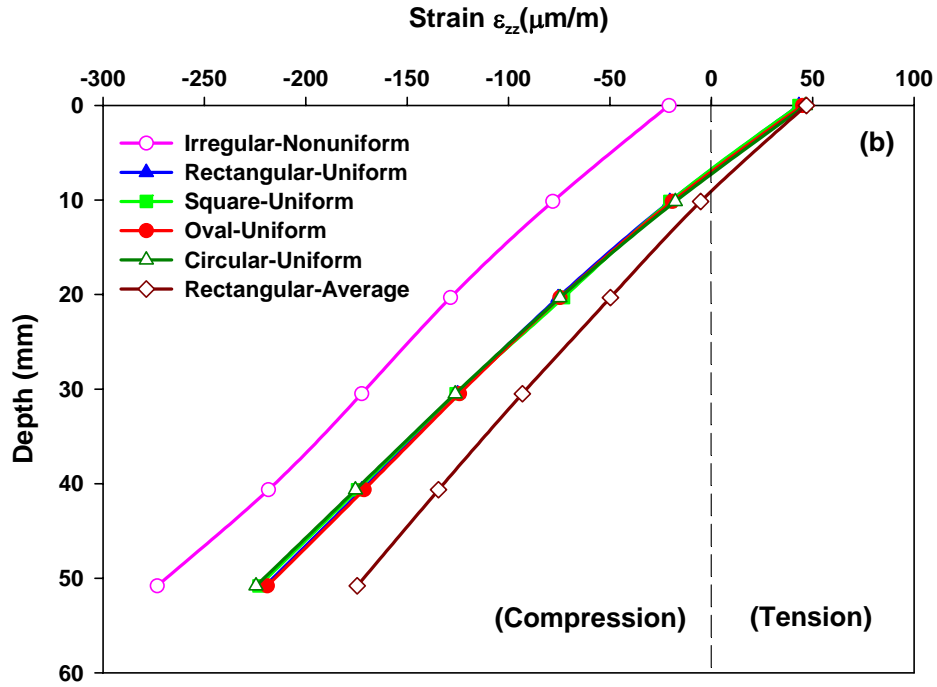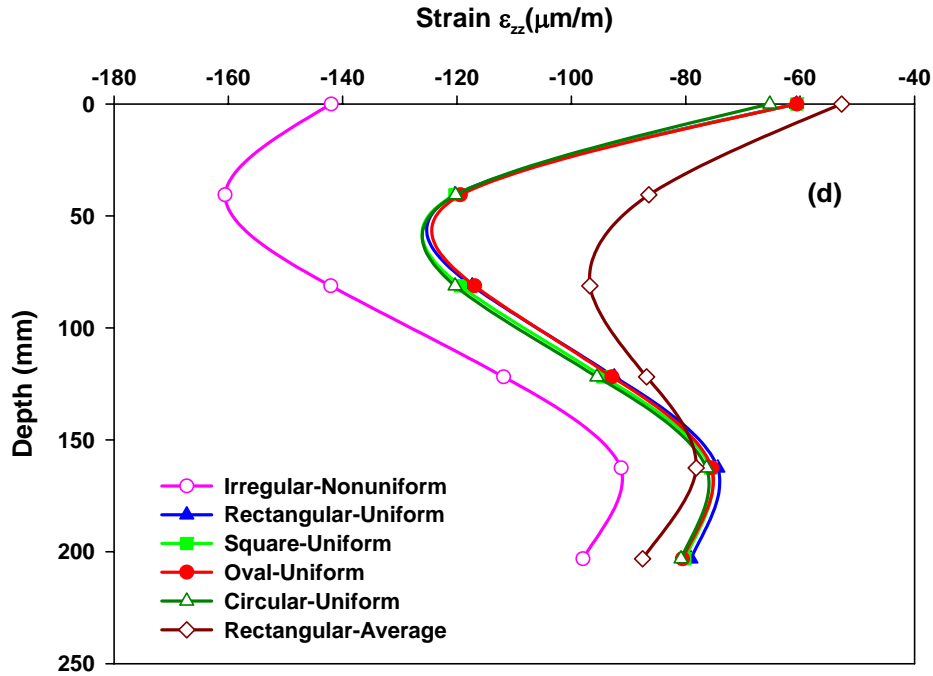
Figure 5.3, Pavement response under different pressures and loading areas in a 50.8 mm AC layer: (a) horizontal strain ε_{xx}, (b) vertical strain ε_{zz}; and a 203.2 mm AC layer: (c) horizontal strain ε_{xx}, (d) vertical strain ε_{zz}.

Stress σ_{zz} (MPa)

(b)

Legend:
- Irregular-Nonuniform
- Rectangular-Uniform
- Square-Uniform
- Oval-Uniform
- Circular-Uniform
- Rectangular-Average

Stress σ_{xx} (MPa)

(c)

Legend:
- Irregular-Nonuniform
- Rectangular-Uniform
- Square-Uniform
- Oval-Uniform
- Circular-Uniform
- Rectangular-Average

(Compression) | (Tension)
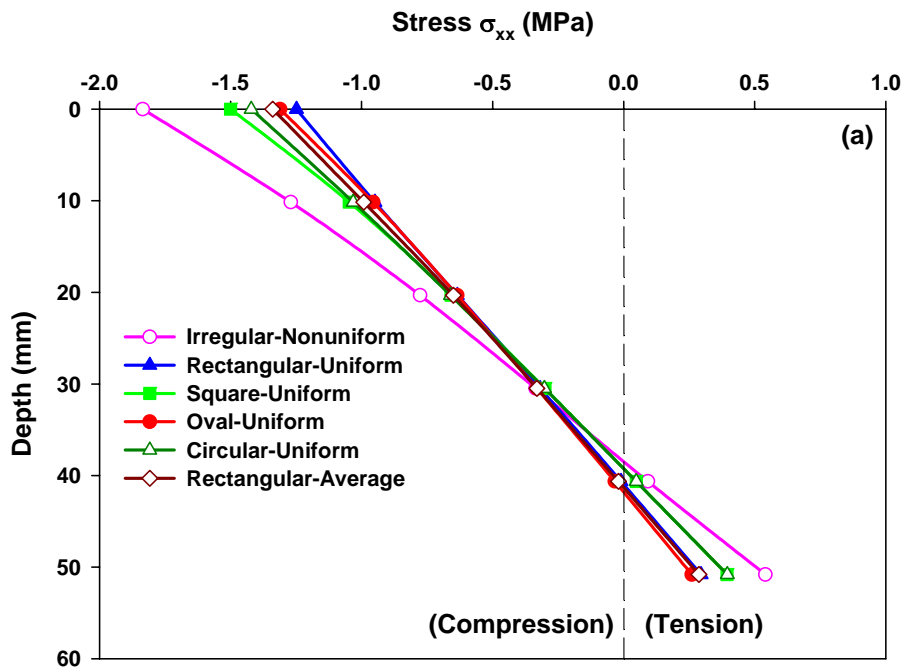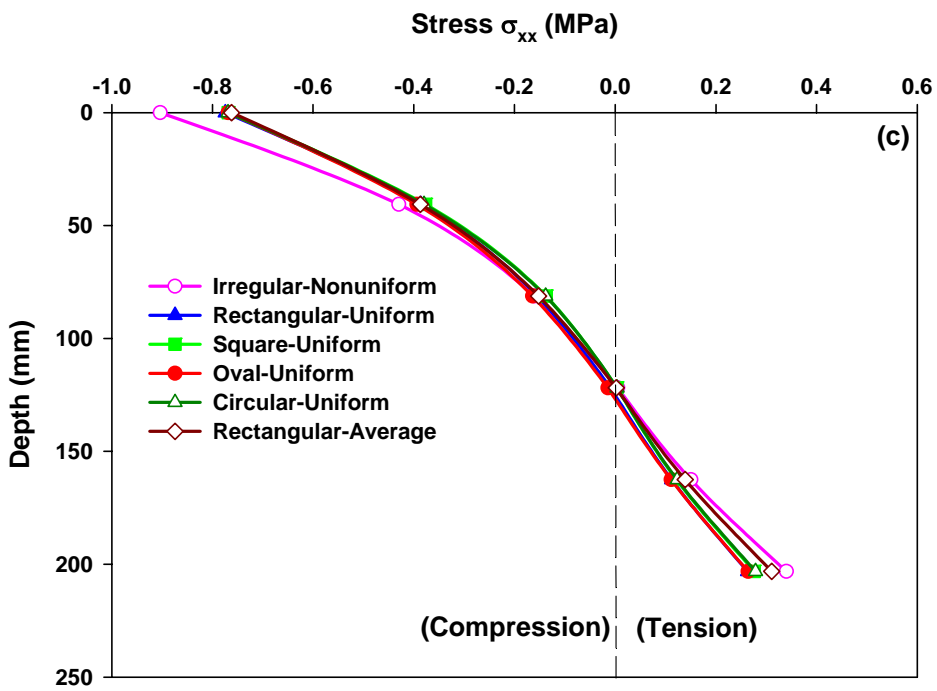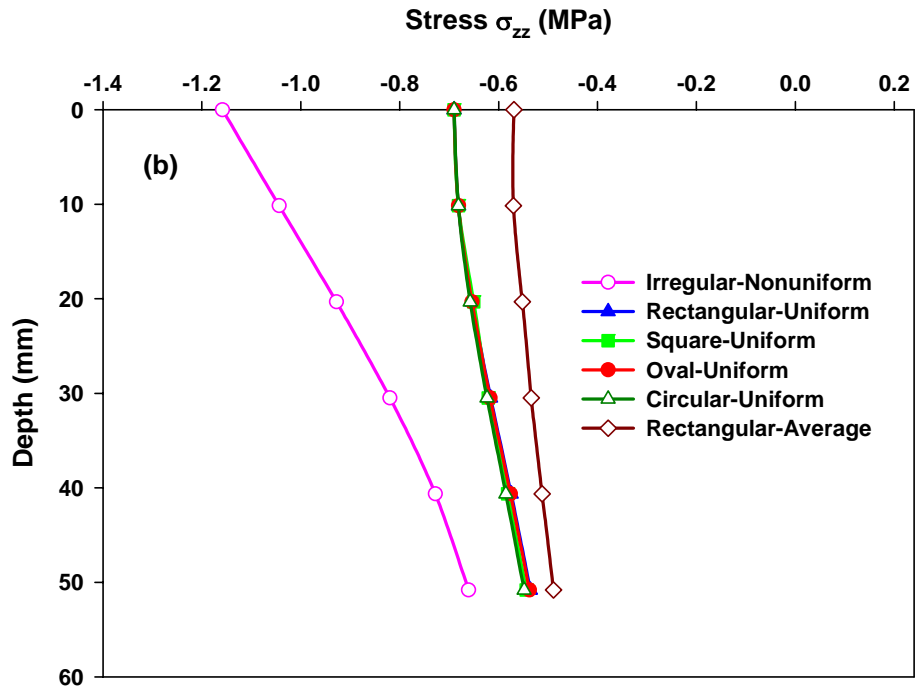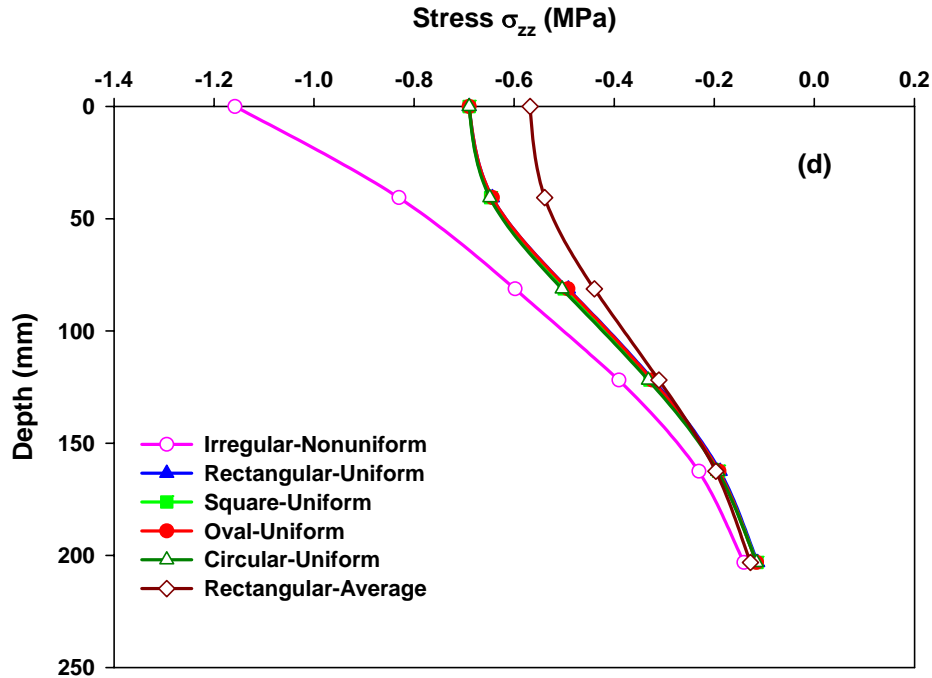
Figure 5.4, Pavement response under different pressures and loading areas in a 50.8 mm AC layer: (a) horizontal stress σ_{xx}, (b) vertical stress σ_{zz}; and a 203.2 mm AC layer: (c) horizontal stress σ_{xx}, (d) vertical stress σ_{zz}.

In general, the use of different footprint areas in Cases 2 through 5 showed negligible effect on the vertical strain regardless of the thickness of the AC layer when compared to each other while showed variation when compared to Cases 1 and 6. However, the effect of the footprint area was more pronounced on the horizontal strains. It can be seen from Figures 5.3(a,c) that none of the assumed cases (Cases 2 through 6) was able to produce reasonable strains compared to Case 1. On the other hand, the use of the average measured pressure as the contact pressure (Case 6) always underestimated the strains except at the top half of the thick AC layer where horizontal strains were higher than other cases but lower than the strains using the circular footprint area.

Figure 5.4 show the variation of the horizontal (Figures 5.4(a,c)) and vertical (Figures 5.4(b,d)) stresses for Cases 1 through 6 in thin and thick AC layers. The results indicate that Cases 2 through 5 produced relatively the same vertical stresses compared to each other while Case 6 produced different vertical stresses since the average measured contact pressure (569 kPa) in Case 6 was less than the tire pressure (690 kPa). However, the effect of the loading configuration and footprint area on the vertical stresses decreases as the depth in the thick AC layer increases.

The effect of the loading configuration and footprint area showed negligible effect on the horizontal stresses in the thick AC layer while it showed relative variations at the top of the thin AC layer. In all cases, the assumed load configuration and footprint area failed to produce reasonable results compared to those calculated using the measured loads and geometry.

The effect of the AC layer thickness on the response of the underlying layers was shown in Figures 5.5 and 5.6 using Case 1. These figures show, as anticipated, that more strains are transferred to the underlying layers through the AC layer as the thickness of the AC layer decreases. However, in thin AC layers the vertical strains increase with depth within the AC layer then decrease in the underlying layers (base, subbase, and subgrade layers) which can be attributed to the relatively low rigidity of the thin AC layer compared to the underlying layer. In general, the horizontal strains decreased with depth as the thickness of the AC layer increased.

Understanding the variation of the horizontal strains at the bottom of the AC layer will help in understanding the effect of the calculated strains on the fatigue cracking prediction using Equations 5.7 and 5.8. As it can be seen in Figure 5.7, the horizontal strain at the bottom of the AC layer increases as the thickness of the AC layer increases to an optimum point then decreases as the thickness increases regardless of the case configuration. However, the selection of the loading configuration and the geometry influences the mechanical response along the bottom of the thin AC layers. Figure 5.7 shows that the horizontal strains at the bottom of the 25.4 mm AC layer are compressive when using Cases 2, 4, and 6 while they are tensile when using the other cases indicating the invalidity of using Cases 2, 4, and 6 to study the pavement response in thin AC layers for fatigue cracking purposes and shows the importance of the loading and geometry configuration in pavement analysis. On the other hand, for AC layers larger than 152.4 mm (6 inches), Case 6 showed relatively close agreement (less than 9% difference) with Case 1 (measured case). For all cases, the horizontal strains at the bottom of the AC layer were underestimated compared to Case 1.
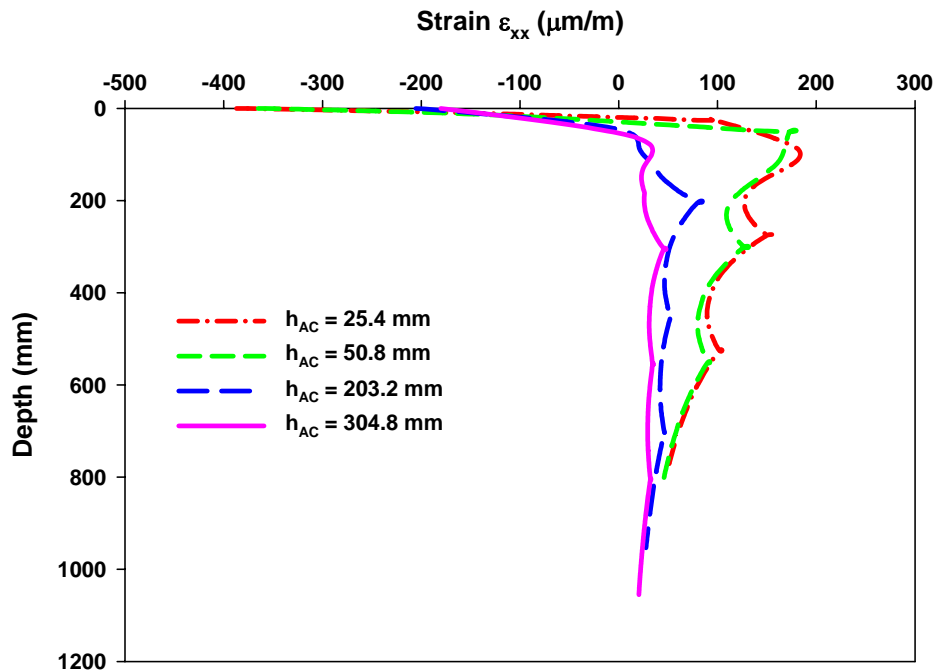
Figure 5.5, Horizontal strain ε_{xx} under the measured load and footprint area for different AC layer thicknesses.
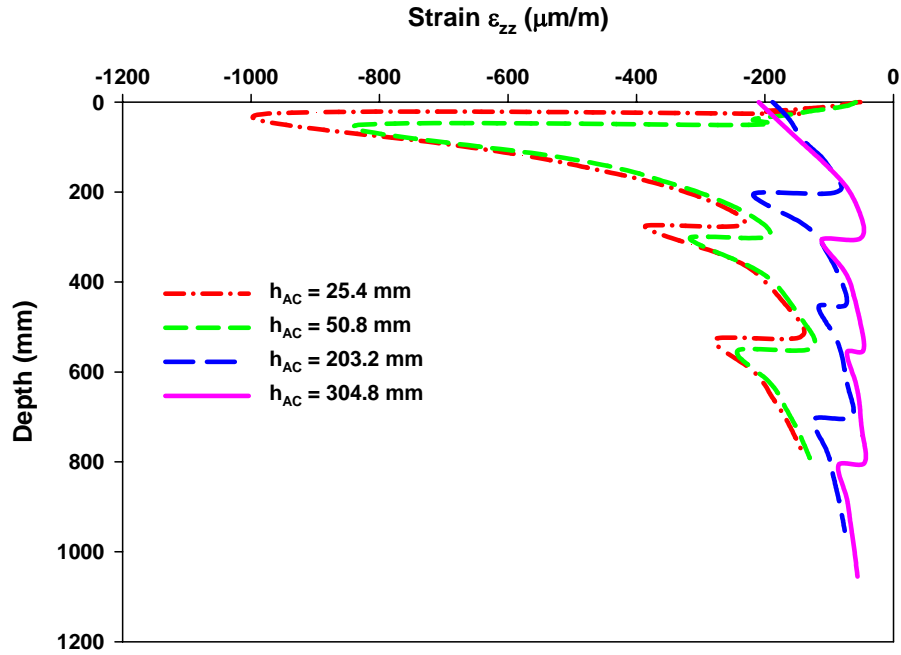
Figure 5.6, Vertical strain ε_{zz} under the measured load and footprint area for different AC layer thicknesses.
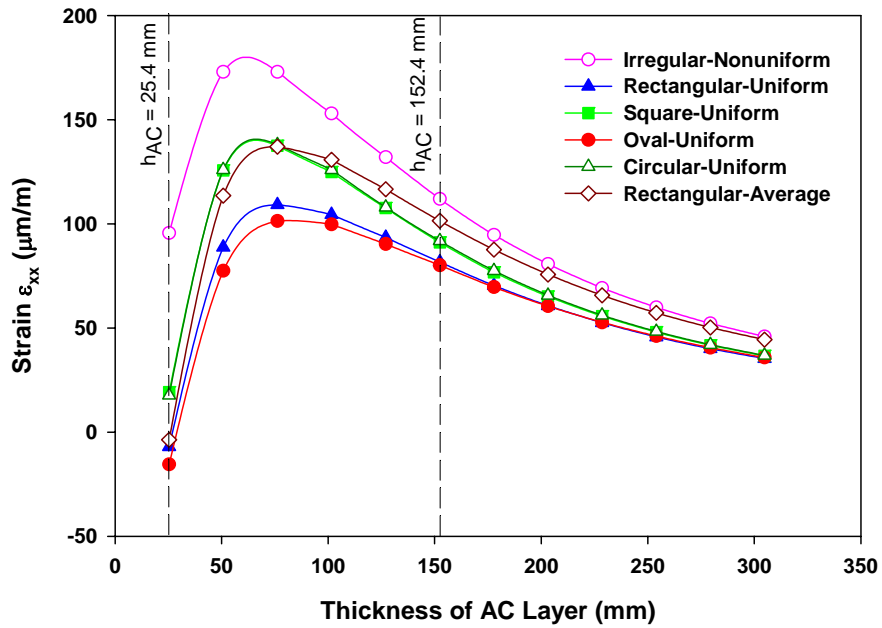

Figure 5.7, Horizontal strain ε_{xx} at the bottom of the AC layer as a function of the AC layer thickness and the loading condition.

The effect of the calculated horizontal strains on the prediction of the number of load repetitions (N_f) fatigue cracking is shown in Figures 5.8 and 5.9. The results show that the

selection of the loading configuration and geometry largely affect the predicted N_f value. The figures show that as the thickness of the AC layer increases the ratio between N_f values using Cases 2 through 6 and using Case 1 decreases. In addition, the figures indicate that the selection of the loading configuration and geometry can overpredict the fatigue life of the pavement by a factor of 56 in thin AC layers and by a factor of 7 in thick AC layers using the Shell Model. Using the Asphalt Institute Model, the fatigue life can be overpredicted by a factor of 14 in thin AC layers and a factor of 4 for thick AC layers when Cases 2 through 6 are used. It should be noted that Figures 5.8 and 5.9 do not show the ratio for the 25.4 mm AC layer due to the invalidity of using compression strains to predict fatigue.
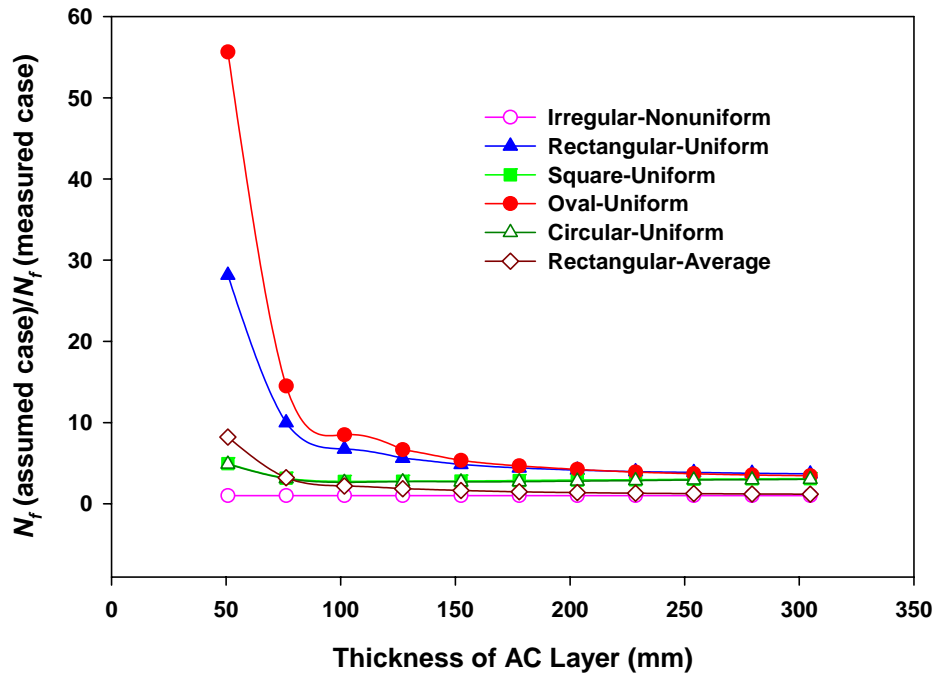
Figure 5.8, Ratio between the estimated number of repeated loads needed for fatigue failure using the measured pressure and area, and the assumed pressure and area (Shell Model).

As anticipated, the vertical strain at the top of the subgrade layer decreases with the increase of the AC layer thickness regardless of the load configuration and geometry, as shown in Figure 5.10. The results show that the vertical strains decrease as the thickness of the AC layer decreases. The conventional use of the circular footprint with the tire inflation pressure (Case 5) always underestimated the vertical strains at the top of the subgrade layer while the use of the rectangular footprint with the average contact pressure (Case 6) showed, relatively, the best agreement with the strains from Case 1. Figure 5.11 shows that the calculated life for rutting using Case 6 was overpredicted only by 3% to 8% while other cases overpredicted the calculated life of rutting by factors of 2.3 (Case 2), 2.6 (Case 3), 2.6 (Case 4), and 6.6 (Case 5).
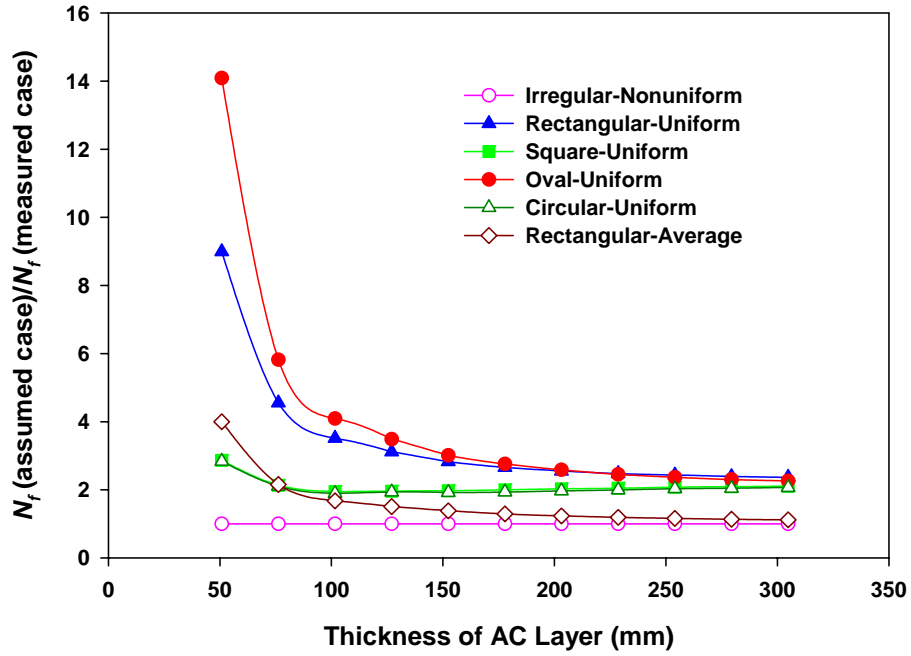
Figure 5.9, Ratio between the estimated number of repeated loads needed for fatigue failure using the measured pressure and area, and the assumed pressure and area (Asphalt Institute Model).
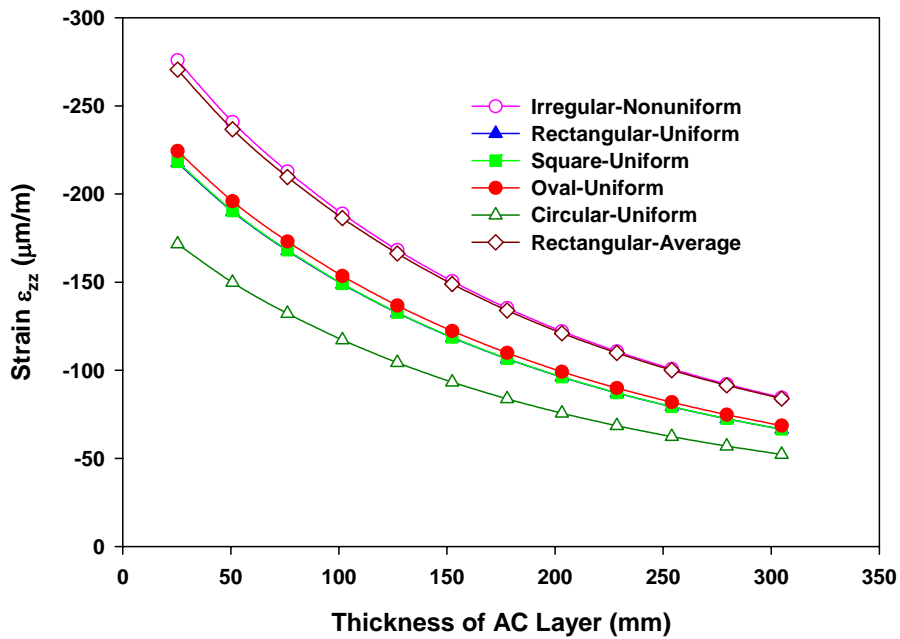
Figure 5.10, Vertical strain ε_{zz} at the top of the subgrade as a function of the AC layer thickness and the loading condition.
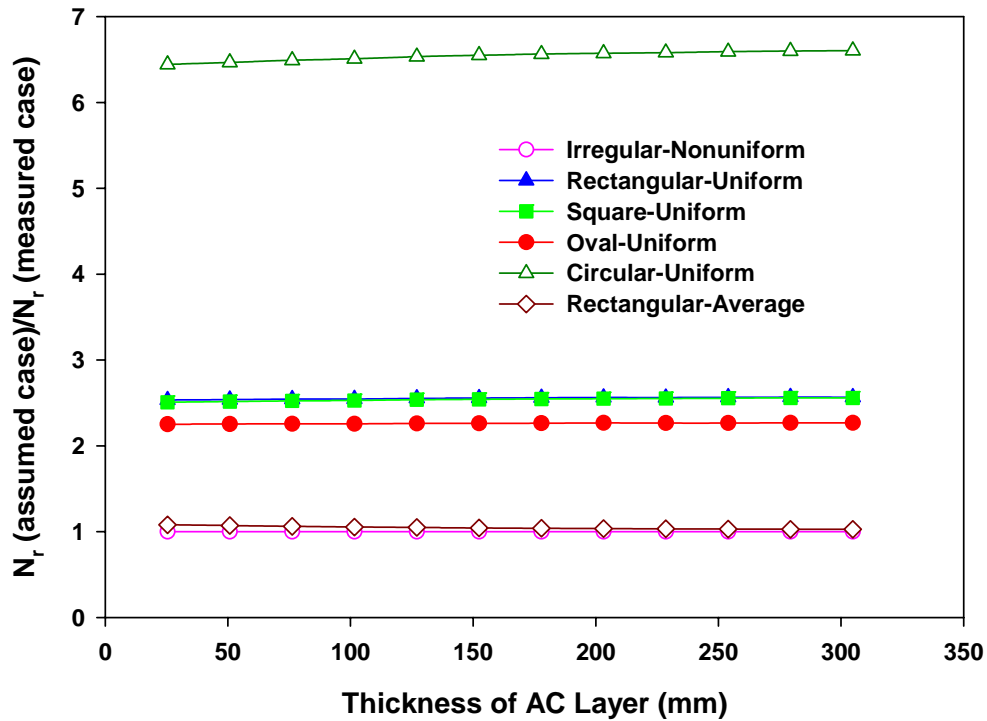
Figure 5.11, Ratio between the estimated number of repeated loads needed for rutting using the measured pressure and area, and the assumed pressure and area.

5.5 CONCLUSIONS

Flexible pavement design and analysis depends largely on analysis performed using multilayered elastic programs. These programs are used normally to analyze circular loaded areas to simulate the tire/pavement contact area (tire footprint) due to limitations in the programs to simulate actual footprint geometries and hence the reliability of the calculated pavement response should be verified. The **MultiSmart3D** program is a powerful multilayered program that can be used for any arbitrary number of elastic layers and footprint geometry. The program was used to study the effect of the loading configuration and footprint geometry on the pavement response by varying the thickness of the AC layer.

The results of the analysis showed that the conventional footprint geometries and pressure assumptions (contact pressure is equal to tire pressure) can overpredict the fatigue life and the rutting life of flexible pavements. In addition, the response of the pavement system can be largely influenced by the selection of the footprint as well as the loading configuration.

It should be noted that the presented results are applicable for this example only and variation in results is anticipated for measured loading configurations and geometries and therefore powerful computational tools such as the **MultiSmart3D** program should be used when applicable to calculate reliable pavement responses.

101

CHAPTER 6

RESPONSE OF PAVEMENT UNDER MULTIPLE LOADING CONFIGURATIONS

6.0 INTRODUCTION

In pavement design, loading configuration is of great importance since the primary goal for pavement engineering is to carry traffic load. Good modeling of loading can predict more accurate stresses and strains within the pavement structure, and hence more reliable lifetime expectance.

Generally speaking, loading configuration consists of tire loads, axle and tire configurations, load repetition, traffic distribution across the pavement, and vehicle speed. While the effect of tire loads, including contact pressure and area, is of concern, which has been discussed in detail in previous chapters, the effect of load repetition, traffic distribution and vehicle speed are other issues beyond the scope of this project, and, therefore, will not be discussed in this exploratory study. The effect of the configuration of axle and tire on the responses of pavement is the focus of the present study.

The configuration of axle and tire, such as the contact number per vehicle and the corresponding spacing, is very critical in pavement analysis and design because it can directly influence the pavement response, failure, and lifetime expectance. Every vehicle has its specific configuration. For example, for specific multiple tires connected by axles, with the tires or axles getting closer, the influence of every single tire or axle on the pavement structure will overlap. As such the responses of the concerned points cannot be simply derived from single load but require the combination of these interactive loads.

6.1 LOAD QUANTIFICATION

Generally speaking the vehicles that a pavement encounters are different one by one, and modeling these different vehicles has always been a challenge in pavement engineering. It is found that although vehicles are different they still share something in common. For example the number of tires and axles are limited, thus based on the vehicles' configurations, they can be classified into 13 classes, as shown in Figure 6.1 (by FHWA as in http://www.sarasota-manateempo.org/Figures/figure1.pdf) and defined as:

Class 1- **Motorcycles:** All two- or three-wheeled motorized vehicles. Typical vehicles in this category have saddle type seats and are steered by handle bars rather than wheels. This category includes motorcycles, motor scooters, mopeds, motor-powered bicycles, and three-wheeled motorcycles.

Class 2- **Passenger Cars:** All sedans, coupes, and station wagons manufactured primarily for the purpose of carrying passengers and including those passenger cars pulling recreational or other light trailers.

Figure 1
FHWA VEHICLE CLASSIFICATION

CLASS GROUP		DESCRIPTION	NO. OF AXLES
1		MOTORCYCLES	2
2		ALL CARS CARS	2
		CARS W/ 1-AXLE TRAILER	3
		CARS W/ 2-AXLE TRAILER	4
3		PICK-UPS & VANS 1 & 2 AXLE TRAILERS	2, 3, & 4
4		BUSES	2 & 3
5		2-AXLE, SINGLE UNIT	2
6		3-AXLE, SINGLE UNIT	3
7		4-AXLE, SINGLE UNIT	4
8		2-AXLE, TRACTOR, 1-AXLE TRAILER (2&1)	3
		2-AXLE, TRACTOR, 2-AXLE TRAILER (2&2)	4
		3-AXLE, TRACTOR, 1-AXLE TRAILER (3&1)	4
9		3-AXLE, TRACTOR, 2-AXLE TRAILER (3&2)	5
		3-AXLE, TRUCK W/ 2-AXLE TRAILER	5
10		TRACTOR W/ SINGLE TRAILER	6 & 7
11		5-AXLE MULTI-TRAILER	5
12		6-AXLE MULTI-TRAILER	6
13	ANY 7 OR MORE AXLE		7 or more
14	NOT USED		
15	UNKNOWN VEHICLE TYPE		
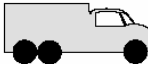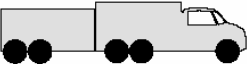
HEAVY TRUCKS

Figure 6.1, FHWA vehicle classification.

103

Class 3- **Other Two-Axle, Four-Tire, Single Unit Vehicles:** All two-axle, four-tire, vehicles other than passenger cars. Included in this classification are pickups, panels, vans, and other vehicles such as campers, motor homes, ambulances, hearses, carryalls, and minibuses. Other two-axle, four-tire single unit vehicles pulling recreational or other light trailers are included in this classification.

Class 4- **Buses:** All vehicles manufactured as traditional passenger-carrying buses with two axles and six tires or three or more axles. This category includes only traditional buses (including school buses) functioning as passenger-carrying vehicles. Modified buses should be considered to be trucks and be appropriately classified.

> **Note:** In reporting information on trucks the following criteria should be used:
> **a**. Truck tractor units traveling without a trailer will be considered as single unit truck.
> **b**. A truck tractor unit pulling other such units in a "saddle mount" configuration will be considered as one single unit truck and will be defined only by axles on the pulling unit.
> **c**. Vehicles shall be defined by the number of axles in contact with the roadway. Therefore, "floating" axles are counted only when they are in the down position.
> **d**. The term "trailer" includes both semi- and full trailers.

Class 5- **Two-Axle, Six-Tire, Single Unit Trucks:** All vehicles on a single frame including trucks, camping and recreational vehicles, motor homes, etc., having two axles and dual rear wheels.

Class 6- **Three-axle Single unit Trucks:** All vehicles on a single frame including trucks, camping and recreational vehicles, motor homes, etc., having three axles.

Class 7- **Four or More Axle Single Unit Trucks:** All trucks on a single frame with four or more axles.

Class 8- **Four or Less Axle Single Trailer Trucks:** All vehicles with four or less axles consisting of two units, one of which is a tractor or straight truck power unit.

Class 9- **Five-Axle Single Trailer Trucks:** All five-axle vehicles consisting of two units, one of which is a tractor or straight truck power unit.

Class 10- **Six or More Axle Single Trailer Trucks:** All vehicles with six or more axles consisting of two units, one of which is a tractor or straight truck power unit.

Class 11- **Five or Less Axle Multi-Trailer Trucks:** All vehicles with five or less axles consisting of three or more units, one of which is a tractor or straight truck power unit.

. Class 12- **Six-Axle Multi-Trailer Trucks:** All six-axle vehicles consisting of three or more units, one of which is a tractor or straight truck power unit.

Class 13- **Seven or More Axle Multi-Trailer Trucks:** All vehicles with seven or more axles consisting of three or more units, one of which is a tractor or straight truck power unit.

Besides the listed 13 classes clearly defined by FHWA, some states also defined the following two classes. For instance, ODOT has the following definitions for Classes 14 and 15:
Class 14- **Will be defined by ODOT personnel for special studies**.

Class 15- **Will, by default, identify any vehicle which does not conform to the classification criteria for Class 1 through Class 14**.

Based on the vehicle classification, the load a pavement encounters in its design life can be quantified using several methods.

6.1.1 EQUIVALENT SINGLE AXLE LOADS (ESALS)

In this load quantification method, the loads with various magnitudes and repetitions are converted into an equivalent number of "standard" or "equivalent" loads based on the amount of damage they induced to the pavement. The commonly used standard load is the 18,000 lb equivalent single axle load. Using this method, all loads (including multi-axle loads) are converted into an equivalent number of 18,000 lb single axle loads. A "load equivalency factor" represents the equivalent number of ESALs for the given weight-axle combination. In existing AASHTO empirical pavement design method, the axle weights and frequencies would be converted into ESALs using fourth power law. Figure 6.2 shows the corresponding load equivalency factor of the FHWA vehicles classification.
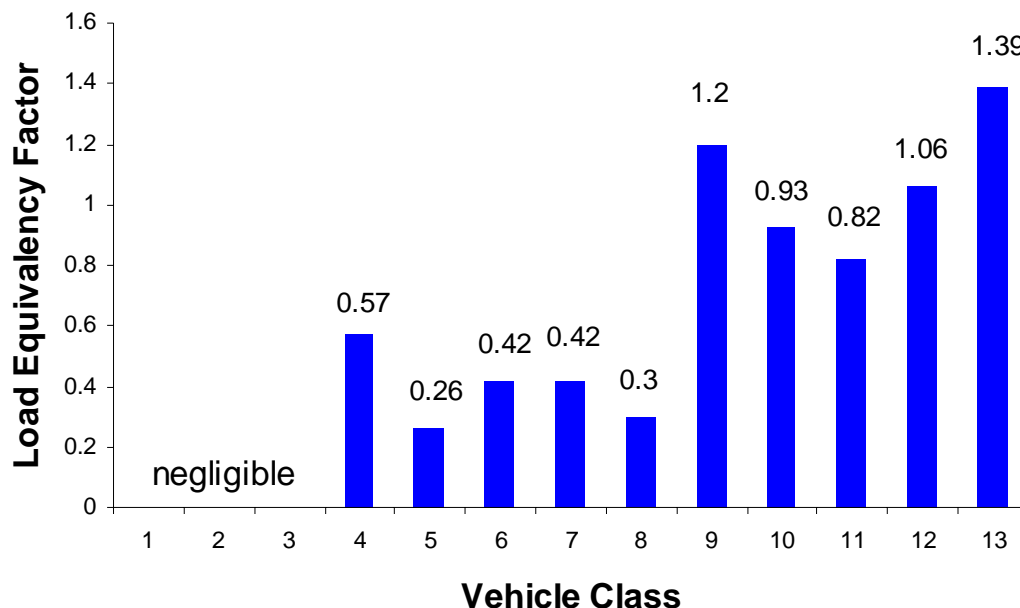

Figure 6.2, The ESALs of FHWA Vehicle Classification

6.1.2 TRAFFIC INDEX (TI)

This load quantification method is associated with the California method of pavement structural design. The traffic index or TI is to express ESALs in terms of an exponential formula. Figure 6.3 illustrates the variation of TI with ESALs.


$$TI = 9 \left(\frac{ESALs}{10^6} \right)^{0.119}$$
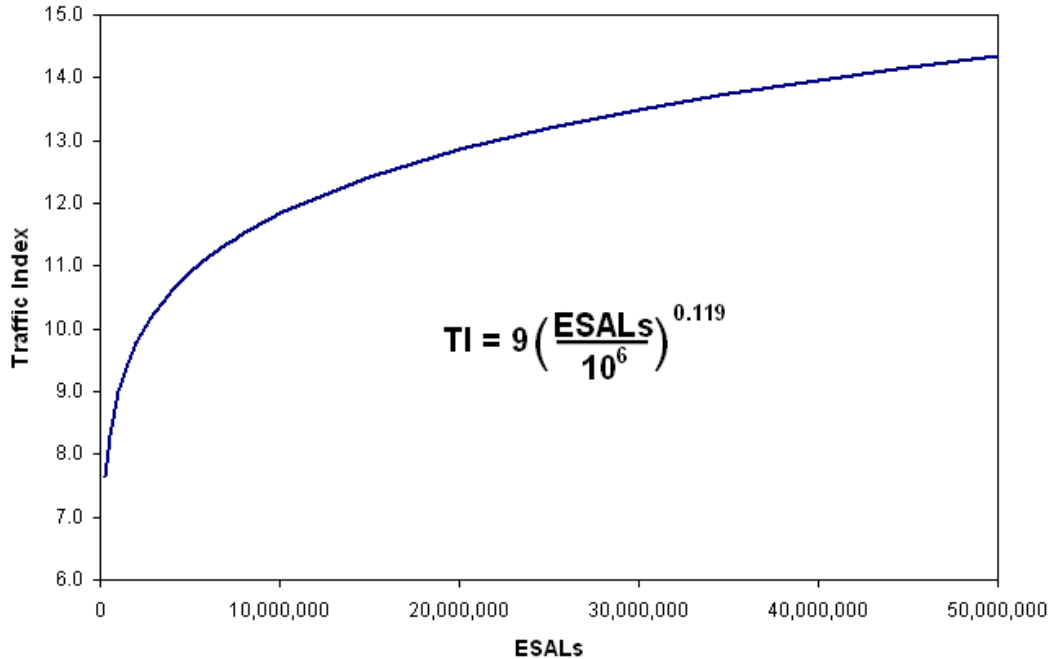
Figure 6.3, The Traffic Index with the variation of ESALs

6.1.3 LOAD SPECTRA

In the new pavement design guide MEPDG, the traffic loads are expressed in the form of load spectra, which is more complicated than the ESALs or TI method. This method requires detailed information on truck traffic volume, temporal variation (hourly, daily, monthly), vehicle class distribution, axle load distribution and axle configuration. According to the design requirements, this information is classified into 3 different levels: level 1 for site specific information, level 2 for regional information and level 3 for default information. The MEPDG stated that the data elements to describe the configuration of typical tire and axle loads can be obtained either directly from manufacturers databases or measured in the field. On the other hand, MEPDG also assumed default values for some of the input information. For example, the average axle width is assumed to be 8.5 inches for typical trucks, typical dual tire spacing for trucks is 12in, average axle spacing is 51.6 inches for tandem and 49.2 inches for tridem and quad axles, and 12, 15, 18 ft for short, medium, and long axle spacing, respectively.

It should be stressed that whether default values or site specific values are used in the pavement design, the responses using load spectra, especially in the loading area will differ from those using ESALs and TI methods. In this exploratory research, the responses of the pavement to multiple loads are calculated using our *MultiSmart3D* program.

106

6.2 MULTIPLE LOADS APPLICATION

An example provided by ODOT was carried out using our **MultiSmart3D** program. The typical flexible pavement section and the load configuration are summarized, respectively, in Tables 6.1 and 6.2. The contact pressure at the surface of the pavement was 125.00psi acting on a circle with a diameter of 4.072in. It should be noticed that these 20 loads belong to a single vehicle which can be viewed as class 14 or 15 defined by ODOT. The coordinate system is chosen such that the *x*- and *y*-axes are on the surface of the pavement (*z*=0) whilst the *z*-axis is vertical to the x-y plane and extends along the depth direction.

Table 6.1, Parameters of the flexible pavement in ODOT example

Layer	Thickness (in)	Resilient Modulus (ksi)	Poisson's Ratio
AC Layer	18.000	350.00	0.35
Base Layer	6.000	30.00	0.35
Subgrade Layer	Infinite Half-Space	4.80	0.44

The responses of the pavement at 8 locations (in inch), i.e., (x,y)= (43.500,59.000), (47.750,59.000), (59.250,59.000), (114.000,59.000), (118.250,59.000), (124.000,59.000), (114.000,118.000), and (124.000,118.000) are calculated. At each location, the Washington State's pavement software, **Everstress5.0**, is also used to calculate the results at 5 specific depths, 17.999, 21.000, 24.000, 0.000, and 18.200 (in).

Figures 6.4 to 6.6 show the variation of displacement, stress, and strain at location (43.500,59.000) along the depth. It is shown that the numerical result by our **MultiSmart3D** program and Everstress5.0 agree well with each other. In addition, it can be clearly observed that there are jumps across the two interfaces for the normal stress along x-direction and the normal strain along z-direction. It is also noted that the maximum displacement along z-direction and the maximum stress along x-direction are reached at the pavement surface. Furthermore, they vary monotonically with depth in every single layer. However, this trend cannot be observed for the normal strain along z-direction where its maximum is obtained at the top of the subgrade layer.

Figures 6.7 to 6.9 show the variation of displacement, stress, and strain along the depth at (x,y=59in) with different x-coordinates to capture the pavement response along both vertical and horizontal directions. From Figure 6.7 it is concluded that, for a fixed pair of (x,y), the vertical displacement decreases with increasing depth, with its maximum displacement being at the surface (which is also called deflection). From Figures 6.8 and 6.9, we observed that the

107

variation of the horizontal stress and vertical strain are much more complicated than the displacement variation. However, it is interesting to notice that the maximum tensile horizontal stresses for different x coordinates are all reached at the bottom of asphalt concrete layer, and that the maximum compressive vertical strains, which are closely related to the rutting failure, are reached at the top of subgrade layer.

Table 6.2, Load configuration in ODOT example

Load No.	X-Position(in)	Y-Position(in)
1	4.50	59.00
2	14.00	59.00
3	34.00	59.00
4	43.50	59.00
5	75.00	59.00
6	84.50	59.00
7	104.50	59.00
8	114.50	59.00
9	134.00	59.00
10	143.50	59.00
11	163.50	59.00
12	173.00	59.00
13	204.50	59.00
14	214.00	59.00
15	234.00	59.00
16	243.50	59.00
17	75.00	118.00
18	84.50	118.00
19	104.50	118.00
20	114.00	118.00

We further remark that, unlike the pavement response due to a single loading where the amplitude of the induced field decreases with increasing radial distance to the loading circle, the maximum field responses in a given horizontal plane due to multiple loads are difficult to

capture because of the interaction among these loads. However, we can still state that the maximum response under uniform multiple loads (same load radius and load magnitude) will be reached at one of the centers of the multiple loads. The general multiple loading case suggests that more field points should be computed in order to capture the horizontal variation of the responses. This then would be very time consuming in computation and thus our fast and efficient *MultiSmart3D* can be applied.

6.3 CONCLUSIONS

In pavement analysis and design, the loading configuration plays an important role. The modeling of loads could be done using either ESALs or TI method. However, both methods are empirical and inaccurate. The newly developed *MultiSmart3D* program is a powerful software product that can be used for any number of loadings. The program was verified by running an example provided by ODOT. It should be noted that the presented studies are not specified to certain axle configuration and that the *MultiSmart3D* program can be easily employed for any specific axle configuration caused by different vehicle classes. Preliminary results show that the responses under multiple loads, especially arbitrary multiple loads, are quite different from those under single load. As such more field points are needed to capture the maximum responses in the whole field, which are critical for pavement design.
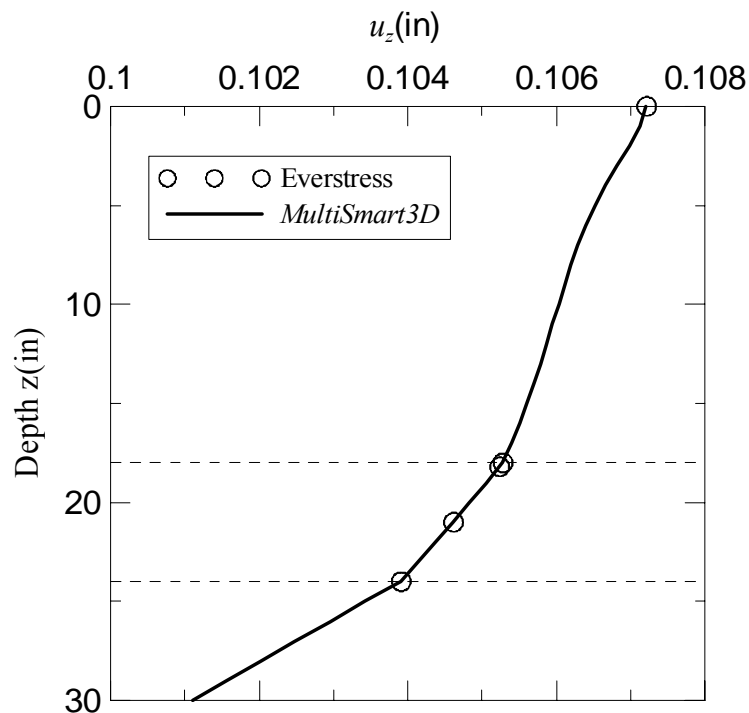
Figure 6.4, Vertical displacement (u_z) variation with depth.
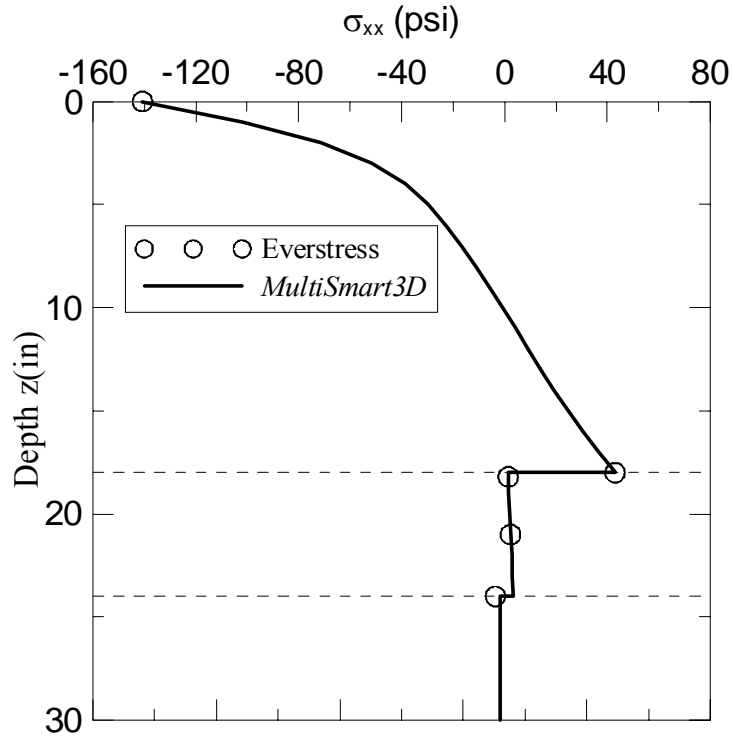
Figure 6.5, Horizontal stress (σ_{xx}) variation with depth.
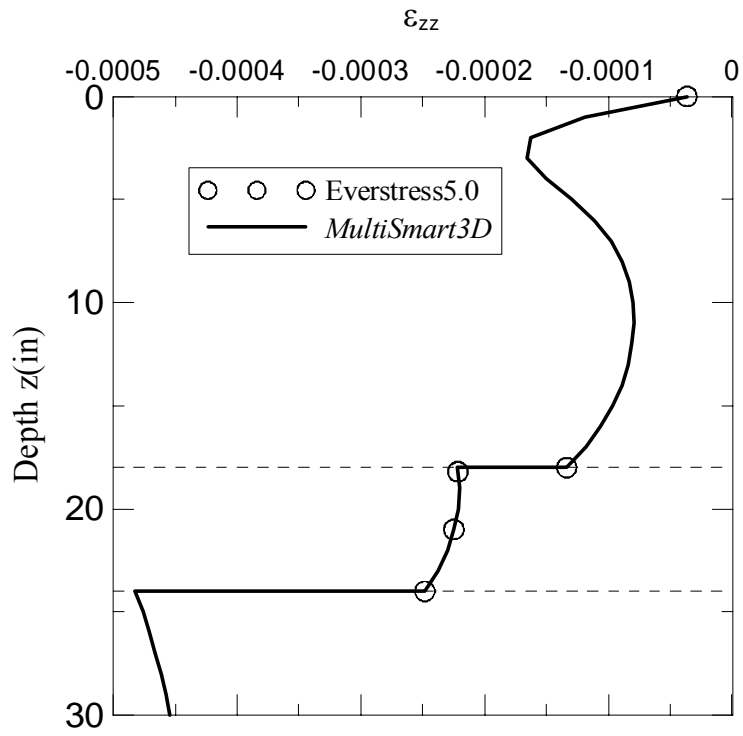

Figure 6.6, Vertical strain (ε_{zz}) variation with depth.
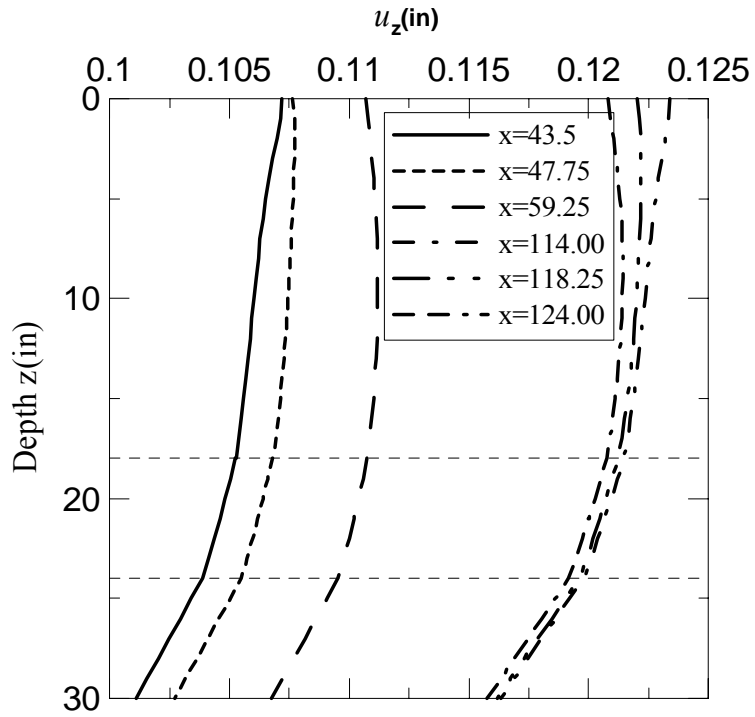
Figure 6.7, Vertical displacement (u_z) variation with depth.
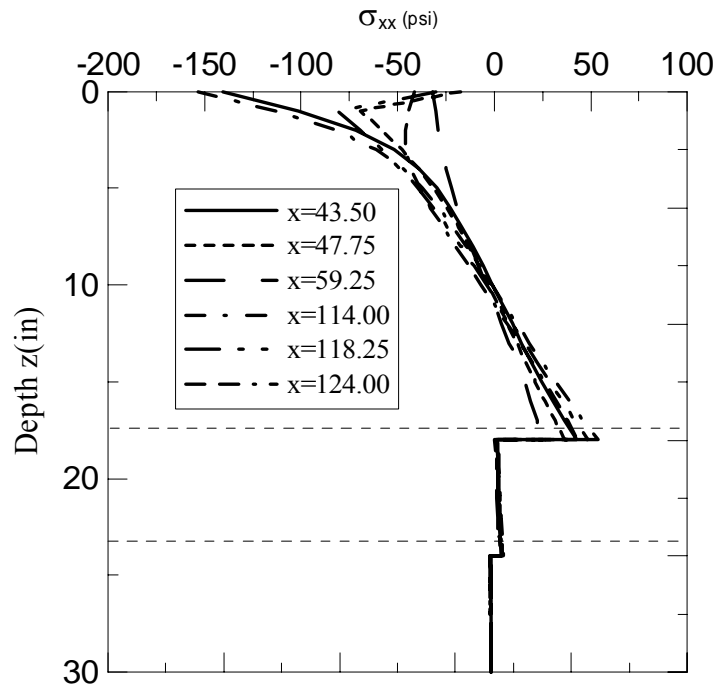
Figure 6.8, Horizontal stress (σ_{xx}) variation with depth.
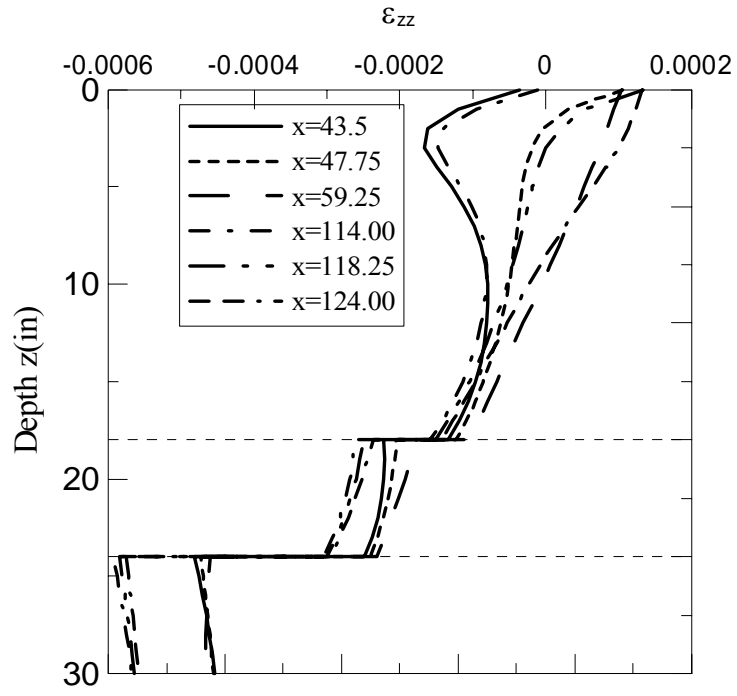
Figure 6.9, Vertical strain (ε_{zz}) variation with depth.

CHAPTER 7

INTRODUCTION TO *MULTISMART3D*

7.0 INTRODUCTION

In transportation engineering, the flexible pavement is usually modeled as a multilayered elastic half-space structure. One typical example is an asphalt concrete layer, base and subbase layer, and subgrade layer with each layer having an average modulus. However, due to the temperature or moisture variation with depth, the modulus of elasticity varies with depth within any layer, just like a functionally graded material structure.

To consider the functionally graded property in pavement design, an effective method is to subdivide every layer into many sublayers with different moduli. To better model the variation of modulus with depth, the number of sublayer required may be very huge, for instance, 100 layers or more. Unfortunately, many tradition pavement analysis programs cannot handle this pavement situation as they can only deal with about 20 discrete layers.

To overcome the limitations of the currently available pavement analysis programs, a powerful and innovative computer program, **MultiSmart3D**, was developed by the **Computer Modeling and Simulation Group** at the University of Akron. This new program can predict accurately and efficiently the response of the pavement consisting of any number of layers/sublayers under any number of loads. Furthermore, the complexity of the tire-pavement loading configuration can also be modeled easily.

7.1 PHILOSOPHY

This novel program is based on the layered elasticity theory, vector function and propagator matrix method. In the following sections, we briefly review the key technical issues of the program.

7.1.1 STATEMENT OF THE PRIMITIVE PROBLEM AND GOVERNING EQUATIONS

We consider the pavement to be a layered half space made up of p parallel, elastic isotropic layers lying over an elastic isotropic half space. The layers are numbered serially with the layer at the top being layer 1 and the last layer p, which is just above the half space (Figure.7.1). We place the cylindrical coordinate on the surface with the z-axis pointing into the layered half space. The k-th layer is bounded by the interfaces $z = z_{k-1}$, z_k. As such, z_{k-1} is the coordinate of the upper interface of the k-th layer, and z_k that of the lower interface. It is obvious that the thickness of the k-th layer is $h_k = z_k - z_{k-1}$, with $z_0 = 0$ and $z_p = H$, where H is the depth of the last layer interface. The interfaces between the adjacent layers are assumed to be welded. The top surface is subject to multiple loads. For a well-posed problem, the solution in the homogeneous half space of the layered system should be also finite when the physical dimension approaches infinity.
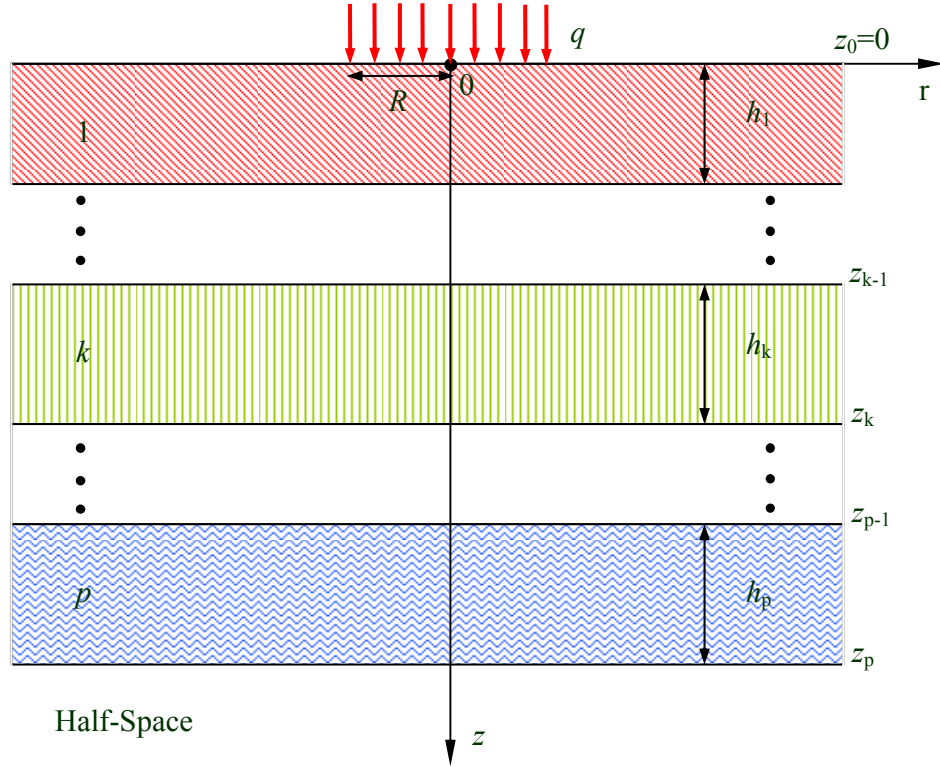
Figure 7.1, A multilayered pavement model.

For the isotropic elastic solid, there are, in each layer, the following governing equations in the cylindrical coordinates:

1) Equilibrium equations without body force:

$$\frac{\partial \sigma_{rr}}{\partial r} + \frac{\partial \sigma_{r\theta}}{r\partial \theta} + \frac{\partial \sigma_{rz}}{\partial z} + \frac{\sigma_{rr} - \sigma_{\theta\theta}}{r} = 0$$

$$\frac{\partial \sigma_{r\theta}}{\partial r} + \frac{\partial \sigma_{\theta\theta}}{r\partial \theta} + \frac{\partial \sigma_{\theta z}}{\partial z} + \frac{2\sigma_{r\theta}}{r} = 0 \qquad \text{Eq. (7.1)}$$

$$\frac{\partial \sigma_{rz}}{\partial r} + \frac{\partial \sigma_{\theta z}}{r\partial \theta} + \frac{\partial \sigma_{zz}}{\partial z} + \frac{\sigma_{rz}}{r} = 0$$

where σ_{ij} is the stress tensor.

2) Constitutive relations:

$$\sigma_{rr} = c_{11}\gamma_{rr} + c_{12}(\gamma_{\theta\theta} + \gamma_{zz})$$

$$\sigma_{\theta z} = c_{44}\gamma_{\theta z} \qquad \text{Eq. (7.2)}$$

where

$$c_{11} = \frac{E(1-v)}{(1+v)(1-2v)} \; ; \; c_{12} = \frac{Ev}{(1+v)(1-2v)} \; ; \; c_{44} = \frac{E}{2(1+v)} \qquad \text{Eq. (7.3)}$$

The constitutive relations for the other normal and shear components can be found similarly. While in Eq. (7.2) γ_{ij} are the engineering strain components, in Eq. (7.3), E and ν are, respectively, Young's modulus and Poisson's ratio.

3) The strain-displacement relations:

$$\gamma_{rr} = \frac{\partial u_r}{\partial r}, \ \gamma_{\theta\theta} = \frac{\partial u_\theta}{r\partial\theta} + \frac{u_r}{r}, \ \gamma_{zz} = \frac{\partial u_z}{\partial z}$$

$$\gamma_{\theta z} = \frac{\partial u_\theta}{\partial z} + \frac{\partial u_z}{r\partial\theta}, \ \gamma_{rz} = \frac{\partial u_z}{\partial r} + \frac{\partial u_r}{\partial z}, \ \gamma_{r\theta} = \frac{\partial u_r}{r\partial\theta} + \frac{\partial u_\theta}{\partial r} - \frac{u_\theta}{r}$$

Eq. (7.4)

where u_i is the displacement field.

7.1.2 GENERAL SOLUTION IN TERMS OF CYLINDRICAL SYSTEM OF VECTOR FUNCTIONS

The cylindrical system of vector functions is very convenient in treating axisymmetric problem and it is defined as (Pan, 1989a,b, 1997)

$$\mathbf{L}(r,\theta;\lambda,m) = \mathbf{e}_z S(r,\theta;\lambda,m),$$

$$\mathbf{M}(r,\theta;\lambda,m) = (\mathbf{e}_r \frac{\partial}{\partial r} + \mathbf{e}_\theta \frac{\partial}{r\partial\theta})S(r,\theta;\lambda,m),$$

Eq. (7.5)

$$\mathbf{N}(r,\theta;\lambda,m) = (\mathbf{e}_r \frac{\partial}{r\partial\theta} - \mathbf{e}_\theta \frac{\partial}{\partial r})S(r,\theta;\lambda,m)$$

with

$$S(r,\theta;\lambda,m) = \frac{1}{\sqrt{2\pi}} J_m(\lambda r)e^{im\theta},$$

Eq. (7.6)

where $J_m(\lambda r)$ is the Bessel function of order m with $m = 0$ corresponding to the axisymmetric deformation, which will be discussed in detail later on. It should be also noticed that the scalar function S in Eq. (7.6) satisfies the Helmholtz equation

$$\frac{\partial^2 S}{\partial r^2} + \frac{\partial S}{r\partial r} + \frac{\partial^2 S}{r^2\partial\theta^2} + \lambda^2 S = 0$$

Eq. (7.7)

The cylindrical system of vector functions is an extension of the Hankel transform and can be directly applied to a vector function. Since this vector function system (Eq. (7.5)) forms an orthogonal and complete space, any integrable vector and/or scalar function can be expressed in terms of it. In particular, the displacement and traction (with the z-axis as the normal) vectors can be expressed as

$$\boldsymbol{u}(r,\theta,z) = \sum_m \int_0^{+\infty} [U_L(z)\boldsymbol{L}(r,\theta) + U_M(z)\boldsymbol{M}(r,\theta) + U_N(z)\boldsymbol{N}(r,\theta)]\lambda d\lambda$$

Eq. (7.8)

$$\boldsymbol{t}(r,\theta,z) \equiv \sigma_{rz}\boldsymbol{e}_r + \sigma_{\theta z}\boldsymbol{e}_\theta + \sigma_{zz}\boldsymbol{e}_z$$

$$= \sum_m \int_0^{+\infty} [T_L(z)\boldsymbol{L}(r,\theta) + T_M(z)\boldsymbol{M}(r,\theta) + T_N(z)\boldsymbol{N}(r,\theta)]\lambda d\lambda$$

Eq. (7.9)

Making use of these expansions along with the strain-displacement and constitutive relations, we have, in general,

$$u_r(r,\theta,z) = \sum_m \int_0^{\infty} (U_M \frac{\partial S}{\partial r} + U_N \frac{\partial S}{r\partial\theta})\lambda d\lambda$$

Eq. (7.10a)

$$u_\theta(r,\theta,z) = \sum_m \int_0^\infty (U_M \frac{\partial S}{r\partial\theta} - U_N \frac{\partial S}{\partial r})\lambda d\lambda \qquad \text{Eq. (7.10b)}$$

$$u_z(r,\theta,z) = \sum_m \int_0^\infty U_L S\lambda d\lambda \qquad \text{Eq. (7.10c)}$$

$$\sigma_{rr}(r,\theta,z) = \sum_m \int_0^\infty [c_{11}(U_M \frac{\partial^2 S}{\partial r^2} + U_N \frac{\partial^2 S}{r\partial r\partial\theta} - U_N \frac{\partial S}{r^2\partial\theta}) + c_{12}(U_M \frac{\partial^2 S}{r^2\partial\theta^2}$$
$$+ U_M \frac{\partial S}{r\partial r} - U_N \frac{\partial^2 S}{r\partial r\partial\theta} + U_N \frac{\partial S}{r^2\partial\theta}) + c_{12} \frac{dU_L}{dz} S]\lambda d\lambda \qquad \text{Eq. (7.11a)}$$

$$\sigma_{\theta\theta}(r,\theta,z) = \sum_m \int_0^\infty [c_{12}(U_M \frac{\partial^2 S}{\partial r^2} + U_N \frac{\partial^2 S}{r\partial r\partial\theta} - U_N \frac{\partial S}{r^2\partial\theta}) + c_{11}(U_M \frac{\partial^2 S}{r^2\partial\theta^2}$$
$$+ U_M \frac{\partial S}{r\partial r} - U_N \frac{\partial^2 S}{r\partial r\partial\theta} + U_N \frac{\partial S}{r^2\partial\theta}) + c_{12} \frac{dU_L}{dz} S]\lambda d\lambda \qquad \text{Eq. (7.11b)}$$

$$\sigma_{zz}(r,\theta,z) = \sum_m \int_0^\infty [-\lambda^2 c_{12} U_M + c_{11} \frac{dU_L}{dz}] S\lambda d\lambda \qquad \text{Eq. (7.11c)}$$

$$\sigma_{\theta z}(r,\theta,z) = c_{44} \sum_m \int_0^\infty (\frac{dU_M}{dz} \frac{\partial S}{r\partial\theta} - \frac{dU_N}{dz} \frac{\partial S}{\partial r} + \frac{1}{r} U_L \frac{\partial S}{\partial\theta})\lambda d\lambda \qquad \text{Eq. (7.11d)}$$

$$\sigma_{rz}(r,\theta,z) = c_{44} \sum_m \int_0^\infty (\frac{dU_M}{dz} \frac{\partial S}{\partial r} + \frac{dU_N}{dz} \frac{\partial S}{r\partial\theta} + U_L \frac{\partial S}{\partial r})\lambda d\lambda \qquad \text{Eq. (7.11e)}$$

$$\sigma_{r\theta}(r,\theta,z) = c_{44} \sum_m \int_0^\infty [U_M(\frac{2\partial^2 S}{r\partial r\partial\theta} - \frac{2\partial S}{r^2\partial\theta}) + U_N(\frac{\partial^2 S}{r^2\partial\theta^2} - \frac{\partial^2 S}{\partial r^2} + \frac{\partial S}{r\partial r})]\lambda d\lambda \qquad \text{Eq. (7.11f)}$$

The relation of the expansion coefficients between T_I and U_I (I=L, M, N) can be found by comparing Eqs. (7.9) to (7.11c,d,e)

$$T_L = -\lambda^2 c_{12} U_M + c_{11} \frac{dU_L}{dz} \qquad \text{Eq. (7.12a)}$$

$$T_M = c_{44}(U_L + \frac{dU_M}{dz}) \qquad \text{Eq. (7.12b)}$$

$$T_N = c_{44} \frac{dU_N}{dz} \qquad \text{Eq. (7.12c)}$$

Substituting the stress expansion (7.11) into the equilibrium equation (7.1), one finds

$$\frac{dT_L}{dz} - \lambda^2 T_M = 0 \qquad \text{Eq. (7.13a)}$$

$$-\lambda^2 c_{11} U_M + c_{12} \frac{dU_L}{dz} + \frac{dT_M}{dz} = 0 \qquad \text{Eq. (7.13b)}$$

$$\frac{dT_N}{dz} - \lambda^2 c_{44} U_N = 0 \qquad \text{Eq. (7.13c)}$$

Noticing that the *N*-type solution is dependent to the *L&M*-type solution, we introduce the followting two sets of coefficient vectors

$$[E] = [U_L, \lambda U_M, T_L/\lambda, T_M]^t \qquad \text{Eq. (7.14a)}$$

$$[E^N(z)] = [U_N(z), T_N(z)/\lambda]^t \qquad \text{Eq. (7.14b)}$$

Then the homogeneous solution in each layer from Eqs. (7.12) and (7.13) are found to be

$$[\boldsymbol{E}(z)] = [\boldsymbol{Z}(z)][\boldsymbol{K}] \qquad \text{Eq. (7.15a)}$$

$$[\boldsymbol{E}^N] = [\boldsymbol{Z}^N(z)][\boldsymbol{K}^N] \qquad \text{Eq. (7.15b)}$$

where $[\boldsymbol{K}]$ and $[\boldsymbol{K}^N]$ are column coefficient vectors of 4×1 and 2×1, respectively, with their elements to be determined by the interface and/or boundary conditions. The matrices $[\boldsymbol{Z}(z)]$ and $[\boldsymbol{Z}^N(z)]$ are the solution matrices given in Pan (1989a,b).

The propagating relations for the coefficient vectors $[\boldsymbol{E}]$ and $[\boldsymbol{E}^N]$ of k-th layer at the z-level z_{k-1} and that at z_k, are found to be

$$[\boldsymbol{E}(z_{k-1})] = [\boldsymbol{a}_k][\boldsymbol{E}(z_k)], \qquad \text{Eq. (7.16a)}$$

$$\left[\boldsymbol{E}^N(z_{k-1})\right] = [\boldsymbol{a}_k^N]\left[\boldsymbol{E}^N(z_k)\right] \qquad \text{Eq. (7.16b)}$$

where $[\boldsymbol{a}_k]$ and $[\boldsymbol{a}_k^N]$ are the propagator matrices for the k-th layer, with their elements given in Pan (1989a,b).

7.1.3 SOLUTION FOR THE SINGLE CIRCULAR LOAD

First we solve the problem with single circular load. Assume that a uniform vertical surface load (*i.e.* pressure or normal stress) of magnitude q is applied within the circle of $r=R$ (Figure 7.1), then the traction boundary condition on the surface $z=0$ is expressed as:

$$\sigma_{zz} = \begin{cases} -q & r < R \\ 0 & r > R \end{cases} \qquad \text{Eq. (7.17)}$$

$$\sigma_{rz} = \sigma_{\theta z} = 0 \quad 0 \leq r \leq \infty$$

Therefore, the corresponding expansion coefficients in the cylindrical systems of vector functions are:

$$T_L(\lambda,0) = -\frac{qR\sqrt{2\pi}}{\lambda} J_1(\lambda R) \qquad \text{Eq. (7.18)}$$

$$T_M(\lambda,0) = T_N(\lambda,0) = 0$$

It is clear that the solution to the *N*-type is identically zero and therefore we need to solve the *L&M*-type problem (axisymmetric) only. We now first solve the problem in the transformed domain (i.e., in terms of the expansion coefficients). Propagating the propagator matrix $[\boldsymbol{a}_k]$ from the top of the homogeneous half space $z = H$ to the surface $z=0$, we find

$$[\boldsymbol{E}(0)] = [\boldsymbol{G}][\boldsymbol{K}_p], \qquad \text{Eq. (7.19)}$$

where

$$[\boldsymbol{G}] = [\boldsymbol{a}_1][\boldsymbol{a}_2] - - - [\boldsymbol{a}_p][\boldsymbol{Z}_p(H)], \qquad \text{Eq. (7.20)}$$

The unknown coefficients $[\boldsymbol{K}_p]$ are those in the half-space. As the solution in the half space should be bounded, the first and third elements in $[\boldsymbol{K}_p]$ should be zero (Pan, 1997). The remaining two unknown coefficients can be determined by the two boundary conditions on the surface $z=0$ as given by Eq. (7.18) (for the *L*- and *M*-components only). After the unknown coefficients in $[\boldsymbol{K}_p]$ are determined, the expansion coefficients at any depth (e.g. in the k-th layer with $z_{k-1} \leq z \leq z_k$) can be obtained exactly as:

$$[E(z)] = [a_k(z - z_{k-1})][a_{k+1}] - - - [a_p][Z_p(H)][K_p].$$ Eq. (7.21)

In general, direct multiplication of the propagator matrix $[a_k]$ can be carried out in order to propagate the transformed domain solution from one layer to the next. However, as discussed in Pan (1997), Yue & Yin (1998), and more recently by Fukahata & Matsu'ura (2005), overflow may occur from multiplication of matrices in Eqs. (7.20) and (7.21). Fortunately, this can be overcome by factoring out the exponentially growing factor in the elements of the propagator matrix. The resulting modified propagator matrices have no element growing exponentially, and therefore there will be no overflow problem for a multilayered half space having any number of layers (no matter what the thickness of each layer).

After solving the problem in the transformed domain, the displacement and stress solutions at any location in the physical domain can be expressed (independent of θ because of symmetry) as:

$$u_r(r,z) = -\frac{1}{\sqrt{2\pi}} \int_0^\infty (\lambda U_M) J_1(\lambda r) \lambda d\lambda$$ Eq. (7.22a)

$$u_\theta(r,z) = 0$$ Eq. (7.22b)

$$u_z(r,z) = \frac{1}{\sqrt{2\pi}} \int_0^\infty (U_L) J_0(\lambda r) \lambda d\lambda$$ Eq. (7.22c)

$$\sigma_{rz}(r,z) = -\frac{1}{\sqrt{2\pi}} \int_0^\infty (T_M) J_1(\lambda r) \lambda^2 d\lambda$$ Eq. (7.23a)

$$\sigma_{\theta z}(r,z) = \sigma_{r\theta}(r,z) = 0$$ Eq. (7.23b)

$$\sigma_{zz}(r,z) = \frac{1}{\sqrt{2\pi}} \int_0^\infty (\frac{T_L}{\lambda}) J_0(\lambda r) \lambda^2 d\lambda$$ Eq. (7.23c)

$$\sigma_{rr}(r,z) = \frac{\nu}{1-\nu} \sigma_{zz} + \frac{2c_{44}}{\sqrt{2\pi}} \int_0^\infty (\lambda U_M)[-\frac{1}{1-\nu} J_0(\lambda r)\lambda + \frac{J_1(\lambda r)}{r}] \lambda d\lambda$$ Eq. (7.23d)

$$\sigma_{\theta\theta}(r,z) = \frac{2\nu}{1-\nu} \sigma_{zz} - \sigma_{rr} - \frac{1}{\sqrt{2\pi}} \frac{E}{(1-\nu)} \int_0^\infty (\lambda U_M) J_0(\lambda r) \lambda^2 d\lambda$$ Eq. (7.23e)

where the expansion coefficients are functions of z and the transform variable λ.

7.1.4 SOLUTION FOR MULTIPLE CIRCULAR LOADS

Based on the solution for the single circular load, the solution for the multiple circular loads with different loading radii and magnitudes can be derived by the virtue of coordinate transformation and superposition. In other words, for N different loads, the total solution can be expressed as

$$\begin{Bmatrix} u_x(x,y,z) \\ u_y(x,y,z) \\ u_z(x,y,z) \end{Bmatrix} = \sum_{i=1}^{N} \left([S^i]^T \begin{Bmatrix} u_r(r,\theta,z) \\ u_\theta(r,\theta,z) \\ u_z(r,\theta,z) \end{Bmatrix}^i \right)$$ Eq. (7.24a)

$$\begin{bmatrix} \sigma_{xx} & \sigma_{xy} & \sigma_{xz} \\ & \sigma_{yy} & \sigma_{yz} \\ & & \sigma_{zz} \end{bmatrix} = \sum_{i=1}^{N} \left(\left[S^i \right]^T \begin{bmatrix} \sigma_{rr} & \sigma_{r\theta} & \sigma_{rz} \\ & \sigma_{\theta\theta} & \sigma_{\theta z} \\ & & \sigma_{zz} \end{bmatrix}^i \left[S^i \right] \right)$$

<div align="right">Eq. (7.24b)</div>

In Eq. (7.24),

$$[S] = \begin{bmatrix} \cos(\beta) & \sin(\beta) & 0 \\ -\sin(\beta) & \cos(\beta) & 0 \\ & & 1 \end{bmatrix}$$

where superscript i means the $i-th$ circular load, and β is the angle between the projection of the field point on the horizontal plane and the global $x-$ coordinate.

7.2 TUTORIAL

Based on the theoretical work presented above, a software product, was developed using FORTRAN. A friendly GUI version was also designed by incorporating the core code into VC++. The executive program is generated and named *MultiSmart3D*.

Double Click the executive program *MultiSmart3D*, the GUI is shown
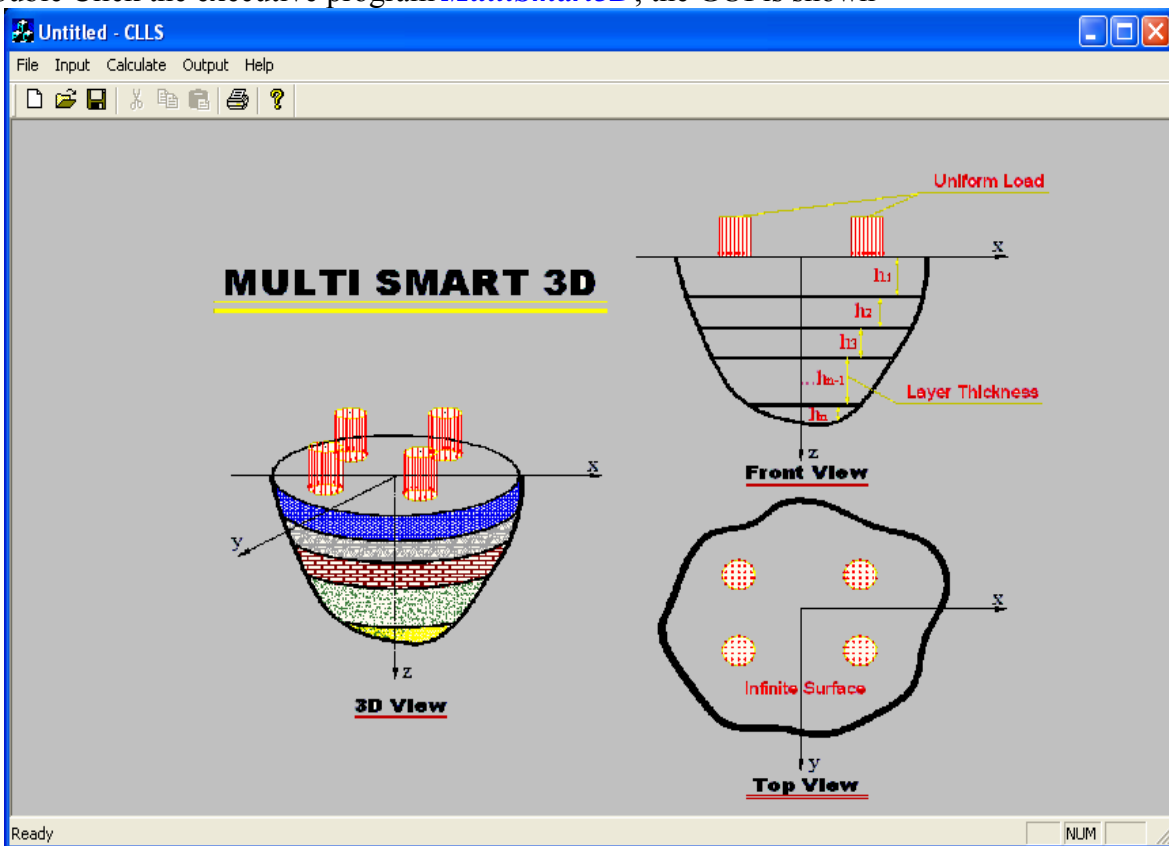

Figure 7.2, The GUI in *MultiSmart3D*.

Click "**File**", **open**, **start** or **save** the input file.
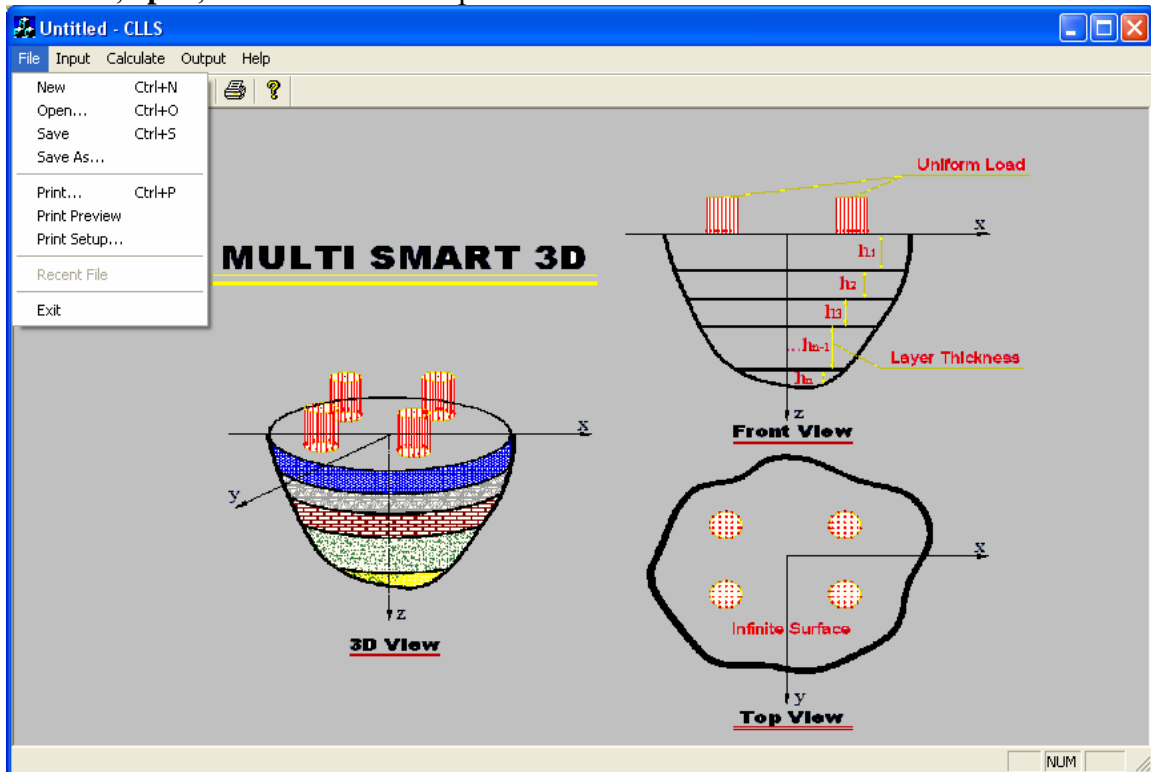
Figure 7.3, "File" option in *MultiSmart3D*.

Click the file you want to open, "sample2" for example
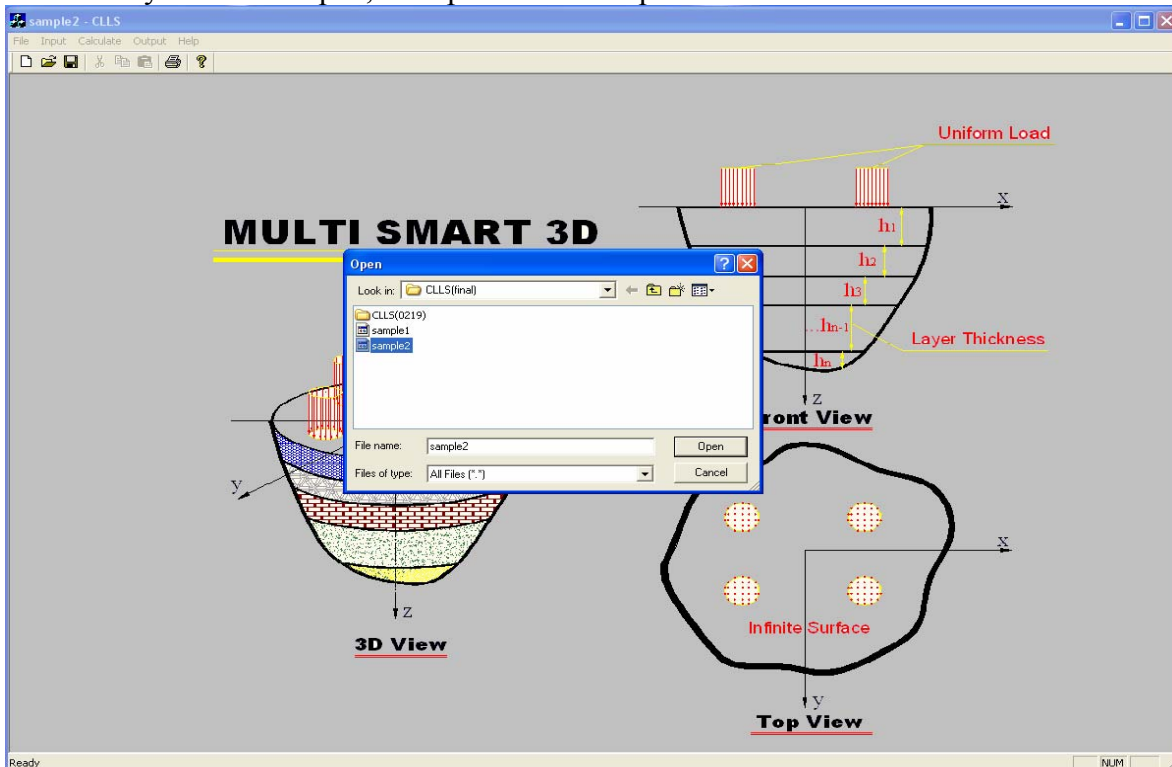
Figure 7.4, Open file in *MultiSmart3D*.

The title is changed to "sample2", Click "**Input**" → "**Input Info**" to "**General Info**"
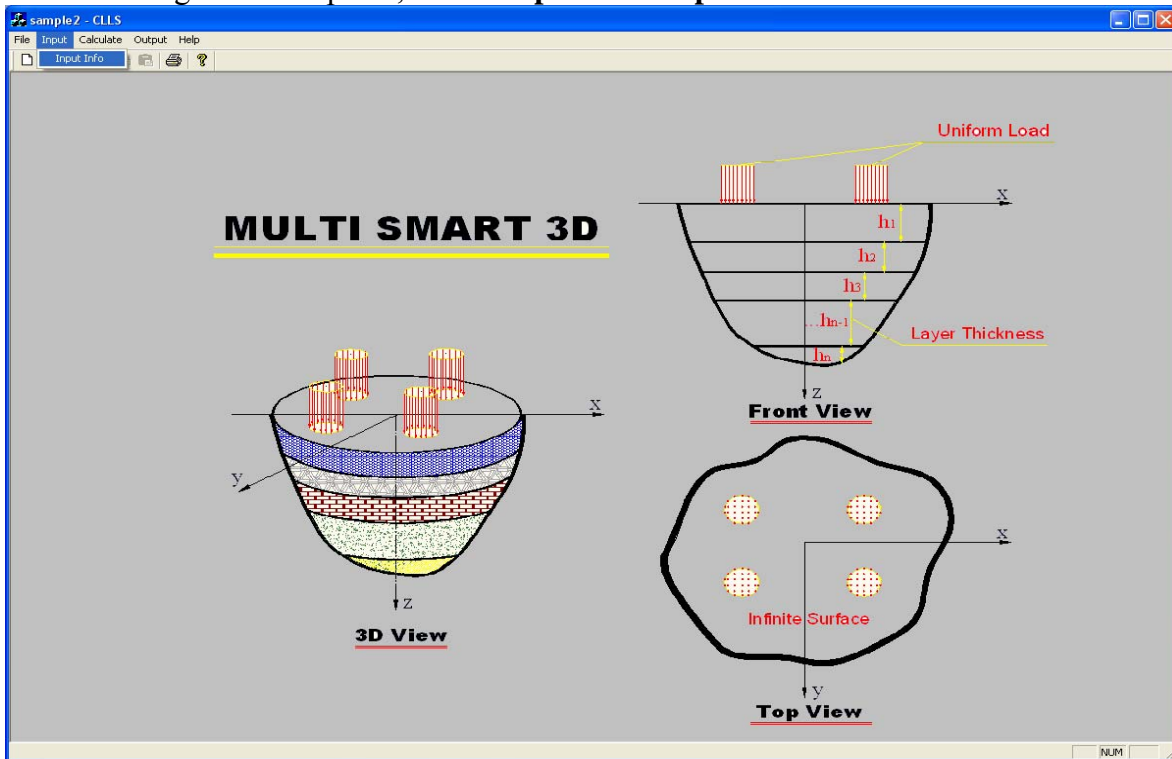
Figure 7.5, "Input" option in *MultiSmart3D*.

In "**General Info**", input general information including unit, case and boundary condition type.
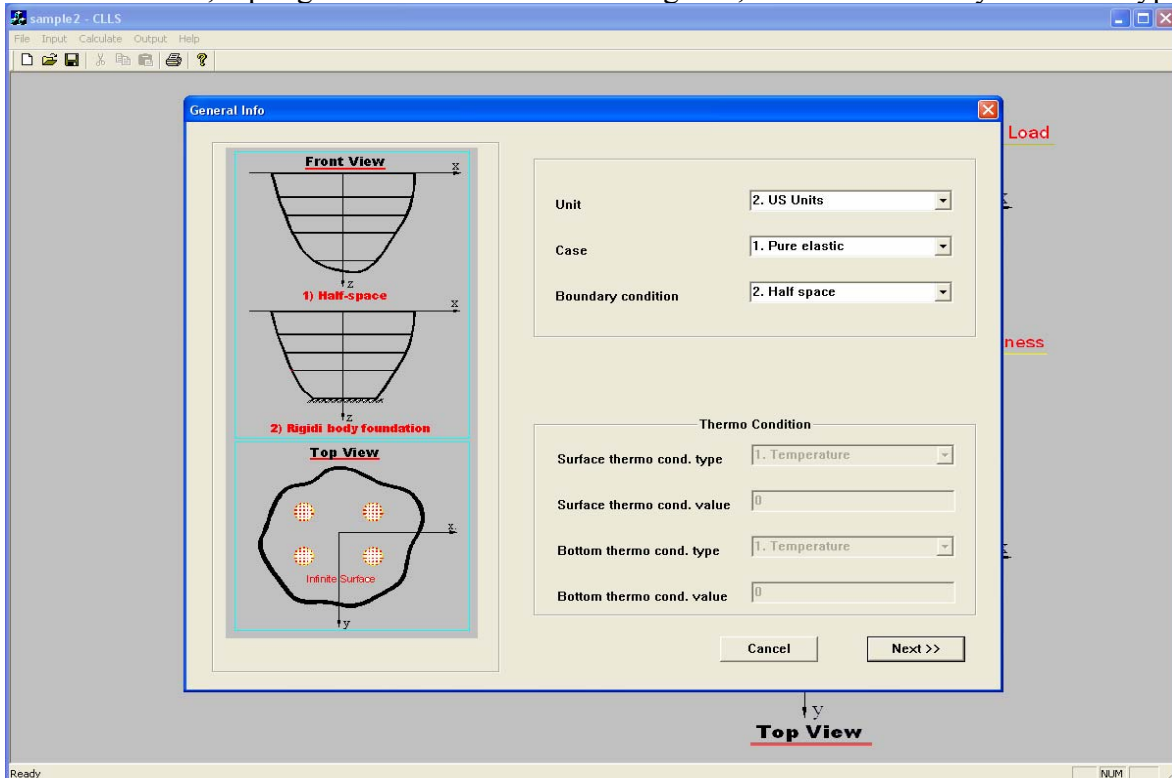
Figure 7.6, General input information in *MultiSmart3D* (1).

In "**General Info**", we can choose two unit systems, "SI Units" or "US Units". Click"**Next**" to "**Layer Info**"
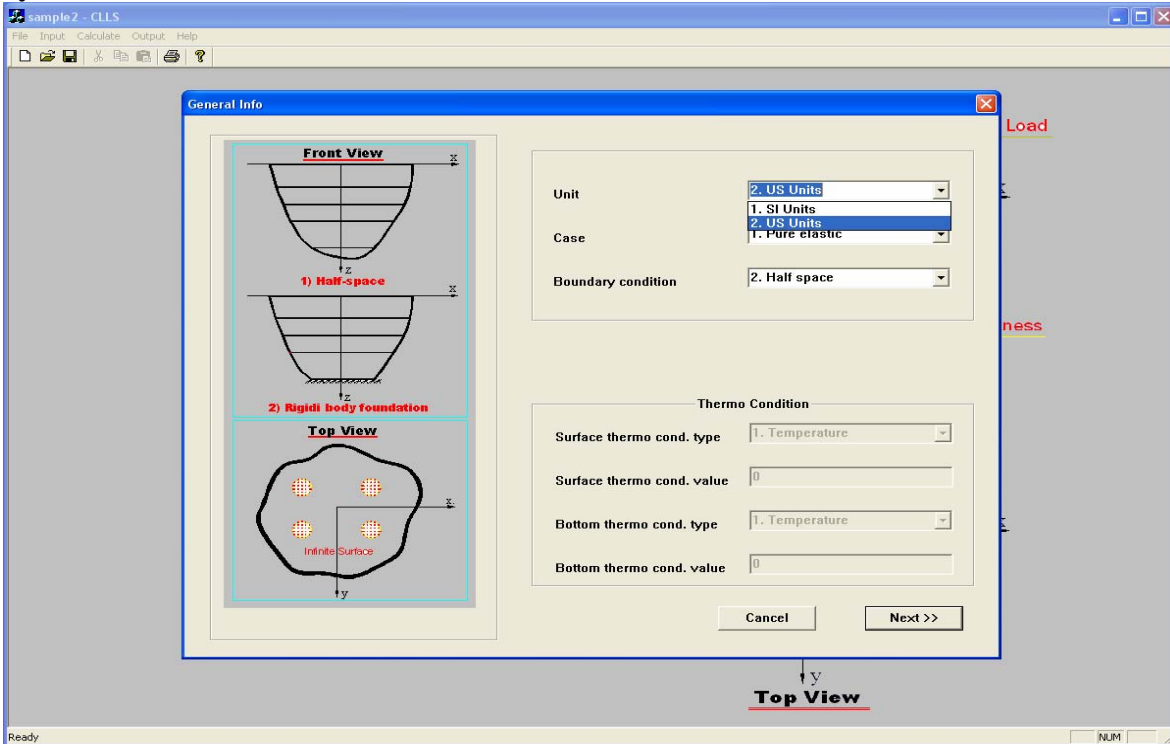
Figure 7.7, General input information in *MultiSmart3D* (2).

In "**Layer Info**", input layer information. Click "**Next**" to "**Load Info**"
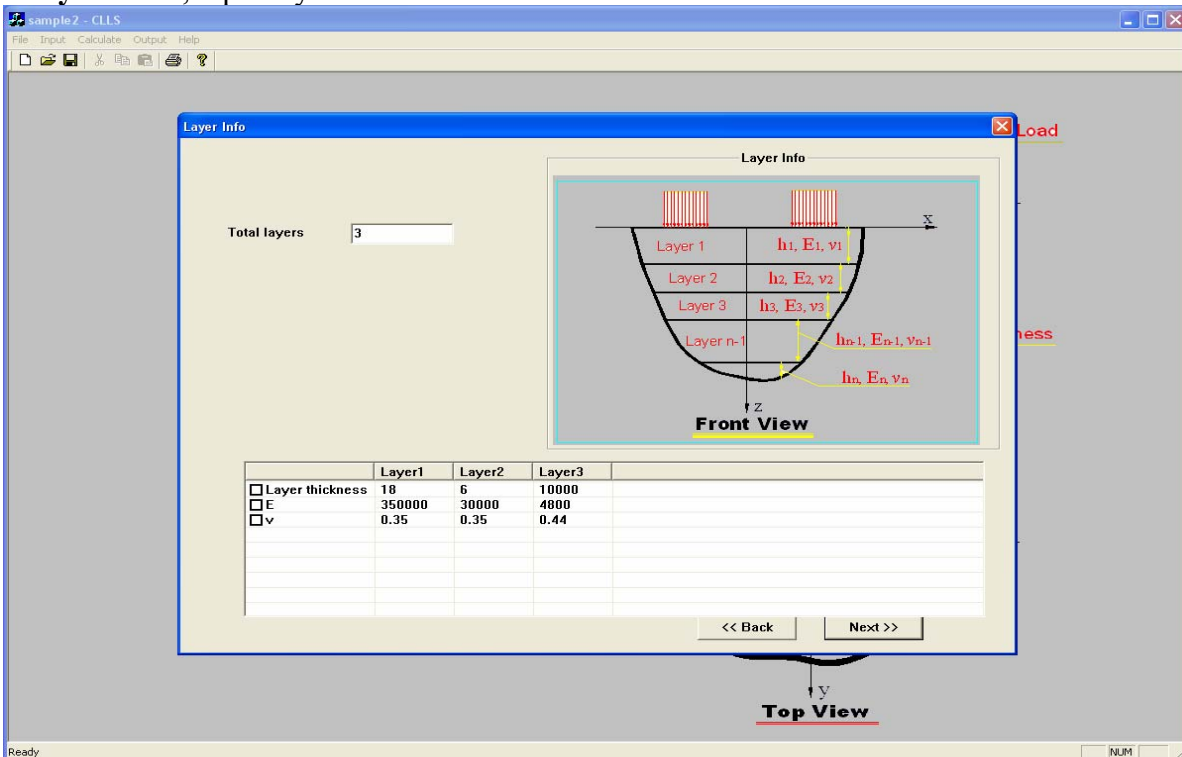
Figure.7.8, Layer parameters in *MultiSmart3D*.

In "**Load Info**", input load information, including load number and position. Click "**Next**" to "**Output Info**"
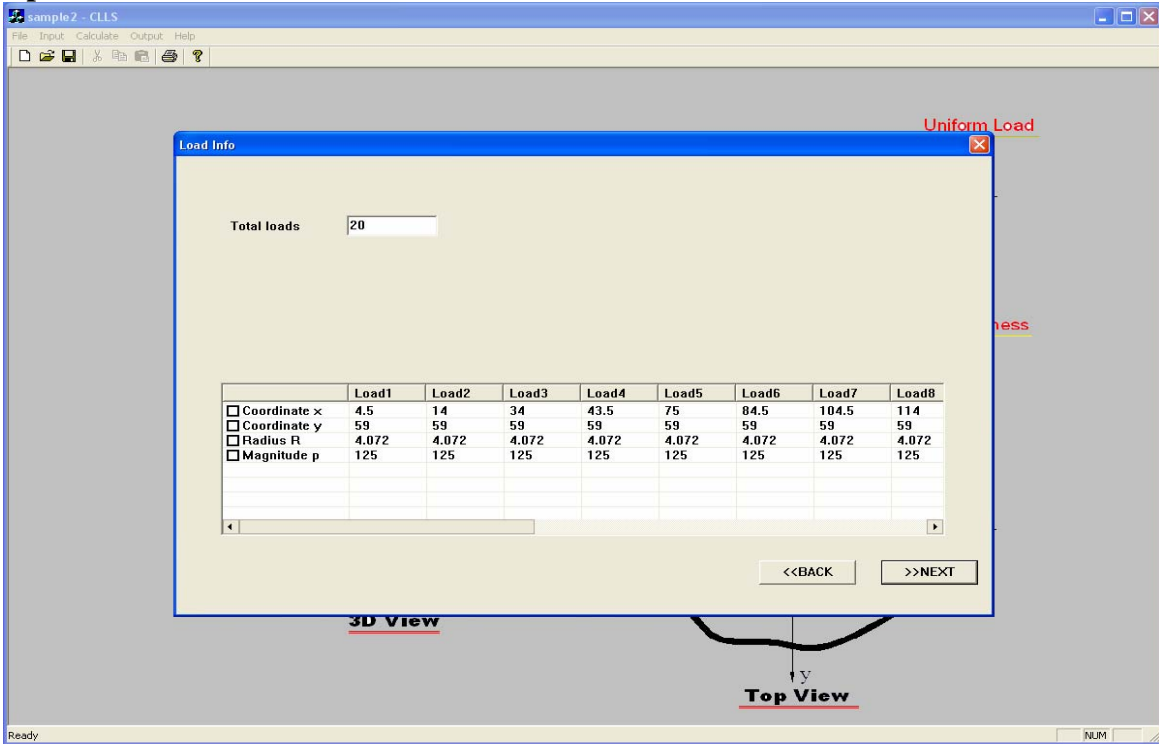
Figure 7.9, Load parameters in *MultiSmart3D*.

In "**Output Info**", input output option, field point number and position.
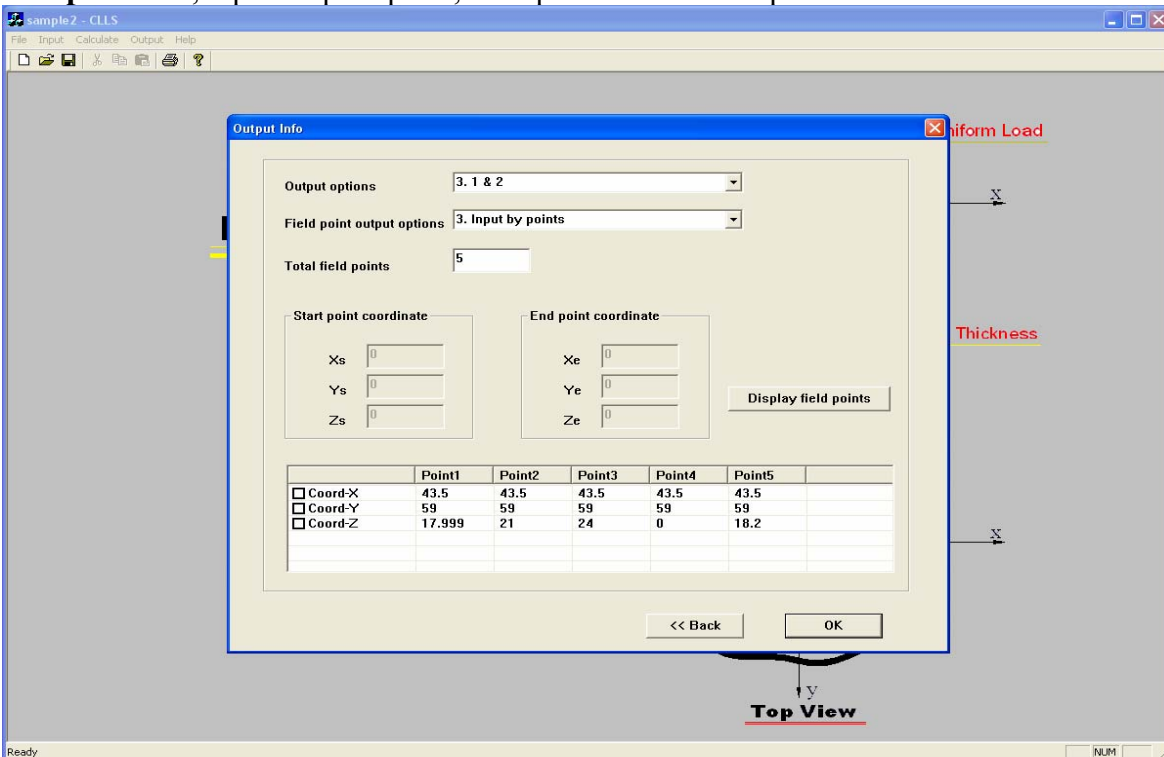
Figure 7.10, Output parameters in *MultiSmart3D* (1).

In "**Output Info**", output option, choose outputting"1.Only displacement (thermo item)","2.Only stress and strain (thermo item)", or"3.1 &2".
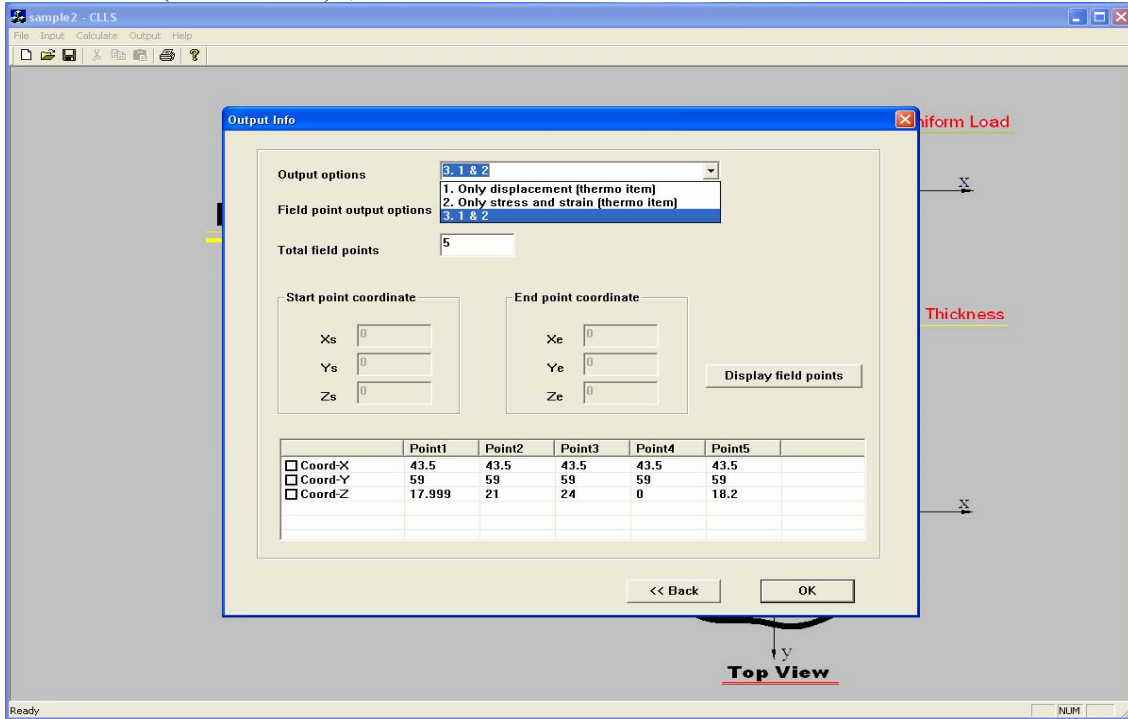
Figure 7.11, Output parameters in *MultiSmart3D* (2).

In "**Output Info**", field point output option, choose output"1.Vertical (total field point>2)"," Horizontal (total field point>2)", or"3.Input by points". Click "**OK**", finish input work.
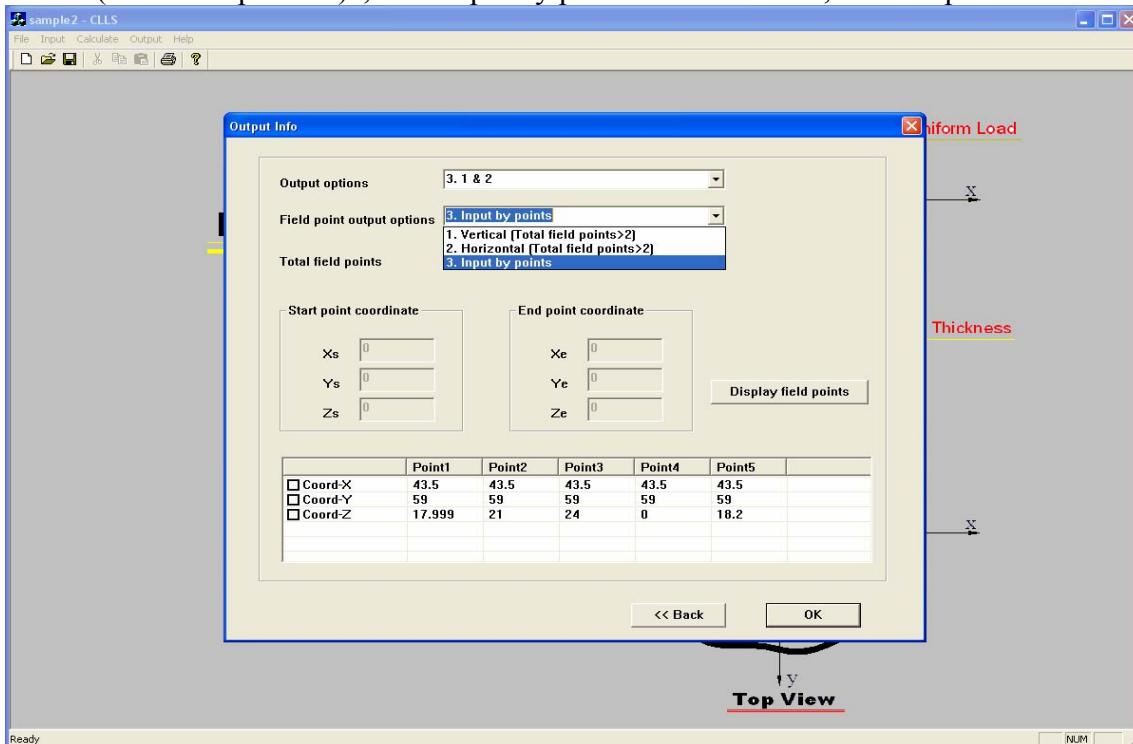
Figure 7.12, Output parameters in *MultiSmart3D* (3).

Click "**Calculate**", to calculate the results
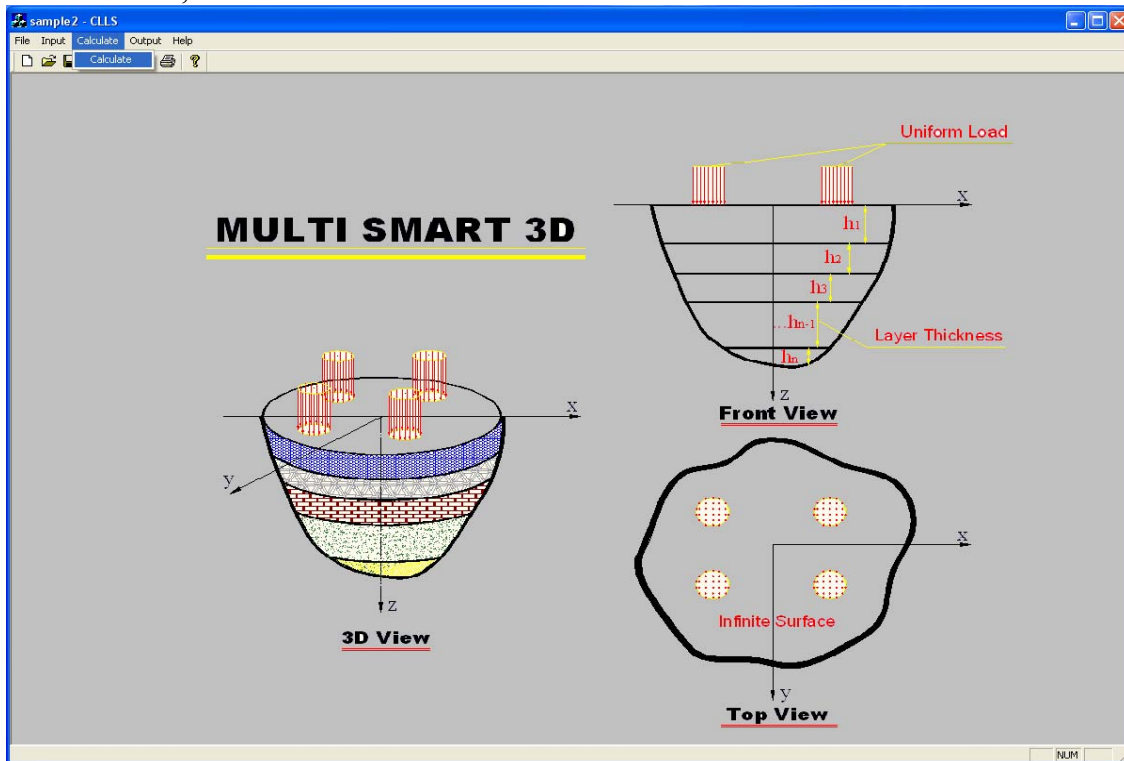
Figure 7.13, Calculation module in *MultiSmart3D*.

In calculating
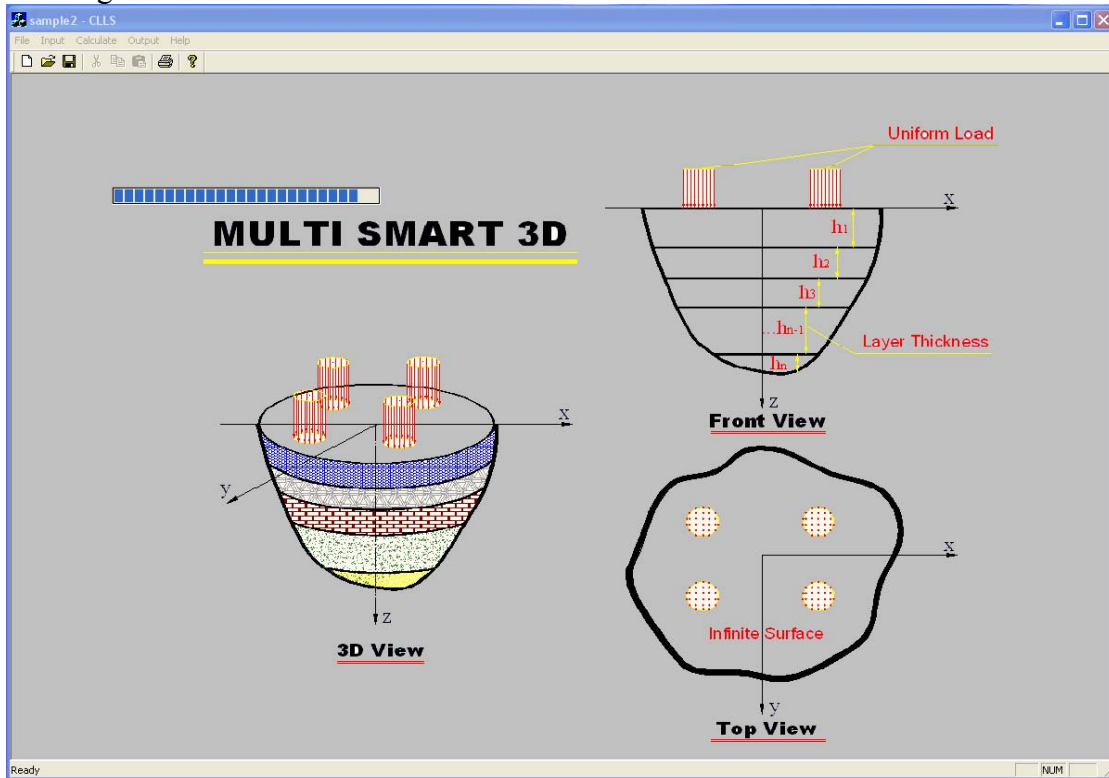
Figure 7.14, Calculation process in *MultiSmart3D*.

Calculating finished, "**Solution Done**", Click"**OK**"
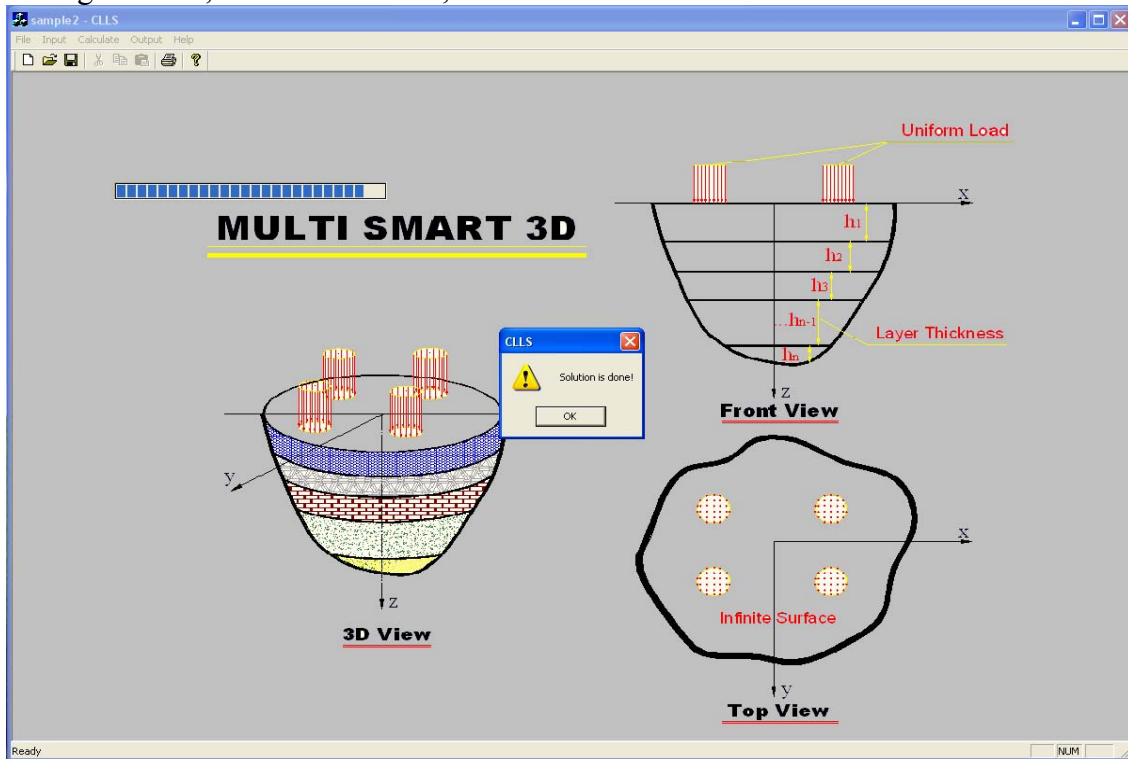
Figure 7.15, Calculation finished in *MultiSmart3D*.

Click "**Output**", choose checking input "Input check", or outputting" Displacement"," Stress","
Strain", and" Thermo"
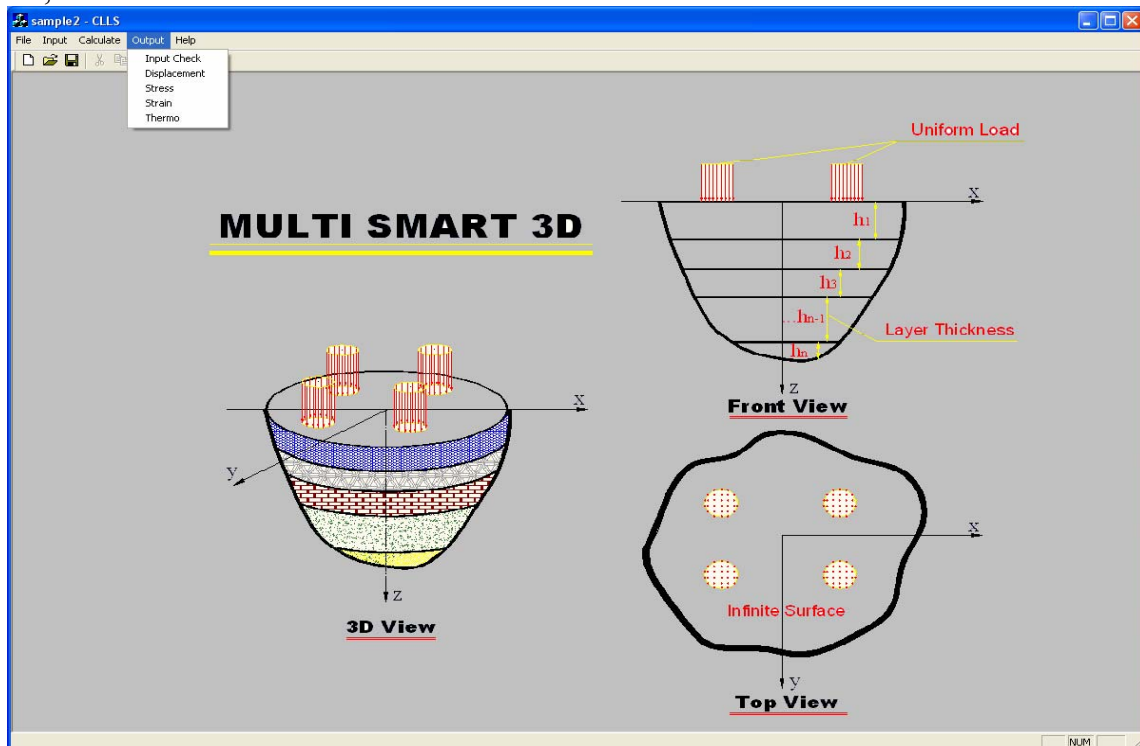
Figure 7.16, "Output" option in *MultiSmart3D*.

Click "**Input check**", check the input dates, which should be consistent to those in **Input**.


```
CheckInput - Notepad
File  Edit  Format  View  Help
---------- Input Check ----------
----------------------------------
---------- General Info ----------
Unit : US Unit
Case : Pure elastic
Boundary condition : Half space
----------------------------------
---------- Layer Info ----------
Total layers =3
    Layer No    Layer thickness            E              v
           0               18         350000           0.35
           1                6          30000           0.35
           2            10000           4800           0.44
----------------------------------
---------- Load Info ----------
Total loads =20
    Load No           xc              yc              p              r
           0             4.5             59            125          4.072
           1              14             59            125          4.072
           2              34             59            125          4.072
           3            43.5             59            125          4.072
           4              75             59            125          4.072
           5            84.5             59            125          4.072
           6           104.5             59            125          4.072
           7             114             59            125          4.072
           8             134             59            125          4.072
           9           143.5             59            125          4.072
          10           163.5             59            125          4.072
          11             173             59            125          4.072
          12           204.5             59            125          4.072
          13             214             59            125          4.072
          14             234             59            125          4.072
          15           243.5             59            125          4.072
          16              75            118            125          4.072
          17            84.5            118            125          4.072
          18           104.5            118            125          4.072
          19             114            118            125          4.072
----------------------------------
---------- Output Info ----------
Output Option : Displacement, stress and strain (Thermo item)
Field points input option : Input by point
Total field points = 5
Point No       Coord-X         Coord-Y         Coord-Z
        1          43.5             59          17.999
        2          43.5             59              21
        3          43.5             59              24
        4          43.5             59               0
        5          43.5             59            18.2
```

Figure 7.17, Check input information in *MultiSmart3D*

Click "**Displacement**", output displacement


```
Displacement - Notepad
File  Edit  Format  View  Help
---------- Displacement of field points ----------
---------- Unit: in ----------
 No      Coord-X       Coord-Y       Coord-Z            Ux            Uy            Uz
  1         43.5            59        17.999     -0.00325361   -0.00131242       0.10551
  2         43.5            59            21     -0.00441618   -0.00171989      0.104844
  3         43.5            59            24     -0.00552949   -0.00213464      0.104139
  4         43.5            59             0      0.00380145    0.00146448      0.107445
  5         43.5            59          18.2     -0.00333298   -0.00133957      0.105465
```

Figure 7.18, Displacements predicted with *MultiSmart3D*.

127

Click "**Stress**", output stresses
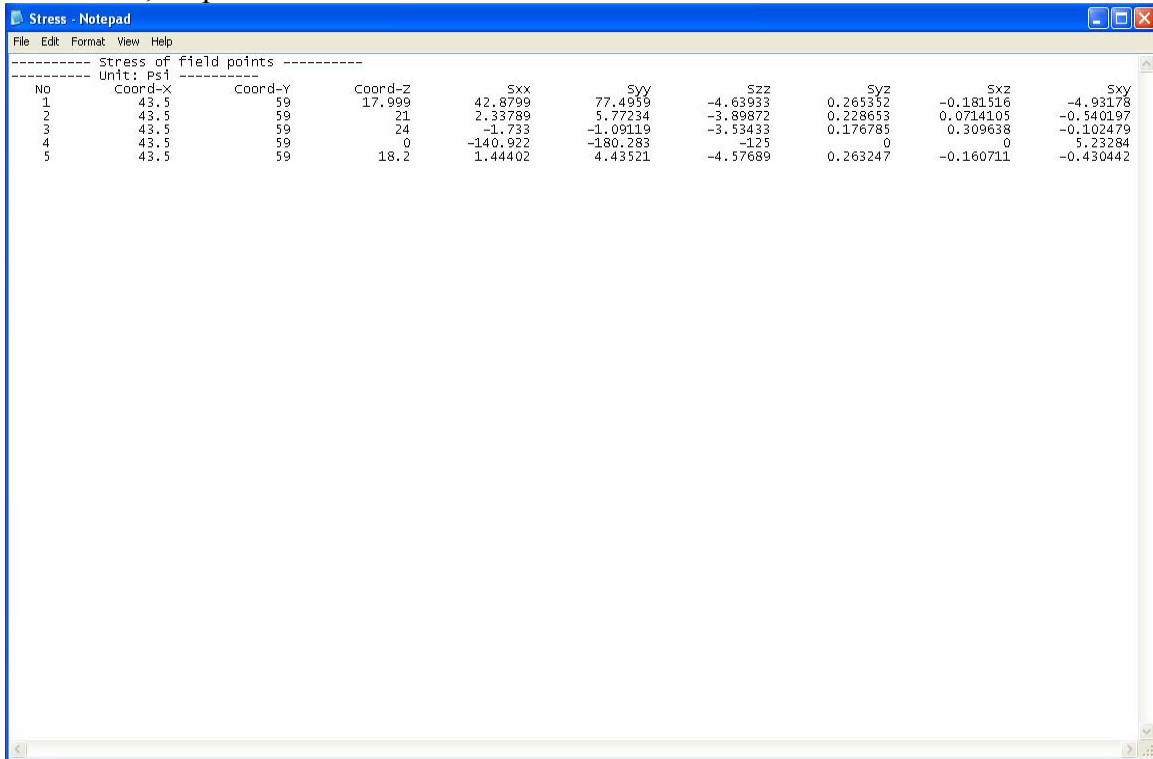
Figure 7.19, Stresses predicted with *MultiSmart3D*.

Click "**Strain**", output strains
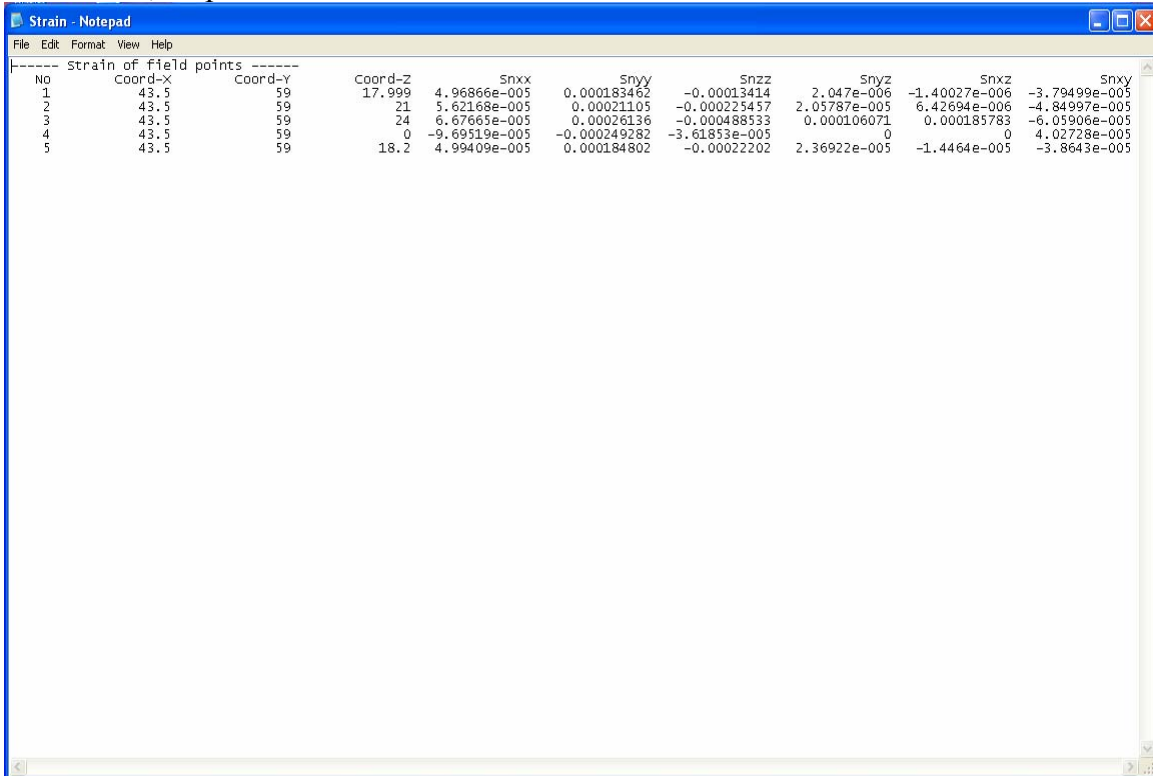
Figure 7.20, Strains predicted with *MultiSmart3D*.

CHAPTER 8

CONCLUSION AND RECOMENDATIONS

8.1 CONCLUSIONS

Based on the system of vector functions, propagator matrix, and adaptive Gauss integration methods, analytical solutions are derived for a multilayered flexible pavement where the resilient modulus can vary arbitrarily in the depth direction (also named as the functionally graded material, or FGM). This new advance will help pavement engineers to consider the effect of the temperature and moisture variations on the pavement response. A powerful and innovative computer program, called *MultiSmart3D*, has been also developed which overcomes the limitations of the currently available pavement analysis programs. The new program can predict accurately and efficiently the response of the pavement consisting of any number of layers/sublayers. The complexity of the tire-pavement loading configuration and multiple loading problems can also be easily modeled. Variation numerical examples have been carried and the correctness of the developed program has been verified. This pavement analysis software tool can be downloaded either from the PI's website at University of Akron or from ODOT's website.

8.2 RECOMMENDATIONS

The relationship between the functionally graded moduli and load response from this research will be useful in the design of flexible pavement. The corresponding *MultiSmart3D* software will be used to analyze permit applications for overloaded vehicles and forensic analysis of pavement sections. This exploratory study will also build up the foundation for the future modulus backcalculation analysis where modulus gradient needs to be included. The developed multilayered elasticity theory can also be extended to the corresponding viscoelasticity theory so that the viscoelastic response of the pavement can also be investigated in the near future.

REFERENCES

1. Abdulshafi, O., Mukhtar, H., and Kedzierski, B. (1994). "Reliability of AASHTO Design Equation for Predicting Pavement Performance of Flexible and Rigid Pavements in Ohio." FHWA/OH/95/006, Ohio Department of Transportation & Federal Highway Administration, CTL Engineering, Inc., Columbus, Ohio.

2. Ahlvin, R. G., and H. H. Ulery (1962), "Tabulated Values for Determining The Complete Pattern of Stresses, Strains, and Deflections Beneath a Uniform Circular Load on a Homogeneous Half Space", Highway Research Board, Bull. 342, 1–13.

3. Ali, H. and Lopez, A. (1996), "Statistical Analysis of Temperature and Moisture Effects on Pavement Structural Properties Based on Seasonal Monitoring Data", Transportation Research Record, No. 1540, 48-55.

4. Al-Qadi, I. L., M. Elseifi, and P. J. Yoo. In-Situ Validation of Mechanistic Pavement Finite Element Modeling, Proceedings of the 2nd International Conference on Pavement Accelerated Facilities, B. Worel and K. Faults, Eds., Minneapolis, MN, Sep 26-29, 2004 (in a CD).

5. Ancey, C. (2005) Notebook Introduction to Fluid Rheology, École Polytechnique Fédérale de Lausanne.

6. Bendana, L.J., Yang, W.S., and Lu, J. "Interpreting Data from the Falling Weight Deflectometer", Engineering Research and Development Bureau, New York State Department of Transportation, Research Report 160, 1994.

7. Blab, R. Introducing Improved Loading Assumptions into Analytical Pavement Models Based on Measured Contact Stresses of Tires. *International Conference on Accelerated Pavement Testing*, Reno, NV, 1999.

8. Bonnaure, F., Gravois, A., and Udron, J. A New Method of Predicting the Fatigue Life of Bituminous Mixes. Journal of the Association of Asphalt Paving Technologist, 1980, Vol. 49, pp. 499-529.

9. Boussinesq, J. "Essai theorique sur l'equilibre d'elasticite des massifs pulverulents compare a celui de massifs solides et sur la poussee des terres sans cohesion", Memoires des Savants Etrangers, Academie de Belgique, 40, Brussels, 1876.

10. Bowles, Joseph E. (1996). *Foundation Analysis and Design*. 5th edition, McGraw-Hill, New York.

11. Burmister, D. M. (1943). "The Theory of Stresses and Displacements in Layered Soil Systems and applications to the Design of Airport Runways," *Proc., Highway Research Board*, Vol. 23, 126-144.

12. Burmister, D. M. (1945). "The General Theory of Stresses and Displacements in layered Soil Systems," *Journal of Applied Physics*, 16, 84-94, 126- 127,296-302.

13. Burmister, D. M., (1958), "Evaluation of Pavement Systems of the WASHO Road Test by Layered Systems Methods", *Highway Research Board Bulletin 177*, 26-54.

14. Computational Modeling and Simulation Group, Department of Civil Engineering *MultiSmart3D* (2005). The University of Akron, Akron, OH.

15. Cho, Y., Liu, C., Dossey, T., and McCullough, B. (1998), Asphalt Overlay Design Methods for Rigid Pavements Considering Rutting, Reflection Cracking, and Fatigue Cracking, Center for Transportation Research, Report 987-9, The University of Texas as Austin.

16. Coree, B., Ceylan, H., and Harrington, D. (2005), Implementing the Mechanistic-Empirical Pavement Design Guide: Technical Report, IHRB Project TR-509, Center for Transportation Research and Education, Iowa State University.

17. COST 333 (1999), Development of New Bituminous Pavement Design Method, FINAL Report of the Action, European Commission, Brussels, Luxembourg.

18. Cundall, P. A., BALL – A Computer Program to Model Granular Media Using the Distinct Element Method. Technical Note TNLN-13, Advance Technology Group, Dames and Moore, London, 1978, pp. 129–163.

19. de Beer, M. and Fisher, C. Contact Stresses of Pneumatic Tires Measured with the Vehicle – Road Surface Pressure Transducer Array (VSPTA) System for the University of California at Berkeley (UCB) and the Nevada Automotive Test Center (NATAC). Restricted Report, Volume I and Volume II, University of California at Berkeley (UCB) and the Nevada Automotive Test Center (NATAC), 1997.

20. Drumm, E., and Meier, R. (2003), LTPP Data Analysis: Daily and Seasonal Variations in Insitu Material Properties, National Cooperative Highway Research Program, Transportation Research Board.

21. Edwards, J. M. and Valkering, C. P. (1974), "Structural Design of Asphalt Pavements for Road Vehicles-the Influence of High Temperatures", Highways and Road Construction, Feburary 1974.

22. Federal Highway Administration (FHWA). (2004). *Highway Statistics 2000*. Office of Highway Policy Information, Federal Highway Administration. Washington, D.C.

23. Figueroa, J. L. (2003). "Long-Term Monitoring of Seasonal and Weather Stations and Analysis of Data from SHRP Pavements." Department of Civil Engineering, Case Western Reserve University, Cleveland, Ohio.

24. Foster, C. R., and Ahlvin, R. G. (1954), "Stresses and Deflections Induced by a Uniform Circular Load", Proceedings, Highway Research Board.

25. Frölich, O. K., (1934) Druckverteilung in Baugrunde, Springer Verlag, Vienna, Austria.

26. Gregers Hildebrand (2002), *Verification of Flexible Pavement Response From a Field Test*, Danish Road Institute, Report 121.

27. Gucunski, N. and Krstic, V. (1996), "Backcalculation of Pavement Profiles from Spectral Analysis of Surface Waves Tests by Neural Networks Using Individual Receiver Spacing Approach", *Transportation Research Record*, No. 1526, p.6-13.

28. Heukelom, W. and C. R. Foster (1960), "Dynamic Testing of Pavements", *Journal of the Soil Mechanics and Foundations Division*, Vol. 86, No. SM1, p. 1-28.

29. Hjelmstad, K. D., Zuo, Q. H., and Kim, J. Elastic Pavement Analysis Using Infinite Elements, Transportation Research Record 1568, TRB, National Research Council, Washington D.C., 1997, pp. 72-76.

30. Huang, Yang H., (1993), *Pavement Analysis and Design*, Prince-Hall, Inc.

31. George, K.P. and Husain, S., "Thickness design for flexible pavement: A probabilistic approach", Transportation Research Record, 1095 pp 27-36, 1986.

32. Holtz, R., and Kovacs, W., An Introduction to Geotechnical Engineering, Printice Hall, Inc., New Jersy, 1981.

33. Huang, Y. H. (1993) Pavement Analysis and Design, Prentice Hall, New Jersy.

34. Janoo, V., and Berg, R. (1991),"Layer Moduli Determination during Freeze-Thaw Periods", Nondestructive Deflection Testing and Backcalculation for Pavements, Proceedings, Transportation Research Board, No. 1377, PP.26-35.

35. Liang, R. Y. (1997). "Mixture Design and Performance Prediction of Rubber-Modified Asphalt in Ohio." FHWA/OH-98/003, Ohio Department of Transportation & Federal Highway Administration, Department of Civil Engineering, University of Akron, Akron, Ohio.

36. Liang, R. Y. (2001). "Durability and Performance Characteristics of Hot Mix Asphalt Containing Polymer Additives – Phase I: Laboratory Study." FHWA/OH-2001/018, Ohio Department of Transportation & Federal Highway Administration, Department of Civil Engineering, University of Akron, Akron, Ohio.

37. Lukanen, E. O., R. N. Stubstad, and R. C. Briggs (2000), Temperature Predictions and Adjustment Factors for Asphalt Pavements. Research Report FHWA-RD-98-085, Federal Highway Administration, McLean, VA.

38. Luo, R., and Prozzi, J. A. Evaluation of the Joint Effect of Wheel Load and Tire Pressure on Pavement Performance, University of Texas, Research Report SWUTC/05/167245-1, 2005.

39. Mamlouk, M. S. (1985), "Use of Dynamic Analysis in Predicting Field Multilayer Pavement Moduli", *Transportation Research Record*, No. 1043.

40. Masada, T., and Sargand, S. M. (2002). "Laboratory Characterization of Materials & Data Management for Ohio-SHRP Projects." FHWA/OH-01/07, Ohio Department of Transportation & Federal Highway Administration, ORITE, Department of Civil Engineering, Ohio University, Athens, Ohio.

41. Masada, T, Sargand, S., Abdalla, B., and Figueroa, J. L. (2004), Material Properties for Implementation of Mechanistic-Empirical Pavement Design Procedures, Ohio Research Institute for Transportation & the Environment (ORITE).

42. MEPDG, National Research Council. Guide for Mechanistic-Empirical Design (MEPDG). National Cooperative Highway Research Program (NCHRP), 2004.

43. Nazarian, S. (1984), *In Situ Determination of Elastic Moduli of Soil Deposits and Pavement Systems by Spectral-Analysis-of-Surface-Waves Method*, Ph.D. Dissertation, University of Texas at Austin, Texas, USA.

44. Newmark, N.M. (1935) "Simplified Computation of Vertical Pressures in Elastic Foundations", University of Illinois Engineering Experiment Station Circular 24, Urbana, Illinois.

45. Ongel, A. and Harvey, J., Analysis of 30 years of pavement temperatures using the enhanced integrated climate model (EICM). Pavement Research Centre, 2004, University of California Davis.

46. Ovik, J., Birgisson, B. and Newcomb, D. (1999), "Characterizing Seasonal Variations in Flexible Pavement Material Properties", Transportation Research Record 1684, pp.1-7.

47. Pan, E., Static response of a transversely isotropic and layered half-space to general dislocation sources. *Phys. Earth Planet. Inter.,* 1989a, **58**, pp. 103-117.

48. Pan, E., Static response of a transversely isotropic and layered half-space to general surface loads. *Phys. Earth Planet. Inter.,* 1989b, **54**, pp. 353-363.

49. Pan, E., Thermoelastic deformation of a transversely isotropic and layered half-space by surface loads and internal sources. *Phys. Earth Planet. Inter.,* 1990, **60**, pp. 254-264.

50. Pan, E., Static Green's functions in multilayered half-spaces. *Applied Mathematical Modelling,* 1997, **21**, pp. 509-521.

51. Park, D., Fernando, E., and Leidy, J. Evaluation of Predicted Pavement Response with Measured Tire Contact Stresses, Transportation Research Record 1919, TRB, National Research Council, Washington D.C., 2005, pp. 160-170.

52. Read, J., and Whiteoak, D. (2003), The Shell Bitumen Handbook, Shell Bitumen, Thomas Telford Publishing, Fifth Edition, 460 pp.

53. Potter, D.W, and Donald, G.S. Revision of the NAASRA Interim Guide to Pavement thickness Design, Technical Note No. 2. Australian Road Research Vol. 15, No.2, June, 1985.

54. Rolt, J. (2000), "Long-Life Pavements", The World Bank Regional Seminar on Innovative Road Rehabilitation and Recycling Technologies, Amman, Jordan, 24 - 26 October 2000.

55. Sargand, S. M., and Hazen, G. A. (1991). "Evaluation of Resilient Modulus by Back-Calculation Technique." FHWA/OH-91/005, Ohio Department of Transportation & Federal Highway Administration, Department of Civil Engineering, Ohio University, Athens, Ohio.

56. Sargand, S. M., and Edwards, W. F. (2002). "Determination of Pavement Layer Stiffness on the Ohio SHRP Test Road Using Backcalculation Technique." Ohio Department of Transportation & Federal Highway Administration, ORITE, Department of Civil Engineering, Ohio University, Athens, Ohio.

57. Schiffman, R. L. (1962) "General Solution of Stresses and Displacements in Layered Elastic Systems", International Conference on the Structural Design of Asphalt Pavement", Proceedings, University of Michigan, Ann Arbor, USA.

58. Scrivner, F., Peohl, R., Moore, W., and Phillips, M. (1969), Detecting Seasonal Changes in Load-Carrying Capabilities of Flexible Pavements, National Cooperative Highway Research Program, Highway Research Board, Report No. 76.

59. Shook, J. F., Finn, F. N., Witczak, M. W., and Monismith, C. L. Thickness Design of Asphalt Pavements – The Asphalt Institute Method. 5th International Conference on the Structural Design of Asphalt Pavements, 1982, **1**, pp. 17-44.

60. Skok, E.L., Clyne, T.R., Johnson, E., Timm, D.H., and Brown, M.L. Best Practices for the Design and Construction of Low Volume Roads Revised, Minnesota Department of Transportation Research Services Section, November 2003 (MN/RC-2002-17REV).

61. Szendrei, M. E., and C. R. Freeme (1970), *Dynamic Techniques for Testing Pavement Structures*, National Institute of Road Research, Bulletin 9, South Africa, 1970.

62. Ullidtz, P. Pavement Analysis, Developments in Civil Engineering, Elsevier, Amestrdam, 1987.

63. Ullidtz, P. (1995), Stresses and Strains in a Two-Dimensional Particulate Material", 74th Annual Meeting of the Transportation Research Board, Washington, D.C.

64. Ullidtz, P. (1998), Modelling Flexible Pavement Response and Performance, Polyteknisk Forlag.

65. Westergaard, H.M. (1938) "A Problem of Elasticity Suggested by a Problem in Soil Mechanics: A Soft Material Reinforced by Numerous Strong Horizontal Sheets," in Contributions to the Mechanics of Solids, Stephen Timoshenko 60th Anniversary Volume, Macmillian, New York, pp. 268-277.

66. Witczak, M. W., "The Universal Airport Pavement Design System, Report II: Asphalt Mixture Material Characterization", University of Maryland Report, May 1989.

67. Witczak, M., Roque, R., Hiltunen, D. and Buttler, W. (2000), Superpave Suppot and Performance Models Management, NCHRP 9-19, Task B, University of Arizona.

68. Yoder, E.J., (1959). Principles of Pavement Design, John Wiley & Sons, Inc., London.

69. Yoder, E.J., and M.W. Witczak. Principles of Pavement Design. John Wiley and Sons, Inc., New York, 1974.

70. Zeng, X. and Hlasko, H. (2005) *Cone Penetrometer Equipped with Piezoelectric Sensors for Measurement of Soil Stiffness in Highway Pavement,* Report No. FHWA/OH-2005/15, Ohio Department of Transportation, Columbus, Ohio.

71. http://www.dot.state.oh.us/techservsite/offceorg/traffmonit/TMReports/default.htm

72. http://www.hawaiiasphalt.com/HAPI/modules/06_design_factors/06_loads.htm